1-1-2017

Zwitterionic Polymer Materials For Nanoparticle Stabilization, Cell Encapsulation And Anti-Fouling Coating

Wei Wang
Wayne State University,

ZWITTERIONIC POLYMER MATERIALS FOR NANOPARTICLE STABILIZATION, CELL ENCAPSULATION AND ANTI-FOULING COATING

by

WEI WANG

DISSERTATION

Submitted to the Graduate School

of Wayne State University,

Detroit, Michigan

in partial fulfillment of the requirements

for the degree of

DOCTOR OF PHILOSOPHY

2017

MAJOR: Materials Science and Engineering

Approved By:

_____

Advisor Date

_____

Committee Member: Date

_____

_____

_____

ACKNOWLEDGEMENTS

During my four-year PhD study, I want to first sincerely thank my advisor, Dr. Zhiqiang Cao, for his instruction and support on both my life and academic development. I benefitted a lot by learning from him for efficient time management and diligent dedication on researches. Most of my research ideas were generated and greatly promoted by the in-depth discussions and brainstorm with him. I also appreciated a lot for the sharing of his valuable experiences on research methods and training on scientific writing and presentation. His working style with great enthusiasm, focus and efficiency will continuously influence my career.

I would also appreciate my committee members, Dr. Howard Matthew, Dr. Guangzhao Mao, Dr. Mohammad Mehrmohammadi and Dr. Anjaneyulu Kowluru for their insightful comments and suggestions on my dissertation. Also, I want to appreciate graduate program director, Dr. Yinlun Huang for his instruction on my academic development.

I would also acknowledge the Wayne State Faculty Startup Founding for the carbon nanoparticle project, Juvenile Diabetes Research Foundation (JDRF) and National Institute of Health (NIH) for the islet encapsulation project and National Science Foundation (NSF) for the anti-biofilm coating project.

I would like to thank all my lab mates, Yang Lu, Dr. Zhanguo Yue, Dr. Jinbin Xie, Dr. Zhigang Wang, Hui Zhu, Dr. Ershuai Zhang, Dr. Jianhai Yang and Dr. Ke Wang for their help and friendship. I appreciate Dr. Zhi Mei from Lugimen Center for the support on SEM and TEM, Dr. Yanmei Yuan from Medical School for tissue sectioning and

staining, Ayad Nacy for the help on FT-IR measurement, Xuecheng Yu and Linxiao Xie for the help on AFM imaging, Elisabeth Steel for the mechanical test, Jinchao Xi and Chunsong Yu for the absorbance measurement and Kevin Miles for the help on materials and tools sterilization.

I would also express my deepest gratitude for my wife, Yanjie Cao, my parents and grandmother for their endless love and emotional support. I wouldn't finish my PhD study without their continuous encouragement.

In the end, I would like to thank all the nice persons who have helped me in one way or another during my Ph.D. candidacy.

TABLE OF CONTENTS

ACKNOWLEDGEMENTS……ii

LIST OF TABLES……vi

LIST OF FIGURES……vii

CHAPTER 1. INTRODUCTION……1

1.1 Zwitterionic polymers stabilize nanoparticles……4

1.2 Zwitterionic hydrogel for islet encapsulation……5

1.3 Zwitterionic coating for biofilm resistance……6

CHAPTER 2. ONE STEP SYNTHESIS OF ZWITTERIONIC POLYMER STABILIZED CARBON NANOPARTICLES……7

2.1 Introduction……7

2.2 Materials and Methods……8

2.3 Results and discussions……12

CHAPTER 3. ZWITTERIONIC HYDROGEL IMPLANTS PROMOTE FUNCTIONAL BLOOD VESSEL GROWTH FOR ISLET ENCAPSULATION……25

3.1 Introduction……25

3.2 Materials and Methods……27

3.3 Results……34

3.4 Discussion……42

CHAPTER 4. A MACRO-CROSSLINKER FOR DURABLE ANTI-FOULING COATING……57

4.1 Introduction……57

4.2 Materials and Methods……59

4.3 Results and discussions……62

CHAPTER 5. SUPER-DURABLE COATING FABRICATED FROM A DOUBLE-SIDED TAPE WITH LONG-TERM “ZERO” BACTERIA ADHESION……75

5.1 Introduction……..75

5.2 Materials and Methods……77

5.3 Results and discussions……82

CHAPTER 6. CONCLUSION AND OUTLOOK……96

REFERENCES……99

ABSTRACT……..113

AUTOBIOGRAPHICAL STATEMENT……114

LIST OF TABLES

Table 2-1 Structures for zwitterionic polymers and zeta-potentials for these free polymers and the resulting NPs……18

LIST OF FIGURES

Figure 2-1 Illustration of making carbonized core-zwitterionic polymer shell NPs directly from zwitterionic polymers……18

Figure 2-2 (a) TEM image and statistic size distribution of PCB-1 NPs (b) TEM image and statistic size distribution of PMPC NPs……19

Figure 2-3 (a) NMR spectra of parent CB-1 polymer and synthesized PCB-1 NPs, (b) NMR spectra of parent MPC polymer and synthesized PMPC NPs……..20

Figure 2-4 (a) short-term and (b) long-term colloid stability of PCB-1, PMPC, and CA NPs in PBS buffer……21

Figure 2-5 Colloid stability (a) in BSA/PBS and (b) in fibrinogen/PBS buffer……22

Figure 2-6 Colloid stability in freeze-drying condition of PCB-1 NPs, PMPC NPs and CA NPs……23

Figure 2-7 (a) MTT results of CB-1, MPC and CA NPs. (b) Fluorescent property of zwitterionic NPs under UV (365 nm) excitation……24

Figure 3-1 (a) Molecular structure of carboxybetaine acrylamide (CBAA) monomer and MBAA crosslinker which that used for making the PCBAA hydrogel. (b) represented histology images on blood vessel formation of hydrogel samples, healthy tissue and self-heal incision after one month transplantation. (c) The calculated density of blood vessels of all samples in (b). (d) Calculated blood vessel density for Long-term PCBAA hydrogel implantation in mice for half a year…… ..47

Figure 3-2 Representative images of MECA-32 antibody staining of PCBAA hydrogel/tissue interface after 2, 3, 4, and 6 months of implantation……..48

Figure 3-3 (a) A represented image of MECA-32 antibody staining of B16F10 melanoma tumor tissue. Scale bar = 50 μm. (b) Calculated blood vessel density of PCBAA hydrogel/tissue interface, normal tissue and tumor tissue, based on MECA-32 staining results……..48

Figure 3-4 (a) Illustration of green dye injection experiment. The mice with implanted samples receive tail vein injection of FITC-dextran in PBS solution. The samples and surrounding tissue were retrieved for imaging. (b) Represented images of FITC-dextran stained blood vessels for all hydrogel samples under fluorescence microscope. Scale bar = 50 μm. (c) images showing blood vessels grown into the hole in the center of a hydrogel disk and narrow space between two hydrogel disks. Scale

bar = 400 µm. (d) Schematic representation of the two approaches in (c). (e) Blood vessels near to PCBAA hydrogel implants were perfused with green FITC-dextran. Gel/tissue interface was labeled by white dash lines. 20 µm away from the interface was depicted by red dash lines. Scale bar = 50 µm……49

Figure 3-5 Blood vessel density for PCBAA, Alginate SLG20 and PEGDA 10K hydrogel/tissue interface, calculated from FITC-Dextran staining……50

Figure 3-6 Fluorescent image on tissues interfaced with PCBAA hydrogel disk containing a premade hole. The hydrogel disk was implanted for 2 months followed by FITC-Dextran perfusion on blood vessels……50

Figure 3-7 a) dye accumulation of all explanted hydrogel samples (after different time points) under UV lamp after receiving i.v. injection of Evans Blue dye in PBS. (b) Fluorescent intensity quantification from (a)……51

Figure 3-8 Evans Blue dye accumulation on Alginate SLG20, PEGDA 10K and PCBAA hydrogels that have been implanted for 15 days……52

Figure 3-9 The first line exhibited the islets morphology in different materials after 30 days' implantation in normal healthy mice. The second line showed the corresponding glucose response capability of islets in different materials after 30 days' implantation……52

Figure 3-10 (a) Therapeutic curve of PCBAA hydrogel and Alginate SLG20 hydrogel devices with 500 IEq rat islets encapsulated. Live (green) and Dead (red) staining was performed at the end point as indicated. (b) The fraction of cured diabetic mice after being transplanted (non-fasted blood glucose level < 200 mg/dl)……53

Figure 3-11 (a) Macrophages in the vicinity of different material implants were analyzed after 1-month implantation. Representative immunofluorescence histological images were obtained through triple staining with the indicated markers. (b) Percentage of macrophages expressing pro-inflammatory (interleukin 10 (IL-10), transforming growth factor beta 1 (TGF-β1), arginase-1 (Arg-1) and macrophage mannose receptor (MMR)) and anti-inflammatory (tumor necrosis factor alpha (TNF-α), interleukin 1 beta (IL-1 β), interleukin 12 (IL-12) and Inducible nitric oxide synthase (iNOs)) biomarkers……54

Figure 3-12 (a) Therapeutic curve of PCBAA hydrogel, alginate SLG20 gel and alginate SLM100 gel devices with 500 IEq rat islets encapsulated. (b) The fraction of cured diabetic mice after being transplanted (glucose level < 200 mg/dl)……55

Figure 3-13 (a) Representative image of MECA-32 antibody staining of Alginate SLM100 hydrogel/tissue interface. Scale bar = 50 µm. (b) Calculated blood vessel

density of PCBAA hydrogel/tissue interface and alginate SLM hydrogel/tissue interface, based on MECA-32 staining results……56

Figure 4-1 Synthetic route and ^{1}H-NMR of the macro-crosslinker……..69

Figure 4-2 ^{1}H-NMR of PCBMA macro-crssolinker with different double bond density (labeled by CBMA/double bond molar ratio)……..70

Figure 4-3 (a) Coating thickness of different methods and (b) SEM image of macro-crosslinker coating……71

Figure 4-4 (a) Time course contact angles for coating surfaces made from different methods and (b) water drop on macro-crosslinker coating on day 8……72

Figure 4-5 (a) Protein binding test on coatings obtained from different methods before and after one week exposure in flowing PBS, and E. coli adhesion test on coatings obtained from (b) bare PU, (c) PCBMA brush coating, (d) PCBMA+MBAA brush coating and (e) PCBMA macro-crosslinker coating with (f) calculated adhesion density……73

Figure 4-6 Mechanism of (a) fragile brush coating and (b) durable macro-crosslinker coating……74

Figure 5-1 (a) structure of DURA-Z tape, (b) DURA-Z tape under pulling, bending wrenching and rolling, and (c) fabrication of DURA-Z coating on PU substrate.....90

Figure 5-2 (a) SEM imaging on the surface and sectioning of uncoated PU, superglue and DURA-Z coated substrates (scale bar = 100 μm), (b) water contact angles on bare PU, superglue and DURA-Z coated substrates, (c) IR spectra of bare PU surface, superglue coated PU surface, DURA-Z coated surface and zwitterionic PCBAA hydrogel surface, and (d) illustration of the formation of DURA-Z coating……90

Figure 5-3 AFM images of bare PU substrate, superglue and DURA-Z coated PU substrates. Scale bar = 50 μm……91

Figure 5-4 Antifouling property of DURA-Z coating after durability tests. (a) 3-month incubation in water and (b) 50 days exposure to PBS shearing at room temperature. Data are presented as mean of replicates (n=3) ± standard deviation……..91

Figure 5-5 Antifouling property of DURA-Z coating after various durability and mechanical damage tests. (a) 30 days exposure to PBS shearing under body temperature, (b) 30 days exposure to perpendicular water flush, (c) 20 cycles of abrasion test under 570 kPa, and (d) random scratch by a scalpel. The antifouling property was evaluated by the resistance of human fibrinogen binding on the surface

(absorbed protein) before and after the coating being challenged……92

Figure 5-6 representative SEM images of bacteria adhesion on bare PU, superglue and DURA-Z coated PU substrates after 30 days of co-culture with E. coli bacteria at (a) shaking condition and (b) static condition. Attached bacterial density was calculated for (c) shaking condition and (d) static condition……92

Figure 5-7 representative SEM images showing bacteria adhesion on DURA-Z coating after 30 days of culture with bacteria at static condition without any rinsing……93

Figure 5-8 (a) DURA-Z coating on wood, stainless steel, and glass substrates. (b) Easy removal and re-application of DURA-Z coating on stainless steel substrate, and (c) corresponding antifouling property……93

Figure 5-9 Antifouling property of DURA-Z coating on wood, stainless steel and glass substrates after two-month incubation in water. All data are presented as mean of replicates (n=3) ± standard deviation……94

Figure 5-10 (a) representative SEM images of bacteria adhesion on wood, stainless steel, glass and DURA-Z coating on these substrates after 30 days of co-culture with bacteria at shaking condition, and (b) calculated bacterial density on wood, stainless steel, glass and DURA-Z coatings on these substrates……..95

Figure 5-11 (a) PCBAA polymer powder and (b) PCBAA water solution were glued on PU substrates. The coated surface showed hydrophobic nature after incubation in water, as indicated by the non-spread water droplet……95

CHAPTER 1. INTRODUCTION

Zwitterionic polymers possess a positively charged group and a negatively charged group in each repeating unit[1]. The specific poly-salt-like structure rendered zwitterionic polymer a super-hydrophilic nature[2-3]. These years, intense studies have been focused on the unique properties and potential applications of zwitterionic polymers in biomedical fields such as drug delivery[4-5], implantable devices[6-7], and tissue engineering[8-9].

Common zwitterionic materials include poly-phosphobetaine (PPC), poly-sulfobetaine (PSB), and poly-carboxybetaine (PCB). PSB materials such as poly(sulfobetaine methacrylate) (PSBMA) have been wildly studied as medical device coating[10] and marine coating applications[11]. PSB materials are generally easy to synthesize with low expense. However, the sulfonic acid groups on PSB polymer have shown to exhibit toxicity for cells in biomedical applications[12]. Different from PSB materials, the PPC materials are considered to be biomimetic since it had a phosphorylcholine head group in each repeating unit, which is found abundant in the cell membrane[13]. Nevertheless, the synthesis procedure of phosphobetaine monomers, such as 2-methacryloyloxyethyl phosphorylcholine (MPC), is complex with associated high expense[14].

The PCB has been studied intensively for structural and chemical properties[15]. Compared with PPC and PSB, PCB retains their advantages and shows further unique properties that cannot be achieved by other types of zwitterion materials. Surface plasma resonance (SPR) sensor study exhibited that gold substrate coated with PCB

polymer was able to achieve super-low fouling of protein binding (<0.3 ng/cm2) in complex physiological environments[16-17]. In addition, the PCB materials can be regarded as biomimetic since the carboxy-betaine chemical group is very similar to the glycine betaine, which is one of the solutes in human body fluid that is crucial for regulating the osmotic pressure of cells and the estimated daily glycine betaine intake of an adult from 0.1 to 2.5 g[18]. PCB materials have not been found to be toxic in both in-vitro and in vivo animal studies[19]. Furthermore, the carboxyl group of PCB can be used to immobilize functional biomolecules or fluorescent dye molecules via simple 1-ethyl-3-(3-dimethyl-aminopropyl)-carbodiimide and N-hydroxy-succinimide (EDC-NHS) chemistry to extend the functionality of the material[20]. Lastly, the synthesis of the PCB monomer such as carboxybetaine methacrylate (CBMA) and carboxybetaine acrylamide (CBAA) is typically a one-step reaction with cheap reagents involved[21].

When using zwitterionic polymers to modify materials for a variety of applications, a common challenge exists that most zwitterionic monomers and polymers are highly polar and not able to be dissolved in organic solvents. When the materials to be modified are hydrophobic, which is frequently the case, it is hard to find an appropriate solvent to co-dissolve the zwitterionic monomer/polymer and the hydrophobic materials to conducting the modifying reaction[22]. PCB is unique that it has a precursor form, CB-tBu (tertbutyl ester of CB monomer), that could be dissolved in many organic solvents such as DMF and acetonitrile, and after the modification reaction, PCB can be re-generated by hydrolyzing the tBu ester groups.

This strategy greatly broadens the applications of PCB materials in many application scenarios[4].

Based on the unique super-hydrophilic property, the zwitterionic polymer materials had been studied for their potentials in various applications. Surfaces coated with zwitterionic polymers were found to effectively reduce more than 95% of the adhesion of the protein and microorganism in physiological environments such as blood plasma[17] and seawaters[11]. Meanwhile, nanoparticles such as PLGA nanoparticles and liposome modified by zwitterionic PCBMA polymers were found to show unprecedented colloidal stability and increased circulation time in blood[23]. Zwitterionic polymers stabilized nanoparticles have shown great improvement in diagnostic and therapeutic performance compared with nanoparticles stabilized by the commonly used polyethyleneglycol (PEG), the golden standard for nanoparticle modification[24].

In addition to anti-biofouling and nanoparticle stabilizing properties, recent research revealed many great properties of PCB materials for biomedical applications. It was found that a pure PCBMA hydrogel implant was able to resist foreign body reaction, which was rarely reported in other common biomaterials such as polyethylene glycol (PEG), alginate and Poly-hydroxyethyl-methacrylate (PHEMA)[6, 25]. Meanwhile, other research reported that a non-fouling PCBMA hydrogel surface enabled stem cells to retain their stem cell phenotype and multipotency, independent of differentiation-promoting media, cytoskeletal-manipulation agents, and the stiffness of the hydrogel matrix. The differentiation of stem cells can be

controlled by altering the fouling moieties on the PCBMA gel surface[8].

The focus of this thesis is to study the potentials of the zwitterionic PCB materials in solving several key challenges in various applications as stabilizing materials for nanoparticles, hydrogels, and surface coatings, respectively. Specifically, this thesis involves the work of a one-step synthesis of zwitterionic polymer modified carbon nanoparticles, pancreatic islets encapsulation by PCB hydrogel materials and subsequent transplantation to achieve long-term diabetic reversal effect, and a durable zwitterionic PCB polymer coating for various substrates to resist long-term biofilm formation. These subjects are introduced separately in the following paragraphs.

1.1 Zwitterionic polymers for nanoparticles surface modification

Anti-fouling polymer materials, especially zwitterionic materials, had been utilized to modify nanoparticles to improve their colloidal stability, the key to maintain the unique properties of nanoparticles[5, 26-28]. Super-hydrophilic zwitterionic polymer chains attract a dense layer of water molecules to separate nanoparticles from aggregation[29]. Nevertheless, nanoparticle modification with zwitterionic materials is not straightforward. Since most zwitterionic materials were unable to be dissolved in organic solvent, conjugation of zwitterionic polymers to hydrophobic nanoparticle surface was usually hard and involved complex procedures[4] (usually involved 5-6 steps). Easy modification of nanoparticles by super-hydrophilic polymers remained a grand challenge in this field. In this work, for the first time, we directly made ultra-stable nanoparticles from zwitterionic polymers by the facile one-step

microwave method. The resulting nanoparticle showed superior colloid stability in bio-relevant media and even at the freeze-drying conditions. This work will be discussed in Chapter 2.

1.2 Zwitterionic hydrogel for islet encapsulation

Polymer hydrogel materials had long been studied as a promising solution for Type 1 Diabetes (T1D) by delivering insulin independence without immunosuppressant[30-33]. Polymer hydrogel layer was able to provide protection for transplanted from the attack of the host's immune system and are believed to control blood glucose in a long term[34-35]. The major challenge is that current encapsulation materials can well protect the islets inside, but they became the target of the host's immune system instead[36]. A process called foreign body reaction can virtually happen on all existing implanted polymer hydrogel[37], which would suffocate islets by cutting off the oxygen transport from blood and also hinders glucose/insulin transport for the implant to achieve therapeutic function[38]. It remained a challenge for hydrogel materials to sustain long-term blood accessibility[39]. Our research demonstrated that a zwitterionic material based hydrogel system was able to perfectly integrate with host tissues and remains instantly accessible by circulating blood even after long-term implantation at least for five months. It was further demonstrated that with such perfect body integration, blood nutrients can be easily transported to the hydrogel implant to support the survival and maintain the blood glucose control ability of islet cells. The hydrogel/ rat islet constructs have been s.c. implanted to non-immunosuppressed STZ-mice, and the preliminary result shows insulin

independence of the diabetic mice for at least two months. These works will be described in Chapter 3.

1.3 Durable zwitterionic coating for long-term biofilm resistance

Zwitterionic polymer coatings had been demonstrated to effectively resist microorganism adhesion[40-44]. The super-hydrophilic anti-fouling polymers prevent the attachment of single bacteria cell onto the coating and therefore prevent the formation of biofilm[45]. PCB materials were proved to be efficient in resisting 95% Pseudomonas aeruginosa and Staphylococcus epidermis bacteria adhesion and reducing the formation of biofilm[46]. However, unlike hydrophobic polymer coatings, super-hydrophilic zwitterionic polymer coatings drastically tend to dissolve into water environment[47]. This leads to gradual exposure of the coated surface over time and hinders the use of zwitterionic coating in applications that require long-term durability[48]. Therefore, improving the durability and toughness of zwitterionic polymer coating could lead to the success of long-term biofilm resistance. We developed several methods to improve the toughness and durability of zwitterionic coatings and achieved long-term bacteria biofilm (gram-negative, gram-positive and fungi) resistance on various substrates for up to one month challenge in the bacteria culture media. These works will be discussed in Chapter 4 and 5.

CHAPTER 2. ONE-STEP SYNTHESIS OF ZWITTERIONIC POLYMERS STABILIZED CARBON NANOPARTICLES

2.1 Introduction

Zwitterionic polymers had been utilized to modify hydrophobic core to render nanoparticle with colloid stability, especially in bio-related environment. However, these methods were either involving complex chemical synthesis or low in efficiency due to unpredicted NP surface environment. In this Chapter, we designed novel strategy to make ultra-stable core-shell nanoparticles directly from zwitterionic polymer through one step reaction, completely different from any existing methods. Resulting nanoparticles were stable in bio-related environment and even harsh freeze-drying condition. This work provides a completely new concept to achieve making stable nanoparticles through green chemistry and was expected to inspire future functional NPs to be developed.

Colloid stability is crucial for nanoparticles (NPs) to remain nano-effects in various functioning media. NPs with hydrophobic core suffered from aggregation problem seriously, especially in bio-related media, which hindered their applications in drug delivery and imaging[49-52]. Typically, anti-fouling polymers, capable of resisting nonspecific protein adsorption, were utilized to modify a NP core to prevent it from aggregation[53]. This modification has been done through various methods, e.g., via surface adsorption[54-55], chemical conjugation[4] (e.g., the commonly used “graft-to” method to modify the surface with anti-fouling materials such as PEG[56-57]), and particle encapsulation in polymeric micelles[58-61], to produce hydrophobic core-anti-fouling polymer shell NPs. These methods however either involved complex

chemical synthesis procedures[62-63] or were low in efficiency due to unpredicted NP surface environment[64]. As an alternative method to these complex modification procedures, we explore the feasibility to make the NPs directly from anti-fouling polymers with superior colloid stability. To the best of our knowledge, a hydrophobic NP stabilized by anti-fouling polymers made purely from the polymer itself has not been reported.

Inspired by the facile one-step microwave method to fabricate carbon nanoparticles[65-66], for the first time, we directly made ultra-stable NPs from zwitterionic polymers with part of the polymer chain carbonized into the hydrophobic core and the rest of the intact polymer as the hydrophilic stabilizing shell. Zwitterionic polymers were chosen, since they have demonstrated their excellent anti-fouling properties in resisting non-specific binding from proteins, cells and microorganisms[67]. NPs previously modified with zwitterionic polymers showed good colloid stability and long-circulation time in blood[23]. The synthesized carbon-core polymer-shell structure was confirmed using NMR and TEM. The directly made NPs were found to be ultra-stable in bio-relevant media and even the harsh freeze-drying conditions (with no cyro-protectant in presence), note that most existing NPs could not survive from such extreme lyophilizing conditions.

2.2 Materials and Methods

2.2.1 Materials

Methacryloyloxyethyl phosphorylcholine (MPC 97%), 2-Methacryloyloxy-ethyl -dimethyl 3-sulfopropyl ammonium hydroxide (SBMA 97%), Tert-Butyl bromoacetate

(98%), 2-(Dimethylamino) ethyl mathacrylate (DMA 98%), Amberlite IRN78 hydroxide form, Quinine hemisulfate salt monohydrate (98%), Acetone (99.5%), Phosphate buttered Saline tablet (PBS), Albumin from bovine serum (BSA 98%) and Fibrinogen from bovine plasma (65-85%) were purchased from Sigma-Aldrich, St. Louis, MO. Ethyl Ether Anhydrous (99.9%) and Boric Anhydride were obtained from Fisher Chemical. Co. Acetonitrile anhydrous (99.9%) was purchased from ACROS Organics. B-Propiolactone (95%) was supplied by Wako Pure Chemical Industries Ltd. Deuterium Oxide (D2O 99.9%) was obtained from Cambridge Isotope Laboratories, Inc. USA. PD-10 desalt columns were purchased from GE Healthcare, UK. Boric Anhydride was utilized to dry acetone and all other chemicals were used without further purification.

2.2.2 Synthesis of PSB NPs, PMPC NPs, PCB-2 NPs

5 mg photo-initiator was added to 5 ml degassed DI water and 100 mg SBMA, MPC, CBMA-2 (synthesis as previous report) monomer was dissolved 0.5 ml photo-initiator solution. Polymerization was initiated by exposing the solution under UV (365 nm, 6 W) for 2 minutes with stirring. Then resulted polymer solution was diluted to 2.5 ml and went through salt filter column (cutoff molecular weight 2000) to remove residue monomer and initiator. Pure polymer (Mw 10k) solution was poured into a flask and the flask was set in the center of a domestic microwave oven. After heating under 1200 W for 5 minutes, light brown substance emerged in the bottom of the flask. 10 ml DI water was added and stirred for 1 h. Resulting solution was centrifuged at 4400 rpm for 10 min to remove the insoluble, yielding a clear light

brown NPs solution with florescence under UV. The general yeild was 56.65%.

2.2.3 Synthesis of PCB-1 NPs

CBMA t-butyl monomer was synthesized as previous report[4]. 200 mg of CBMA tbul monomer was hydrolyzed in 2 ml TFA for 5h. TFA solution was dropped in anhydrous ethyl ether to remove TFA and precipitate CBMA-1 zwitterionic monomer. After vacuum dried, monomer was dissolved in 0.5 ml photo-initiator solution described above in ice bath. Basic resin was used to adjust solution pH to 7 and the yielding solution was exposed under UV to initiate polymerization. The resulting PCB-1 was similarly purified and made into NPs as described in the last section.

2.2.4 NPs purification

2 g sucrose,was dissolved in 10 ml DI water to prepare sucrose stock solution. 1.4 ml sucrose solution was added to a centrifuge tube and 0.1 ml NPs raw solution was slowly added to obtain a well-defined NP region on the top of sucrose solution. Centrifuge the tube for 1 h at 15000 rpm at room temperature and expose the tube to UV. NP region in the sucrose column showed blue florescence and was collected using a pipette. The collected solution will go through a PD-10 column to remove contaminated sucrose.

2.2.5 Nanoparticle Characterization:

The morphology and microstructure of the PMPC NPs and PCB-1 NPs were examined by transmission electron microscopy (TEM) on JEOL 2010 TEM with LaB6 Filament Gun (JEOL Ltd. Tokyo, Japan) under accelerating voltage of 200 kV. Purified sample solutions were dropped onto a 300-mesh copper grid coated with a lacy

carbon film to make TEM sample. Nuclear Magnetic Resonance H^1 spectrum of zwitterionic polymer and purified NPs were conducted on Varian Mercury-400 MHz NMR. Polymer and purified NPs were lyophilized and dissolved in Deuterium Oxide (D_2O). Molecular weight of the MPC and CB-1 polymer are determined by a Waters Alliance 2695 Separations Module equipped with a Waters Ultrahydrogel Linear column and a Waters 2414 reflex detector. The mobile phase was PBS buffer solution at a flow rate of 0.7 ml/min at 35 °C. Poly(ethylene oxide) from Polymer Laboratories were used as standards. UV absorption of NPs was conducted on a Multiskan GO UV–Vis Spectrophotometer (Thermo Scientific, USA).

2.2.6 Fluorescence Property measurement

The maximum absorptions were 354 nm for PMPC NPs and 367 nm for PCB-1 NPs. Maximum emissions are 436 nm for PMPC NPs and 455 nm for PCB-1 NPs. Quantum yield of the PMPC NPs and PCB-1 NPs were determined by comparative method. Quinine hemisulfate in 0.1 M H2SO4 was utilized as the standard whose QY was reported to be 54%. The integrated fluorescence intensity is the area under the PL curve in the wavelength range from 380 to 650 nm with 365 nm excitation. Absolute values were calculated according to the following equation:

$$QY_{CDs} = QY_{ST} * \frac{Grad_{CDs}}{Grad_{ST}} * \frac{\eta^2_{CDs}}{\eta^2_{ST}}$$

Where ST denotes the standard, Grad is the gradient from the plot of integrated fluorescence intensity vs absorbance, and η is the refractive index of the solvent. To prevent the re-absorption effect, absorbance in the 10 mm fluorescence cuvette should never exceed 0.1 at the excitation wavelength. The resulted QY for PMPC NPs

and PCB-1 NPs were 8.92 ± 0.60 % and 7.02 ± 0.59 %, respectively.

2.2.7 MTT cytotoxicity assays

The cytotoxicity of the PMPC NPs and PCB-1 NPs was determined by MTT assay. NIH/3T3 Fibroblast were grown in 96-well plates in full Dulbecco's Modified Eagle's Medium and 10% FBS under 5% CO_2 at 37 °C to allow 80-90% confluence. For each well, cells were washed with PBS and incubated with 200 µl full medium containing varied concentration of PMPC NPs, PCB-1 NPs and CA NPs for 24 h. Cells were washed with PBS to remove NPs and incubated with 100 µl full medium plus 50 µl of 12 mM MTT stock solution for another 4 h. Then, MTT containing medium was replaced with 150 µl DMSO to dissolve the formed crystal at 37 °C for 10 min. Absorbance (Abs) was measured at 570 nm with pure DMSO as the blank reading. Cells with no NPs incubation were used as the controls and cell viability upon NPs treatment was estimated in triplicate: cell viability (%) = Abssample / Abscontrol x 100.

2.3 Result and discussion

The synthetic route to core-shell zwitterionic NPs composed of one single step, microwave heating of zwitterionic polymers **(Figure 2-1).** Typically, Zwitterionic polymers were synthesized through UV initiated polymerization of respective monomers. Then, a beaker containing 100 mg of zwitterionic polymer (Mw 8-10 KDa) in 5 ml DI water was placed at the centre of the rotation plate of a 1000 W microwave oven and heated for 5 minutes. As water evaporated, light brown substance was obtained in the bottom of the beaker. This microwave method is

simple, facile and green, however, there are several obstacles to overcome before obtaining the targeted core-shell zwitterionic NPs.

The primary challenge is that microwave oven heating can't be easily controlled and resulting polymer NPs are contaminated with unreacted polymers and have broad size distribution (PDI > 0.6 as measured by dynamic light scattering, DLS). Conventional purification methods such as centrifugation, filtration, or dialysis can't effectively remove the contaminating polymers or obtain homogeneously sized NPs. We found a sucrose gradient centrifugation method can be effective to purify the rough products[68]. NPs migrate under the centrifugation force with their migration pattern retained by sucrose while linear free polymers barely moved and stayed on top of the sucrose column. This was confirmed by control experiment where free polymer solution alone was loaded on top of the sucrose column and DLS results showed no polymer presented in the NPs layer. By exposing the centrifuge tube to UV light, polymer protected NPs can be visualized and retrieved (fluorescent property will be discussed below). Further removal of sucrose was achieved by using a PD-10 column and highly purified polymer protected NPs (free from unreacted polymers with narrow size distribution, diameter < 30 nm, PDI < 0.15) can be obtained.

The next challenge we met is that zwitterionic polymer chosen should stand high temperature of the microwave heating reaction. While part of the polymer carbonized into the NP core, the other part of the polymer should be thermally intact maintaining the anti-fouling zwitterionic structure. Our initial testing with

poly(sulfobetaine) (PSB)[69] and poly(carboxybetaine)-2 (PCB-2) **(Table 2-1)**, two common zwitterionic polymers we previously worked on, was not successful; the obtained NPs were positively charged as indicated by zeta-potential measurement in water. This could be explained by the thermo-instability of SB and CB-2 units; when heated at high temperature, the quaternary amine group tends to undergo "elimination reaction" splitting into a tertiary amine and an acrylic group[70]. The resulting NPs thus showed positive net charges due to the protonated tertiary amines formed on the protecting polymer shell. By contrast, poly -(2-methacry-loyloxyethyl phosphorylcholine) (PMPC)[71-74] and poly -(carboxybetaine)-1 (PCB-1)[75] polymers were found to render resulting NPs with zwitterionic property, as characterized by a slightly negative zeta potential of the resulting NPs. It should be noted that their parent zwitterionic polymers gave similar negative zeta potentials in the control experiment **(Table 2-1)**. Among four kinds of polymer derived NPs, only PMPC and PCB-1 NPs were chosen for further study due to their zwitterionic shell nature.

It was hypothesized that the zwitterionic polymer was partially burnt into the carbon core while the remaining part forming a super-hydrophilic shell. The structure of the purified zwitterionic NPs was further examined using transmission electron microscopy (TEM) and nuclear Magnetic resonance H^1 (NMR). Organic molecules are known for their carbonization under microwave heating conditions[76-77]. Carbon core structure for PCB-1 NPs and PMPC NPs could be detected under the TEM **(Figure 2-2)**. Average core diameters for PMPC NPs and PCB-1 NPs were 12 nm and 11 nm,

respectively. NMR results **(Figure 2-3)** showed a perfect match between the peaks of polymer shell of NPs and the parent free polymers, indicating that the protecting polymer structure remained intact on the NP surface.

For potential biological applications, NPs have to be stable in complex environment where bio-elements (e.g., proteins) were present. It is expected that the synthesized zwitterionic NPs are well protected from aggregation by the zwitterionic shell in the bio-related media. As non-zwitterionic polymer NP controls, we synthesized CA NPs, from citric acid and ethylenediamine through the same microwave method (a well-established fluorescent NP system with ultra-high quantum yield[78]), and purified it via the same sucrose centrifugation procedure. The resulting CA NPs had slightly negative zeta potential (-1.78 mV), similar to zwitterionic polymer stabilized NPs, but were lack of a zwitterionic polymer shell surface. For colloid stability testing, purified PMPC NPs, PCB-1 NPs and CA CNPs (size < 30 nm PDI < 0.18) were placed in PBS (phosphate buffered saline, salt concentration 153 mM), PBS solution of 5 wt% bovine serum albumin (BSA) and PBS solution of 5 wt% fibrinogen from bovine plasma. The sizes for NPs were measured as a function of time **(Figure 2-4(a) and Figure 2-5)**. No obvious size increase appeared in any of the zwitterionic polymer NPs groups while CA NPs aggregated drastically. It is a general trend that particles tend to be less stable in high salt concentration solution[79]. Zwitterionic PCB-1 NPs, however, retained its original size in a solution with salt concentration as high as 500 mM in a 40-min study (i.e.). CA NPs by contrast doubled its size overnight even in DI water with zero ionic strength.

Long-term stability study **(Figure 2-4(b))** showed that both PMPC NPs and PCB-1 NPs, after one week incubation in PBS, have no significant size increase while CA NPs continuously aggregated.

Lyophilization, a necessary procedure for NP storage and precise weighing, introduces harsh interaction among individual NPs, causing aggregation that could not be segregated even under sonication. To the best of our knowledge, NPs even protected by anti-fouling polymers are very rare to survive from lyophilization induced aggregation. We used lyophilization conditions to further push the limit of stability performance of the zwitterionic core-shell particles. PMPC NPs, PCB-1 NPs, and CA NPs were lyophilized without adding any cryoprotectant and re-dissolved in DI water and their sizes were measured using DLS **(Figure 2-6)**. CA NPs aggregated substantially after freeze-drying while zwitterionic NPs survived such harsh condition by maintaining the particle size. We have previously observed that PCB-1 protected PLGA NPs can sustain the original size through lyophilization, while other NP protecting technology (such as PEG-PLGA) can't but require the addition of cyro-protectant (e,g., 10% sucrose)[80]. It was believed that zwitterionic polymers strongly bind water molecules to prevent hydrophobic interactions among carbon cores in this case, and keep them apart even in a highly dehydrated environment[22]. With excellent stability, both in bio-relevant media and harsh freeze drying conditions, we demonstrated the effectiveness of our strategy to render NPs ultra-stabile properties.

To verify that our way towards stable NPs do not cause cytotoxicity, MTT assay was

conducted **(Figure 2-7(a))**. NIH/3T3 cells remained more than 85% and 80% viability in PMPC NPs and PCB-1 NPs, respectively, at concentration as high as 10 mg/ml, while CA NPs were toxic to cells (30% viability) at concentration as of 5 mg/ml. It is worth-mentioned that the synthesized NPs had fluorescent property **(Figure 2-7(b))**. Under UV excitation, Both the PCB-1 NPs and PMPC NPs exhibited blue light. It was hypothesized that the fluorescent property was related to the core-shell structure, which was previously reported as surface-passivation mechanism[81]. The fluorescent property can lead to potential imaging applications of the resulting zwitterionic NPs[82-83].

In summary, we have demonstrated a novel strategy to make core-shell NPs with superior stability directly and solely from anti-fouling zwitterionic polymers through single step of microwave heating. Only those zwitterionic polymers, that are stable through high temperature microwave heating can produce zwitterionic polymer shell-carbon core NPs, which can be further purified through sucrose gradient centrifugation. It was found that zwitterionic NPs maintained excellent colloid stability in various bio-relevant media, and even under the harshest lyophilization condition. With undetectable cytotoxicity, the new strategy will lead to ultra-stable NPs for drug delivery and imaging application. We expect this green chemistry in making ultra-stable NPs can inspire future functional NPs to be developed.

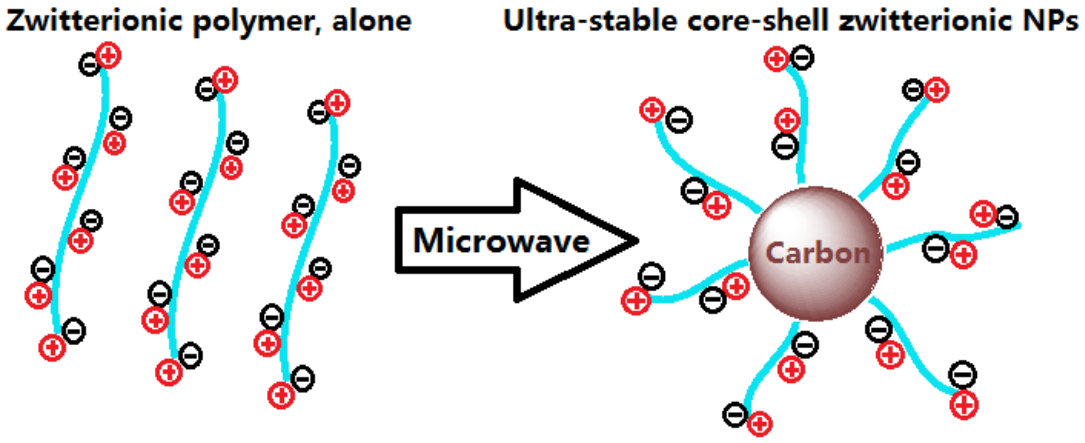

Figure 2-1 Illustration of making carbonized core- zwitterionic polymer shell NPs directly from zwitterionic polymers

Table 2-1 Structures for zwitterionic polymers involved and zeta-potentials for these free polymers and the resulting NPs

	Zwitterionic Polymer Structures	Zeta-potential (mV) Polymer (Parent)	Zeta-potential (mV) NP (Synthesized)
PSB	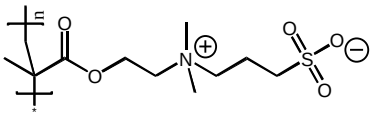	**-3.25±0.56**	**23.05±1.26 (cationic)**
PCB-2	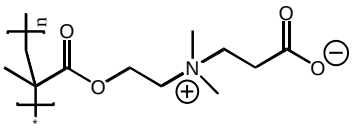	**-4.77±0.32**	**18.73±2.06 (cationic)**
PMPC	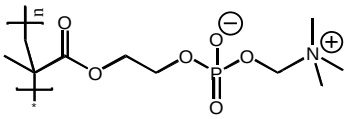	**-2.73±0.13**	**-4.33±0.80 (Zwitterionic)**
PCB-1	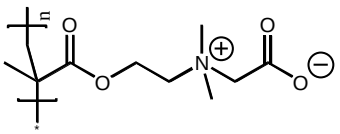	**-3.22±0.45**	**-4.75±0.78 (Zwitterionic)**

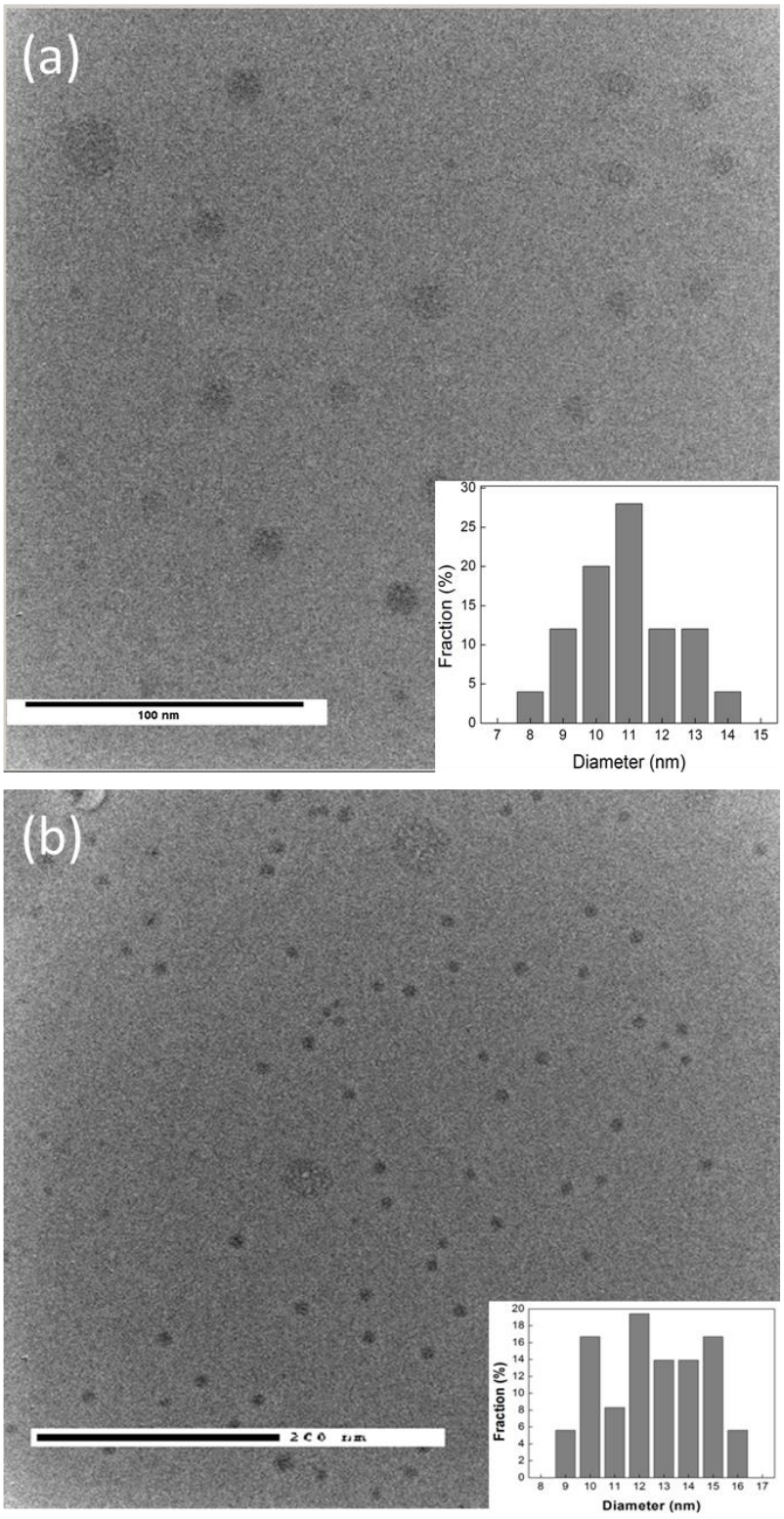

Figure 2-2 (a) TEM image and statistic size distribution of PCB-1 NPs (scale bar: 100 nm) (b) TEM image and statistic size distribution of PMPC NPs (scale bar: 200 nm)

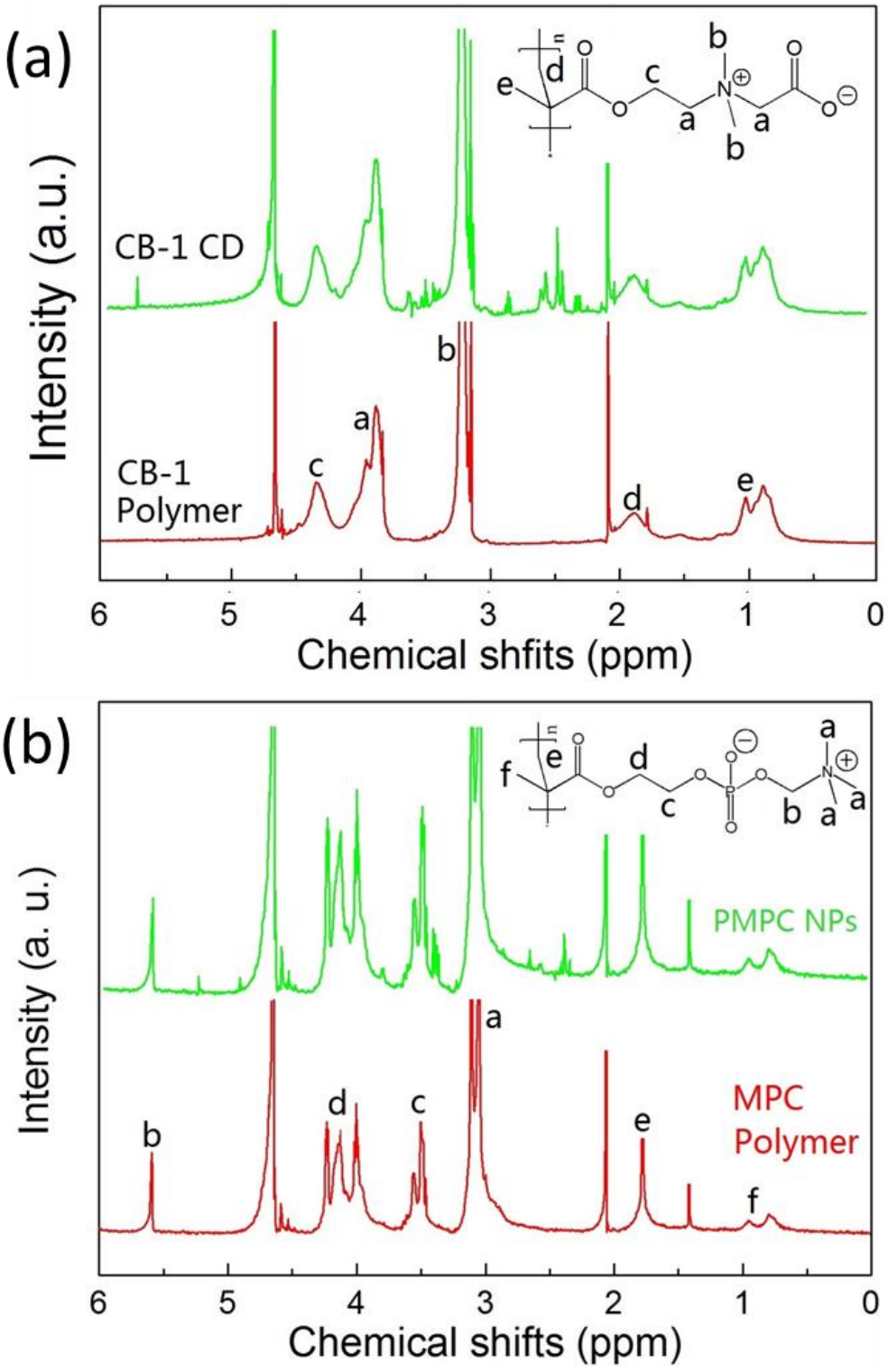

Figure 2-3 (a) NMR spectra of parent CB-1 polymer and synthesized PCB-1 NPs, (b) NMR spectra of parent MPC polymer and synthesized PMPC NPs

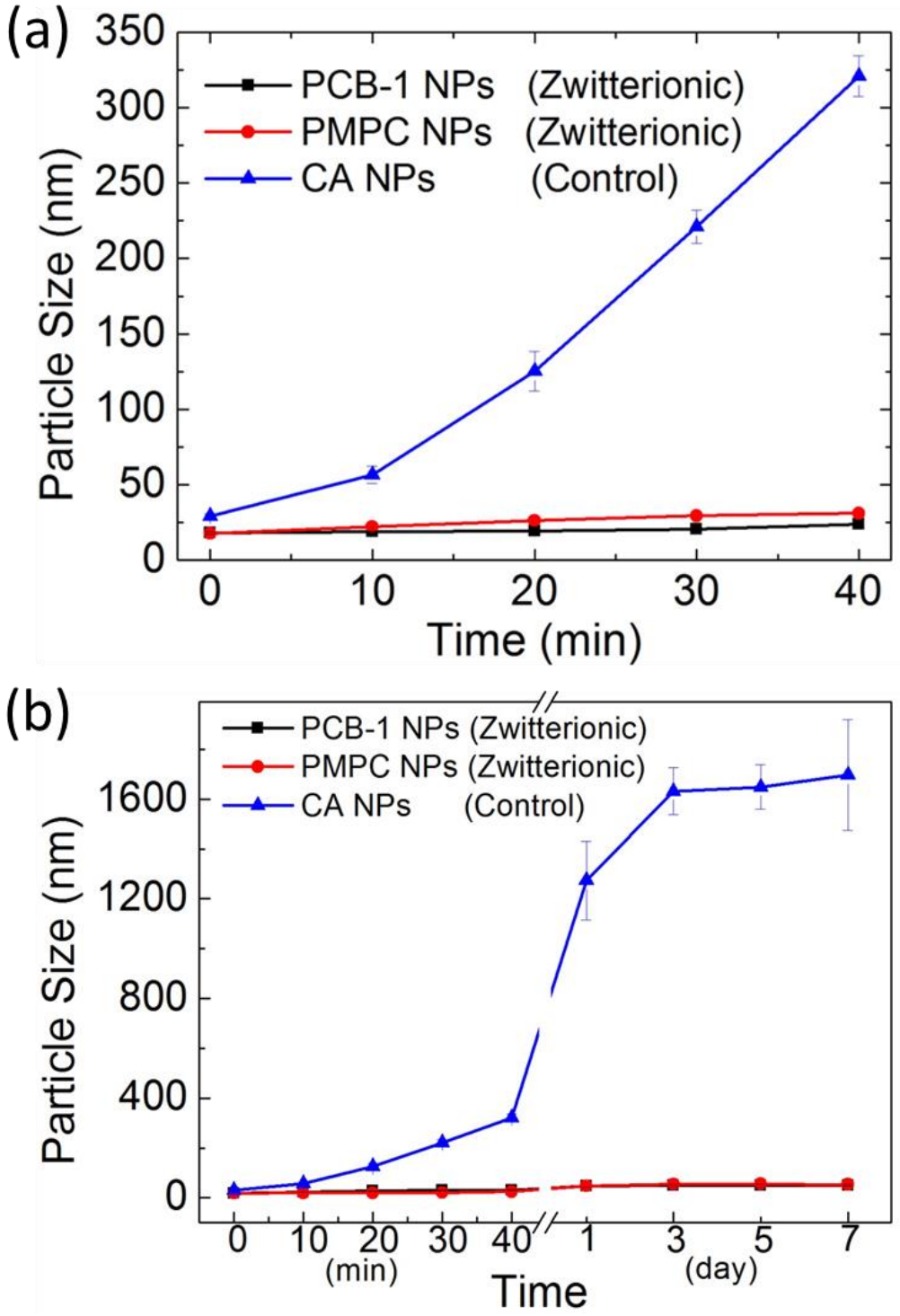

Figure 2-4 (a) short-term and (b) long-term colloid stability of PCB-1, PMPC, and CA NPs in PBS buffer

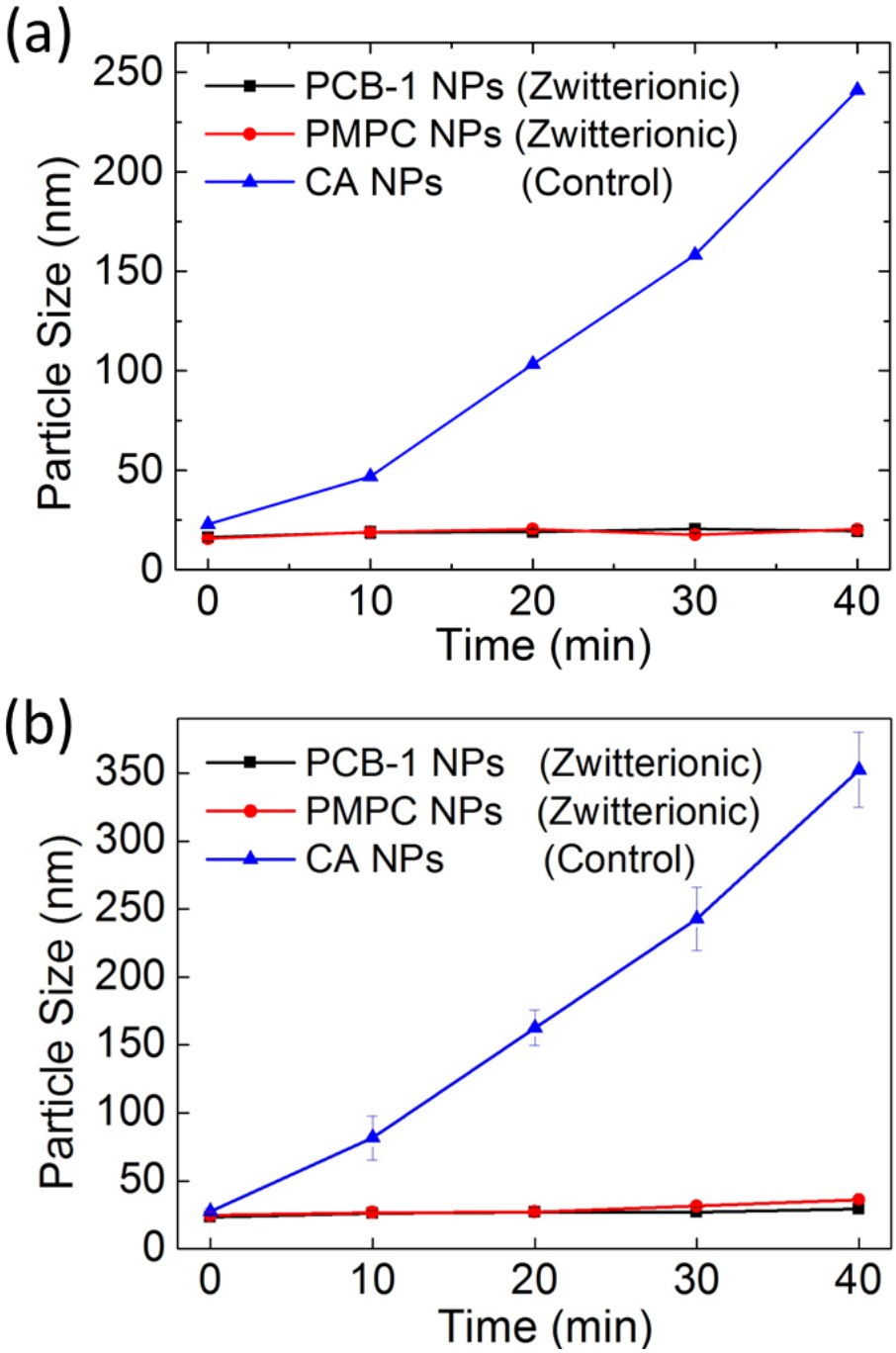

Figure 2-5 Colloid stability (a) in BSA/PBS and (b) in fibrinogen/PBS buffer

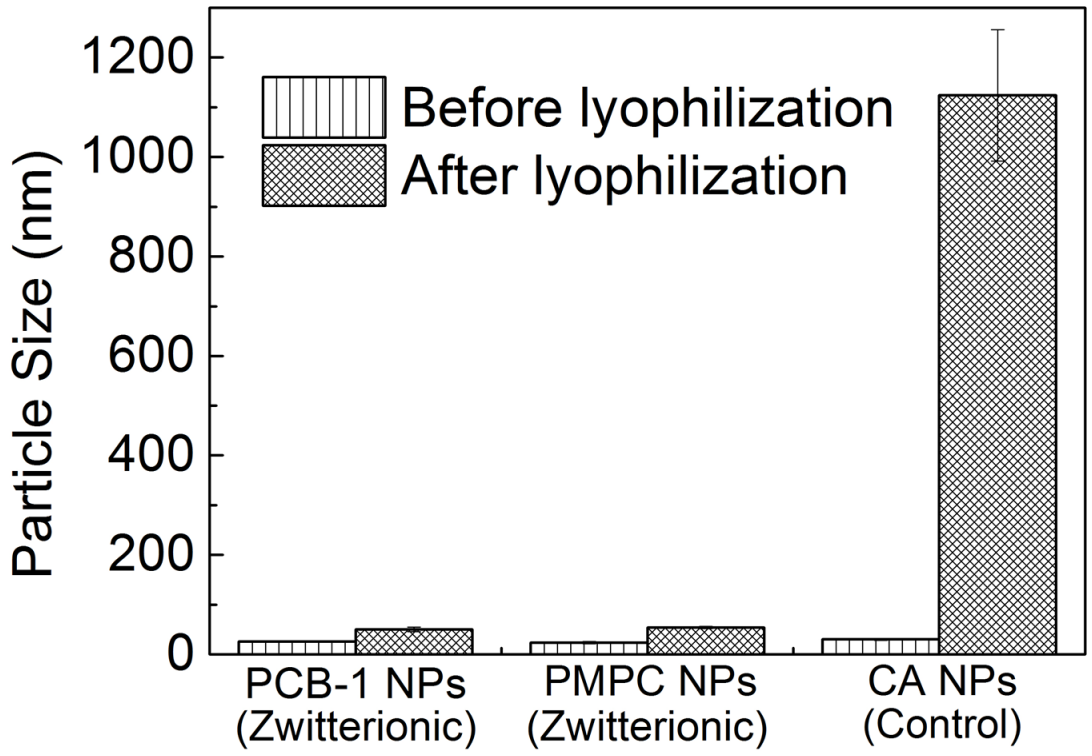

Figure 2-6 Colloid stability in freeze-drying condition of PCB-1 NPs, PMPC NPs and CA NPs

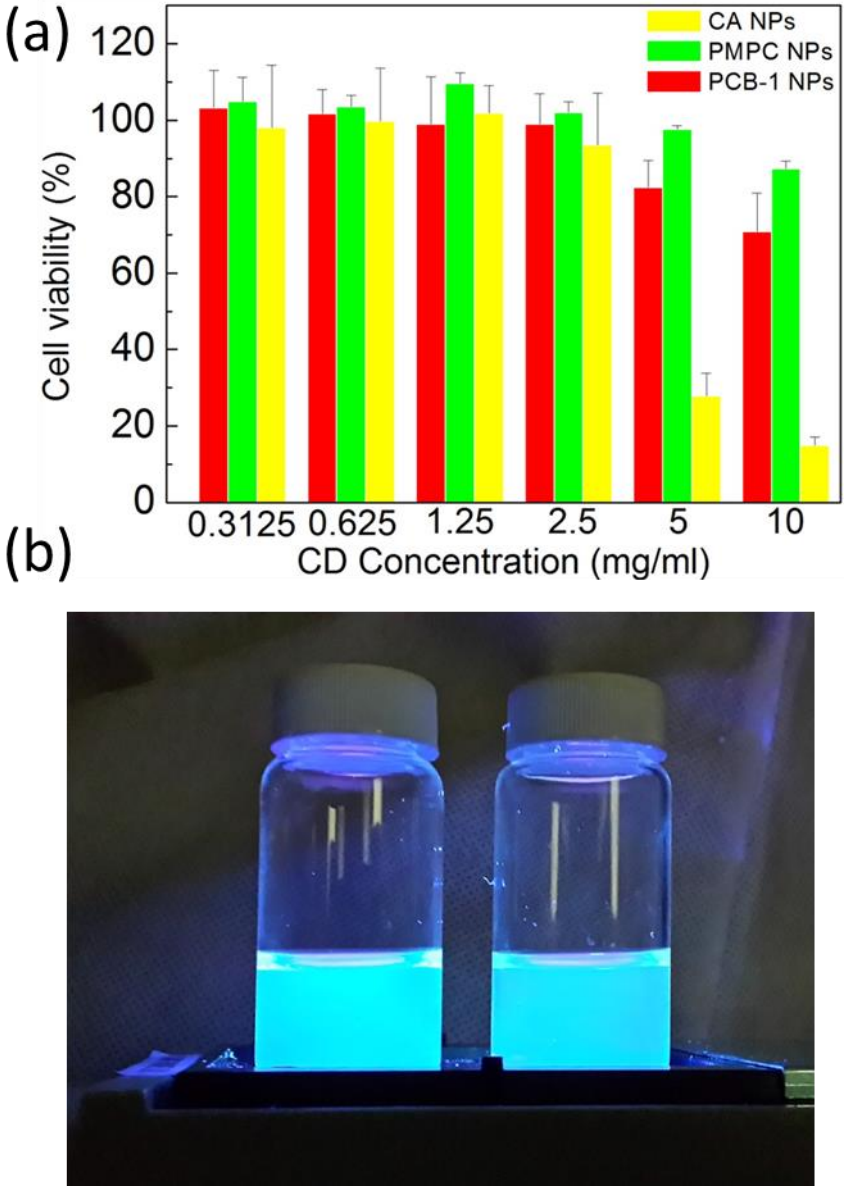

Figure 2-7 (a) MTT results of CB-1, MPC and CA NPs. (b) Fluorescent property of zwitterionic NPs under UV (365 nm) excitation (Lift: PMPC NPs, Right: PCB-1 NPs)

CHAPTER 3. ZWITTERIONIC HYDROGEL IMPLANT PROMOTES FUNCTIONAL BLOOD VESSELS GROWTH AS GOOG AS NATURAL BODY SYSTEM

3.1 Introduction

In this chapter, we will describe the zwitterionic polymer hydrogel as the first synthetic material ever known promoting functional neovascularization as good as natural body system. A zwitterionic carboxy betaine containing hydrogel was found to promote vascularization at the subcutaneous (s.c.) site to the same density level as normal tissue, and to maintain that high-level vasculature for at least 6 months. The newly formed blood vessels were perfused and they approached the implanted zwitterionic gel surface as close as below 20 micrometers away. Consequently, the zwitterionic hydrogel was highly accessible by circulating blood, even after 5 months of implantation. This finding was highlighted by using zwitterionic hydrogel in encapsulating islet of Langerhans for the treatment of Type 1 diabetes. The zwitterionic hydrogel based novel system remarkably outperforms the state-of-the-art technology using alginate encapsulating materials at highly challenging s.c. site.

Implantable devices based on biopolymers are wildly utilized in biomedical fields such as cell encapsulation[84-85], monitoring sensor coating[86-87], controlled drug release[88] and tissue engineering[89]. Most of these applications require adequate body fluid exchange, in which blood was the most crucial to enable the exchange of gasses, nutrients, and metabolites between the blood and device, to sustain the survival of tissue/cell grafts and achieve monitoring or therapeutic effect[90-93]. Blood accessibility, therefore, is the key factor in determining successful implantation wherein a

comparable density of blood vessel with normal tissue is considered to be ideal[94-95]. Nevertheless, most of the biomaterial implants could not escape from foreign body reaction and blood accessibility was cut off soon after transplantation[96-97].

A number of researches had been done to increase blood vessel formation for implanted materials. It was found that materials with microarchitecture were able to promote neovascularization in surrounding area[98], particularly at pore sizes of 30-40 μm[99], but the resulting vessel density is still far below regular tissue level. Delivery of growth factors (e.g., vascular endothelial growth factor and fibroblast growth factors[100-103]), angiogenic genes[104], and stem cells[105-106] facilitates neovascularization and has been studied for combinational delivery with cells in transplantation. However, the blood vessels promoting effect was not able to be maintained when the growth factors or gene were used out[107]. The high cost and potential safety issue also hindered these methods from further advancement in applications.

Here, we developed hybrid hydrogel material containing zwitterionic carboxy betaine (CB) moieties to solve the blood accessibility challenge. A zwitterionic hydrogel material, after subcutaneous (s.c.) implantation, supports the growth of new blood vessels to the same density level as naturally healed wound and healthy tissue, and maintains such high-density vasculature for a long-term (up to 6 months, the longest time point tested). The newly formed blood vessels were functionally perfused, and the nearest vessels are within 20 μm distance from the implant surface. Therefore, the zwitterionic hydrogel implants are highly blood accessible, as indicated by the efficient accumulation of dye molecules on the hydrogel device,

even after 5 months of implantation. This is the first synthetic material ever known promoting functional neovascularization as good as natural body system. To highlight the implication of this finding, the zwitterionic hydrogel was utilized to encapsulate rat islets of Langerhans and s.c. implanted in diabetic mice. We observed that islets encapsulated by state-of-the-art alginate materials (both high guluronate and high mannuronate) failed to control blood glucose starting at day ~10 at the challenging s.c. implantation site, while zwitterionic hydrogel/islet remarkably reversed diabetes through the entire 80 days of implantation. We expect, with natural tissue-like blood accessibility, the zwitterionic hydrogel is a promising platform to improve the long-term performance of most current implantable devices.

3.2 Materials and methods

3.2.1 Materials

CBAA monomers were synthesized as previous reports[108]. PEGDA 10K was purchased from Laysah Bio, Inc. (Lot# 136-18). HEMA monomers were obtained from ACROS ORGANICS (New Jersey, USA). Sterile and low endotoxin alginate SLG20 and alginate SLM100 were purchased from FMC Biopolymer. Evans Blue dye and Fluorescein isothiocyanate-dextran (FITC-dextran) were obtained from Sigma-Aldrich. (St. Louis, USA).

3.2.2 Synthesis of hydrogel materials

The PCBAA and PHEMA hydrogel were fabricated by UV initiation of monomer solution of 50% in a weight ratio in the presence of 0.2% UV initiator

2-Hydroxy-4'-(2-hydroxyethoxy)-2-methylpropiophenone (I-2959) and 1% crosslinker (MBAA). Polyethylene (glycol) diacrylate (PEGDA) hydrogel was synthesized as reported previously that PEGDA solution (10% in weight ratio) was crosslinked under UV in the presence of 0.2% UV initiator (I-2959). Alginate SLG20 and alginate SLM100 hydrogel were formed by mixing the alginate solution (1.4% in 0.9% NaCl) with 20 mM $BaCl_2$ solution. All hydrogel samples were equilibrated in sterile phosphate-buffered saline (PBS) for at least five days with frequent change of PBS to remove all unreacted small molecule. Before implantation, all samples were shaped into discs form (D=5 mm) with 1 mm in thickness either using a punch or lancet. The endotoxin level of implant hydrogels was evaluated using a Limulus Amebocyte Lysate (LAL) endotoxin assay kit (Cambrex Bioscience) with a detection limit of 0.06 endotoxin units (EU)/ml.

3.2.3 Implantation of hydrogel materials

All animal experiments followed federal guidelines and were approved by the IACUC at Wayne State University. C57BL/6 mice (male, 20-30g, from Jackson's Lab) were anesthetized using isoflurane and received meloxicam analgesia. The surgical site (dorsal skin) was shaved and prepped with three alternating scrubs of betadine and alcohol. On prepped animal, a single incision (1.5-2 cm) was made through the dorsal skin. Bilateral subcutaneous pockets are created by blunt dissection through the incision for placement of one material sample per pocket. After implantation, the incisions were closed using wound clips which were removed within two weeks.

Hydrogel implants were kept in mice for a maximum of 6 months before further testing.

3.2.4 Histology study: Blood vessel staining and density calculation

At pre-determined time points, mice with implants were euthanized by CO_2 asphyxiation. The hydrogel samples together with the surrounding tissue were excised by cutting around the area with scissors and scalpels. The explanted samples were then fixed in zinc fixative for 2 days and embedded in paraffin wax. 5 μm sections were cut and mounted onto slides for histological staining. Blood vessels were stained brown using rat anti-mouse MECA-32 antibody kit from BD Biosciences (dilution 1:20; catalog no. 550563), which is an endothelial cell biomarker. Blood vessel density was calculated by counting the average blood vessel number in 0.2 um^2 area with 6 random repeats.

3.2.5 Immunofluorescence staining of macrophage phenotypes

Triple-label immunofluorescence staining was employed to examine phenotypes of macrophages near to the implant/tissue interface, following the previous protocol[6]. Macrophage cells were identified by F4/80 antigen. Phenotype markers include iNOS, IL-1β, TNF-α, and IL-12 (pro-inflammatory markers), and MMR, Arg1, IL-10, and TGFβ1 (anti-inflammatory markers). The tissue slides were incubated with three primary antibodies (rat anti-mouse F4/80 antibody, one pro-inflammatory antibody (rabbit or goat anti-mouse), and one anti-inflammatory antibody (goat or rabbit anti-mouse)), followed by incubation with three secondary antibodies labeled with three different fluorescence tags. Primary antibodies include: rat anti-mouse

F4/80 antibody (BM8) (dilution 1:50; catalog no. 14-4801-82, eBiosciences), rabbit anti-mouse iNOS antibody (dilution 1:50; catalog no. ab15323, Abcam), goat anti-mouse IL-1β antibody (M-20) antibody (dilution 1:50; catalog no. sc-1251, Santa Cruz Biotechnology), rabbit anti-mouse TNF-α antibody (dilution 1:25; catalog no. ab9739, Abcam), goat anti-mouse IL-12 antibody (dilution 1:50; catalog no. NB600-1443, Novus Biologicals), goat anti-mouse MMR antibody (dilution 1:50; catalog no. AF2535, R&D Systems), rabbit anti-mouse Arg1 antibody (H-52) (dilution 1:50; catalog no. sc-20150, Santa Cruz Biotechnology), goat anti-mouse IL-10 antibody (M-18) (dilution 1:50; catalog no. sc-1783, Santa Cruz Biotechnology), rabbit anti-mouse TGFβ1 antibody (V) (dilution 1:50; catalog no. sc-146, Santa Cruz Biotechnology). Secondary antibodies include: donkey anti-rat IgG (dilution 1:200; catalog no. A-21209, Invitrogen), donkey anti-rabbit IgG (dilution 1:200; catalog no. A-21206, Invitrogen), and donkey anti-goat IgG (dilution 1:200; catalog no. A-21081, Invitrogen). For isotype control, rat IgG (dilution 1:80; catalog no. sc-2026, Santa Cruz Biotechnology), goat IgG (dilution 1:80; catalog no. sc-2028, Santa Cruz Biotechnology), and rabbit IgG (dilution 1:80; catalog no. sc-2027, Santa Cruz Biotechnology) were used as primary antibodies. For negative control, no primary antibodies were used.

3.2.6 FITC-dextran injection and histology study

At pre-determined time points, mice with implants were anesthetized using isoflurane. 200 µl FITC-dextran/PBS solution (2 mg per 20 g mouse) was injected through the tail vein. 5 min after injection, mice were euthanized by CO_2

asphyxiation. The hydrogel samples together with the surrounding tissue were collected and then fixed in zinc fixative for 2 days and embedded in paraffin wax. 5 µm sections were cut and mounted onto slides, which was directly visualized under a fluorescent microscope with an excitation wavelength of 488 nm.

3.2.7 Evans Blue injection for accumulation study

At pre-determined time points, mice with implants were anesthetized using isoflurane. 15 mg Evans Blue in PBS buffer was administrated by i.v. injection for a mice with 25 g body weight. 5 min after injection, mice were euthanized by CO_2 asphyxiation. The hydrogel samples were explanted excluding the surrounding tissue and immediately exposed to UV (365 nm) for imaging.

3.2.8 Islet isolation

Rat islets were isolated using a method established by Lacy and Kostianovsky[109] as well as others[110-113] and modified by our lab. Briefly, Sprague-Dawley rats (male, 275-300g, from Charles River Lab) were euthanized by CO_2 and their bile ducts were cannulated with an injection of Collagenase P solution. The distended pancreases were removed and further digested by Collagenase P at 37 ^oC. Digested pancreases were quenched with cold PBS, washed, filtered using a 450 µm sieve, and subjected to Histopaque 1077/PBS gradient purification. Islet layer was taken and further purified by hand-picking islets. Resulting islets were counted and cultured in RPMI 1640 media with 10% fetal bovine serum and 1% penicillin/streptomycin at 37 °C in humidified air containing 5% CO_2.

3.2.9 Islet encapsulation and transplantation

To encapsulate a large number of islets by PCBAA hydrogel for therapeutic purpose, the isolated rat islets will be first encapsulated by 1.4% Alginate SLG20 after mixing the islet/alginate preparation with 20 mM $BaCl_2$ solution, and then be shaped into disks of 3 mm in diameter and 1 mm in thickness. The islet containing small disks will be placed between two glass slides separated by Teflon spacers (2 mm in thickness), suspended in a pre-gel solution (containing zwitterionic CBAA monomer, MBAA crosslinker, and photoinitiator I2959 in PBS), and chemically crosslinked at 365 nm UV. The resulting hydrogel sheets will be removed and equilibrated in cell culture medium, and tailored into macro disks using a 5-mm biopsy punch for transplantation (islets encapsulated within the 5 mm PCBAA disk). SLG20/islet and SLM100/islet controls were obtained by mixing the islet/alginate preparation (1.4% alginate concentration) with 20 mM $BaCl_2$ solution, and then be shaped into disks of 5 mm in diameter and 2 mm in thickness.

C57BL/6 mice (male, 20-30g) received a daily i.p. injection of 5 mg/ml streptozocin (STZ) at 50 mg/kg for 5 consecutive days. STZ-mice were placed on a non-fasted regular diet. 17 days after the first injection, weight and blood glucose were measured to confirm diabetic status. Only mice whose non-fasted blood glucose levels were above 300 mg/dL for two consecutive days were considered diabetic and underwent transplantation. PCBAA/islet, SLG20/islet, and SLM100/islet disks were s.c. implanted in diabetic mice at day 0 following the implantation procedure described above. After implantation, the animals' blood was sampled three times a week before the endpoint. Blood drop was collected from the tail using a lancet and

tested using a commercial glucometer (Clarity One, Clarity Diagnostic Test Group). Typically, the mice blood glucose was observed to drop one or two days after the implantation. Mice with a non-fasted blood glucose below 200 mg/dL were considered normoglycemic. Transplanted mice maintaining normoglycemia (i.e., received PCBAA/islet) and those returning to hyperglycemic state (i.e., received SLG20/islet and SLM100/islet) were subject to explantation. Explanted islets were stained by Live and Dead staining kit (Life technology) to visualize the survival of islets.

3.2.10 Glucose-stimulated insulin secretion (GSIS) assay

Explanted hydrogels with islets encapsulated were pre-incubated for 1 h in FBS-free RPMI 1640 containing 2.8 mmol glucose in a 6-well plate at 37°C incubator in 5% CO_2. In the following 3 hours, RPMI 1640 medium with 2.8 mmol glucose, 28 mmol glucose, and 2.8 mmol glucose was added consecutively, 1 h respectively. After each incubation, the media was collected and stored at -20 °C for future insulin concentration determination. The rat insulin concentration in the culture media was evaluated using Mercodia ultrasensitive rat insulin kit (Uppsala, Sweden) with three repeats for every group.

3.2.11 Statistical Analysis

n = 6 was used for mice per time point or per treatment group unless specified otherwise. The sample size was selected according to previous reports. All tested mice were included in analyses except for ones with unforeseen sickness or morbidity. Animal cohorts where randomly selected and investigators were not blind

to performed experiments. Representative images illustrated are based on n = 3 mice per treatment group unless specified otherwise. Most data were normally distributed and similar variance was determined for groups that are compared. Analysis includes unpaired two-tailed t-test and one-way analysis of variance (ANOVA) with Bonferroni multiple-comparison correction. For data not following normal distribution, non-parametric Mann-Whitney test was used. *: $P < 0.01$, **: $P < 0.001$, ***: $P < 0.0001$ and n.s: no significant difference. For all statistical analyses, significance was accepted at the 95% confidence level.

3.3 Results

3.3.1 Implanted zwitterionic hydrogel healed like a natural wound, and promoted vascularization to the same density level as normal tissue.

The zwitterionic hydrogel was made from zwitterionic carboxybetaine acrylamide (CBAA) monomer (synthesized as previously documented[108]) and a widely used N,N-methylenebis(acrylamide) (MBAA) crosslinker through ultraviolet (UV) induced crosslinking (structure in **Figure 3-1(a)**). The resulting hydrogel was equilibrated in phosphate buffered saline (PBS) and punched into disks of 5 mm in diameter and 1 mm in thickness. Zwitterionic hydrogel disks along with other hydrogel controls of the same dimension were then subcutaneously (s.c.) implanted on normal healthy mice. One month after implantation, hydrogel samples with surrounding tissue were collected for histology study. An incised subcutaneous wound healed for one month (no hydrogel implanted) and a normal healthy subcutaneous tissue were also collected for comparison. By staining the tissue slides with an antibody binding to

MECA-32 on endothelial cells, blood vessels can be visualized (shown by brown color) and their density can be calculated.

The major finding was that the zwitterionic hydrogel implant promoted blood vessel formation which was similar to healthy tissues in vessel density. It was clearly showed that new blood vessels formed near to the zwitterionic PCBAA hydrogel surface (**Figure 3-1(b)**) with a vessel density comparable to physiologically healed and healthy tissues (no significant difference at $p > 0.58$; **Figure 3-1(c)**). On the contrary, the Alginate SLG20 hydrogel, PEGDA 10K hydrogel and PHEMA hydrogel (made from 2-hydroxyethyl methacrylate (HEMA)) had much fewer neovascularization in the surrounding area; this is significantly different from PCBAA hydrogel ($p < 0.0001$). It was worth mentioning that these control materials (alginate, PEG, and PHEMA) have been intensively studied for implantation purposes, such as for tissue engineering[114-115], device coating[116-117], and cell therapies[118-126]. It was further observed that such high level of blood vessel density induced by the zwitterionic hydrogel can last at least 6 month in the transplantation study (no significant change over time at $p > 0.31$; **Figure 3-1(d)**; representative histological images shown in **Figure 3-2**).

We did not observe a sign for uncontrolled blood vessel formation in the surrounding area of the zwitterionic hydrogel, indicating that the hydrogel was not like a tumor that induces uncontrolled neovascularization. A melanoma tumor was developed by s.c. injection of $1x10^5$ murine B16F10 cells s.c. to the back on health mice on the left flank. Two weeks later, tumor tissue was explanted for similar

histological analysis using anti-MECA-32 blood vessel staining. It was found that the tumor blood vessels showed structurally disordered, abnormal morphology (in agreement with the literature[127]) and their density was estimated to be at least three times of that of normal tissue and the tissue interfaced with PCBAA hydrogel (**Figure 3-3**).

3.3.2 The newly formed blood vessels were perfused, and approached the implanted zwitterionic hydrogel surface as close as below 20 μm away.

Based on the finding that the implanted zwitterionic PCBAA hydrogel induced vascularization to a density level comparable to that of a naturally healed wound and normal tissue level, it is essential to know whether these newly formed blood vessels are functional and perfused with circulating blood. To address this question, we injected FITC-dextran solution through the tail vein to healthy mice previously received the s.c. implant of different hydrogel materials for one month. 300 seconds following the injection, implanted hydrogel samples with surrounding tissue were collected for tissue sectioning **(Figure 3-4(a))**. Using a fluorescent microscope, it was discovered that the newly formed vessels were highly perfused with function, which was proved by the green dye in the lumen of the vessels in the surrounding of PCBAA hydrogel. For alginate and PEGDA hydrogel surface tissue, however, no significant amount of green-labeled blood vessel can be observed **(Figure 3-4(b))**. The density of neovascularization could also be calculated based on the green-labeled tissue slides **(Figure 3-5)**, and was found to be comparable to MECA-32 staining results **(Figure 3-1(c))**.

It is particularly worth noting that the newly formed blood vessels approached the zwitterionic hydrogel surface as close as possible. We created a penetrating hole (1 mm in diameter) in the center of the hydrogel disk, or an inter-space between two identical disks **(Figure 3-4(d))**, and s.c. implanted them for one month. Mice then received a tail-vein injection of FITC-dextran, and 5 min later hydrogels together with surrounding tissues were histologically analyzed. It was obvious that new blood vessels grew into the holes and narrow space between zwitterionic hydrogel surfaces after one-month implantation **(Figure 3-4(c))**, and also maintained their presence after two-month implantation **(Figure 3-6)**. We further measured how close these new functional vessels were to the zwitterionic surface in the cases of hydrogel disks, holes, and interspaces, and found that the nearest blood vessels were typically within a perpendicular distance of 20 μm from the gel surface **(Figure 3-4(e))**. Considering a typical animal cell size of 10-20 μm in diameter, the zwitterionic implant surface is expected to be highly accessible by the blood with only one or a few cell layers in between.

3.3.3 Implanted zwitterionic hydrogel was highly accessible by circulating blood for up to five months.

The function or tissue and organ were supported by the blood that transports oxygen, nutrient and metabolic waste[128]. It will be ideal that an implantable device can achieve a similar level of blood accessibility as regular tissue to sustain efficient transport and communication between the device and its environment. Based on the finding that abundant of perfused blood vessels were grown and approached the

zwitterionic gel surface down to 20 μm range, we expect the hydrogel can be easily accessible by circulated blood components. This was evaluated by quantifying the freshly injected dye molecules that circulated through blood and accumulated to the implanted hydrogels. Healthy mice received s.c. implantation of hydrogel samples for up to 5 months, and was then injected with Evans Blue through tail vein. Evans blue was a nontoxic dye that was widely applied as a contrasting agent to improve resolution of small veins[129]. 5 min after injection, mice were sacrificed and hydrogel samples were immediately explanted, visualized under UV **(Figure 3-7(a))**, and quantified for dye accumulation **(Figure 3-7(b))**. It was found that all tested hydrogel samples implanted for 1 day were not able to effectively recruit the dye due to the destruction of nearby blood vessels during the implantation surgery. For zwitterionic PCBAA disk, the dye accumulation was found to be significant at 2 weeks after implantation **(Figure 3-8)**, and reached its maximum during the 2 to 5 months post-implantation window. By contrast, non-zwitterionic controls, PEGDA 10K and Alginate hydrogels, exhibited negligible fluorescent intensity during the entire study period ($p < 0.0001$). This result indicates that the implanted zwitterionic hydrogel is able to maintain superior blood accessibility for a long term, which has rarely been obtained by known implanted synthetic materials.

3.3.4 zwitterionic hydrogel enabled the survival and function of encapsulated xenograft islets and improved therapeutic outcome at subcutaneous site

To highlight the implications of our findings, we studied whether the unique and desirable feature of implanted zwitterionic hydrogel, i.e., normal-tissue like blood

vessel density and superior blood accessibility, can improve the performance of an implantable device. Particularly we employed zwitterionic hydrogel for islets of Langerhans (islets) encapsulation and subsequent xenograft transplantation. Conventional biomaterials such as alginate and PEG have been widely used to encapsulate/immuno-isolate the islets, but their therapeutic potential was jeopardized since nutrients and oxygen can hardly reach the implanted device to sustain the cell viability[130-131]. When islets are transplanted at s.c. site, their viability is even worse since s.c. site is generally less blood accessible comparing with other locations, such as intraperitoneal (i.p.) site[132]. It has been reported that alginate based materials sustained islet survival at the i.p. site but failed at the s.c. site[133], and the i.p. location was mostly used in evaluating performance of islet encapsulating devices[134-135]. Regarding the challenge above, we expect that islets transplantation outcome at the convenient s.c. site can be significantly improved through zwitterionic hydrogel encapsulation.

Our study involved two phases. At phase one, PCBAA and control hydrogel materials (Alginate SLG20 and PEGDA 10K) were used to encapsulate a few rat islets and the hydrogel/islet constructs were s.c. implanted in healthy mice. Each encapsulating construct included 3-6 islets in order to tract and identify the size, location, and survival condition of each islet after explantation. It was found that islets encapsulated by zwitterionic PCBAA hydrogel were healthy under a microscope after one-month implantation, however, islets in the Alginate and PEGDA hydrogels were either dead or hard to be visualized **(Figure 3-9)**. The explanted hydrogel/islet

constructs were further challenged continuously by three glucose concentration levels (2.8, 16.7, 2.8 mmol; each for 1 h) to evaluate the insulin producing capability of the transplanted islets in a glucose challenge methods (**Figure 3-9**). It was showed that islets encapsulated in PCBAA hydrogel sustained their glucose response capability after 30 days in mice (no significant difference, $p > 0.53$), but control materials failed to render islets normal GSIS function ($p < 0.0001$).

At phase two study, we encapsulated larger amount of rat islets and examined whether zwitterionic hydrogel encapsulation outperformed the conventional alginate SLG20 encapsulation in achieving insulin independence of diabetic mice. We chose 500 islet equivalents (IEq) from rat, and transplanted the devices to s.c. site of streptozotocin (STZ)-induced C57BL/6 diabetic mice. Notably, 500 IEq rat islets encapsulated by Alginate SLG20 have been reported to achieve at least ~20 days insulin independence at i.p. site. Here we found that Alginate SLG20 hydrogel/islet started to fail at ~10 days after s.c. transplantation in lowering blood glucose of diabetic mice (therapeutic level is 200 mg/ml) **(Figure 3-10(a))**. Meanwhile, zwitterionic PCBAA gel/islet was found to sustain the diabetes reversal during the entire 80 days of implantation period **(Figure 3-10(b))**. When PCBAA hydrogel/islet was retrieved on day 83, the blood glucose immediately went back to the pre-treatment level. Live and dead staining (green-fluorescent calcein-AM (live)/ red-fluorescent ethidium homodimer-1 (dead)) indicated that the explanted islets protected by PCBAA gel maintained their healthy condition **(Figure 3-10(a))**. The

supreme capability to sustain islet survival and glucose response was due to the great blood vessel formation and tissue integration of PCBAA hydrogel.

3.3.5 Implanted zwitterionic hydrogel had an unusual anti-inflammatory effect on local surrounding tissues.

Among conventional biomaterials for implantable applications, high mannuronate (M) alginate has been identified to be able to promote blood vessel formation to certain extent, and has been used to encapsulate islets and demonstrated control of fasted diabetic non-human primate blood glucose for half a year[136-137]. However, the application of high-M alginate hydrogel was hindered due to the pro-inflammatory reaction produced by the material, with monocytes that produced high level of IL-1 TNF-α and IL-6 which endangered the long-term survival of the islet[138-139]. Here we evaluated the potential inflammatory response of zwitterionic hydrogel materials together with control materials including high M alginate (Alginate SLM100, low endotoxin, from FMC Biopolymer). One month after s.c. implantation of these material disks in healthy mice, the materials with surrounding tissues were explanted and subjected to immunofluorescence histological study. Macrophages in the vicinity of the implant and their expressed pro-inflammatory (TNF-α, IL-1β, IL-12, iNOs) and anti-inflammatory cytokines (IL-10, TGF-β1, Arg-1, MMR) were triple labeled **(Figure 3-11(a))**. Zwitterionic PCBAA stimulate significantly less inflammatory cytokines, particularly compared with Alginate SLM100, PEGDA 10K, and PHEMA ($p<0.0001$), and drastically more anti-inflammatory factors, i.e., IL-10, compared with all tested control biomaterials ($p<0.0001$) **(Figure 3-11(b))**. With superior blood

accessibility plus the unusual anti-inflammatory capability, zwitterionic PCBAA hydrogel is expected to outperform most current biomaterials, including the highly promising high M alginate, in boosting the outcome of current implantable devices. In our islet encapsulation and s.c. transplantation test, we indeed observed that Alginate SLM100/ islet implant failed to control blood glucose starting at day ~10, while zwitterionic PCBAA/islet continuously reversing diabetes through the entire 80 days of implantation (**Figure 3-12**).

3.4 Discussion

Our body evolved a vasculature systems with high density of blood vessels to enable sufficient exchange of oxygen, nutrition and metabolic waste of every single cell. An implantable device, ideally, requires a similar level of blood accessibility to sustain long-term therapeutic or monitoring function. However, most biomaterials could not evade foreign body attack and were unable to support blood vessel formation, no matter they are polymers, metals, or ceramics[140-143]. Our study for the first time showed that (1) zwitterionic hydrogel material supports the growth of new blood vessels to the same density level as naturally healed wound and healthy tissue, and maintains such natural density of vasculature for a long term. It is particularly noted that there is no sign of uncontrolled angiogenesis near to the zwitterionic hydrogel surface; this, however, is frequently observed with tumor vasculature, and when growth factors were overly delivered at the implantation site[144-145]. We further found that (2) the newly formed vessels were highly perfused with function, which was proved by the green dye in the lumen of the vessels in the surrounding of PCBAA

hydrogel, and were discovered to stay very close to the PCBAA hydrogel surface and grow into the holes or the narrow space between two PCBAA hydrogels. By measuring how close these new functional vessels were to the zwitterionic surface in the cases of hydrogel disks, holes, and interspaces, it was found that the nearest blood vessels were typically within a perpendicular distance of 20 μm from the hydrogel surface. This indicated that the zwitterionic implants could be potentially highly accessible by the blood with one or a few cell layers in between. We further verified that (3) zwitterionic hydrogel implants are highly blood accessible, as indicated by the efficient accumulation of Evans blue dye on the hydrogel device, even after 5 months of implantation. It is worth noting that most of the current studies on blood vasculature around biomaterials focused mostly on blood vessel morphologies. Our work provided insights on the function of the newly formed vasculature and the blood accessibility of the implants. With natural tissue-like vasculature and superior blood accessibility, the zwitterionic hydrogel is expected to be a promising platform to improve long-term implantable device outcome (such as being the coating or surface materials for implantable devices).

Our implantation study was exclusively performed on the subcutaneous (s.c.) site for two reasons. First, this location is ideal for many commonly found implantable devices such as vascular access devices, contraceptive devices, blood glucose sensor, cell delivery devices, cardioverter defibrillator: S.c. site is the most welcomed implantation site for the patience. The surgery could be easily performed in a local clinic without general anesthesia. If there is some malfunction happen to the device,

it will be easily retrieved and replaced to elongate the therapeutic function period. Second, s.c. site is known for poor vascularization, and is known to have less blood accessibility comparing to intraperitoneal (i.p.) or other sites. We showed remarkable neovascularization promotion and blood accessibility at this challenging site with zwitterionic hydrogel implants. This effectively addresses the current challenge preventing s.c. implant from achieving long-term device outcome, and also implies that zwitterionic hydrogel implants can perform as efficiently at other implantation sites.

To highlight the capability of the zwitterionic hydrogel in improving implantable device outcome, we studied zwitterionic hydrogel as a novel material for islet encapsulation and transplantation. Islet Encapsulation by biomaterials is a potential solution to treat Type 1 Diabetes with insulin independence free of immunosuppressant[146-148]. Encapsulated islets will be protected by the polymers hydrogels from the attack of the body immune system and are shown to long term manage blood glucose. Nevertheless, there was few clinically relevant product of islet encapsulation even with over decades of research[149]. The crucial point in the successful islet transplantation is to sustain function and survival of the transplanted islets for a long term. Current biomaterials including hollow fiber, natural polymers such as agarose and alginate, and synthetic PEG have been extensively used as islet encapsulation materials[150-152]. These materials, however, resulted in poor blood accessibility after transplantation, which hindered the survival of islets because the blood/oxygen exchange was cut off. This hinders glucose/insulin transport and

prevents the implant from achieving desired long-term therapeutic function[153-155]. Here we observed that with superior blood accessibility, islets encapsulated by zwitterionic hydrogel achieved greatly improved therapeutic outcomes. In the s.c. site, zwitterionic PCBAA hydrogel/islet was able to correct diabetes during the entire 80 days of implantation period, while both Alginate SLG20 gel/islet and SLM100 gel/islet, two state-of-the-art technology, failed to lower blood glucose starting at less than 10 days **(Figure 3-10, Figure 3-12)**.

It is important to compare the zwitterionic PCBAA with Alginate SLM100 (high mannuronate (M)) and SLG20 (high guluronate (G)), two of the most popular alginate materials currently used for islet encapsulation, from both blood vessel promotion and anti-inflammatory standpoints. We consider inflammatory response in this comparison because most islet encapsulating materials are known for stimulating the production of cytotoxic cytokines upon implantation that penetrated to the encapsulated islets and cause islet death. Alginate SLM100 as s.c. implant with islet encapsulated has demonstrated the management of fasted blood glucose for half a year in diabetic primate studies. Our results show that SLM100 after 1-month s.c. implantation promoted new blood vessel growth to a density of 9.6±1.8 blood vessels per 0.2 mm^2, but is still far below the 22.7±3.4 blood vessels per 0.2 mm^2 for PCBAA that matched the normal tissue level (**Figure 3-13**). In addition, SLM100 (high M) was found to stimulate severe inflammatory response than SLG20[156] (high G) (**Figure 3-11**), and high level of IL-6, IL-1 and TNF-α greatly endangered the long-term survival of transplanted islets. SLG20, by contrast, showed fewer pro-inflammatory

reaction compared with high-M alginates (**Figure 3-11**, well-consistent with the literature), and have been alternatively used for islet encapsulation. But SLG20 is even worse in promoting blood vessel growth (3.3±0.3 blood vessels per 0.2 mm^2, **Figure 3-1(c)**). The advantage of zwitterionic PCBAA is obvious: it shows the strongest neovascularization promotion (as good as natural body system), the least inflammatory cytokine secretion, and the highest anti-inflammatory response. By overcoming both the blood vessel and inflammation challenges, zwitterionic PCBAA encapsulation technology has great potential to outperform the state-of-the-art islet encapsulation strategies in supporting long-term viability and function of transplanted islets.

In summary, we report the first synthetic material ever known, namely zwitterionic hydrogel, promoting functional neovascularization as good as natural body system. This finding has a promising impact on current implantable devices in improving the device outcome. To highlight this implication, zwitterionic hydrogel was used to encapsulate islet cells for T1D treatment, with therapeutic outcome remarkably outperforming the state-of-the-art technologies.

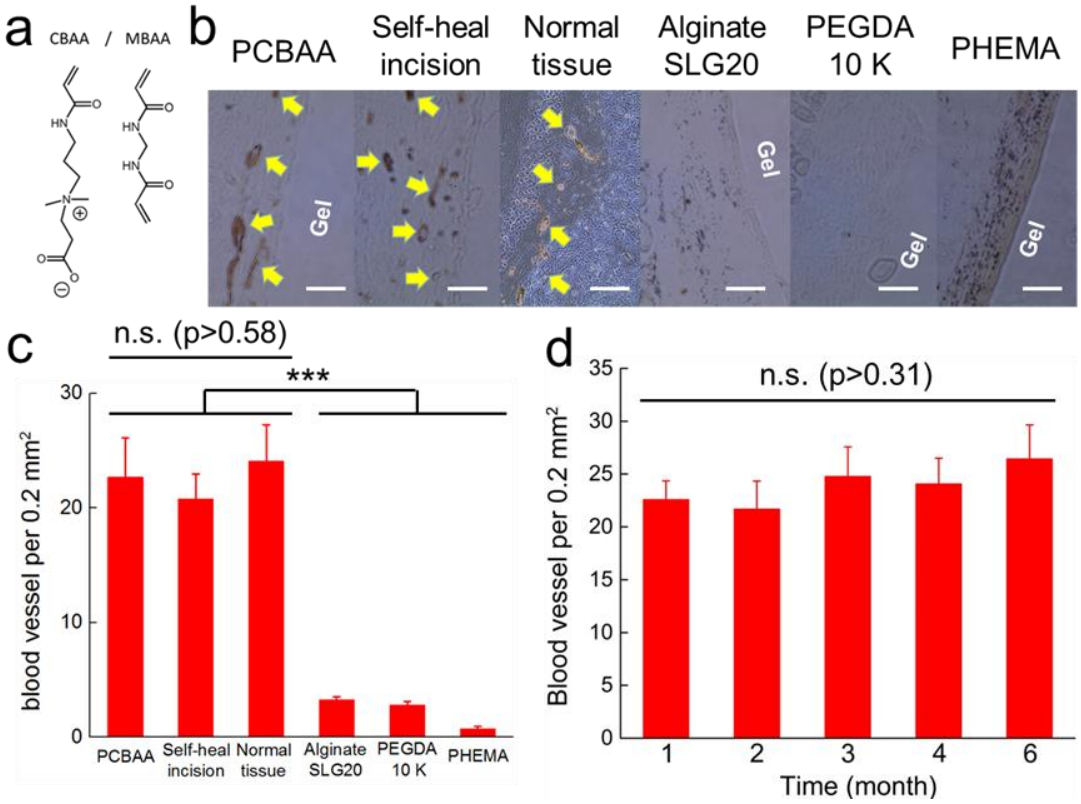

Figure 3-1 (a) Molecular structure of carboxybetaine acrylamide (CBAA) monomer and MBAA crosslinker which that used for making the PCBAA hydrogel. (b) represented histology images on blood vessel formation of hydrogel samples, healthy tissue and self-heal incision after one month transplantation. (c) The calculated density of blood vessels of all samples in (b). (d) Calculated blood vessel density for Long-term PCBAA hydrogel implantation in mice for up to half a year. All data are presented as mean of biological replicates (n=6) ± standard deviation. Statistical analysis: one-way ANOVA with Bonferroni multi-comparison. ***: $p < 0.0001$; n.s.: no significant difference.

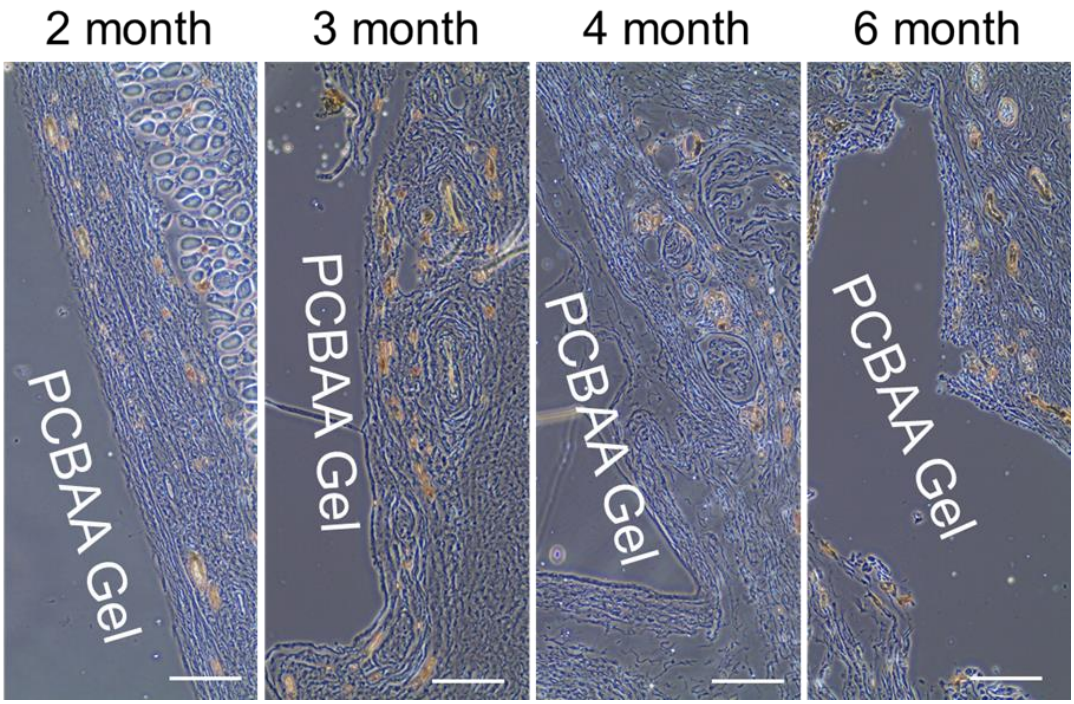

Figure 3-2 Representative images of MECA-32 antibody staining of PCBAA hydrogel/tissue interface after 2, 3, 4, and 6 months of implantation. Scale bar = 50 µm.

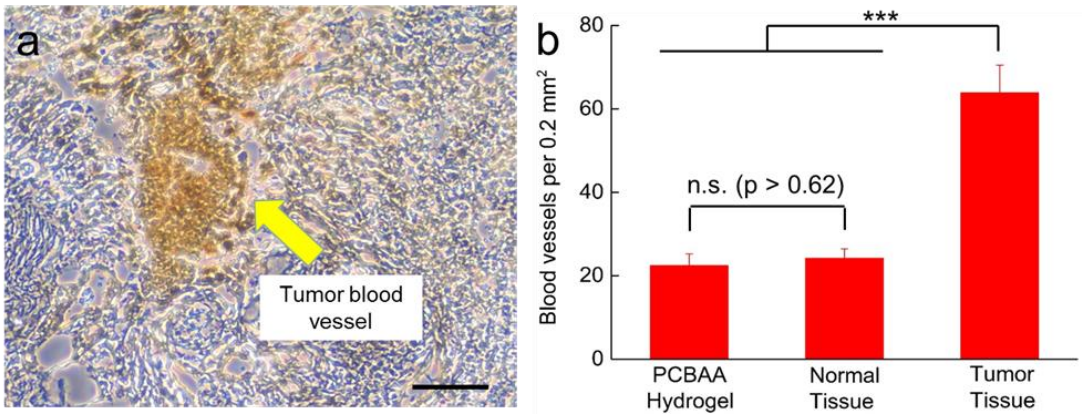

Figure 3-3 (a) A represented image of MECA-32 antibody staining of B16F10 melanoma tumor tissue. Scale bar = 50 µm. (b) Calculated blood vessel density of PCBAA hydrogel/tissue interface, normal tissue and tumor tissue, based on MECA-32 staining results. All data are presented as mean of biological replicates (n=6) ± standard deviation. Statistical analysis: one-way ANOVA with Bonferroni multi-comparison. ***: $p < 0.0001$; n.s.: no significant difference ($p > 0.62$).

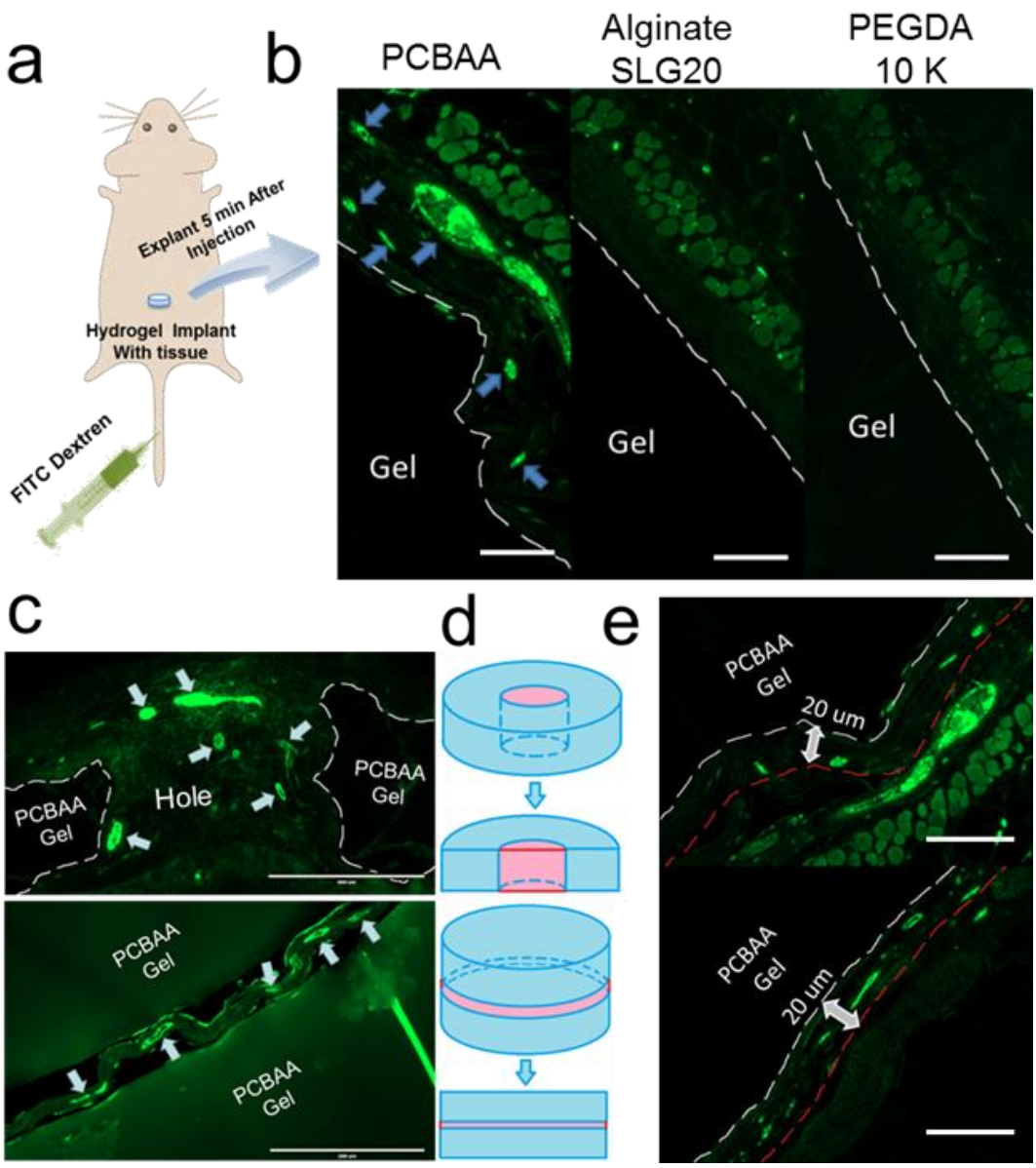

Figure 3-4 (a) Illustration of green dye injection experiment. The mice with implanted samples receive tail vein injection of FITC-dextran in PBS solution. The samples and surrounding tissue were retrieved for imaging. (b) Represented images of FITC-dextran stained blood vessels for all hydrogel samples under fluorescence microscope. Scale bar = 50 µm. (c) images showing blood vessels grown into the hole in the center of a hydrogel disk and narrow space between two hydrogel disks. Scale bar = 400 µm. (d) Schematic representation of the two approaches in (c). (e) Blood vessels near to PCBAA hydrogel implants were perfused with green FITC-dextran. Gel/tissue interface was labeled by white dash lines. 20 µm away from the interface was depicted by red dash lines. Scale bar = 50 µm.

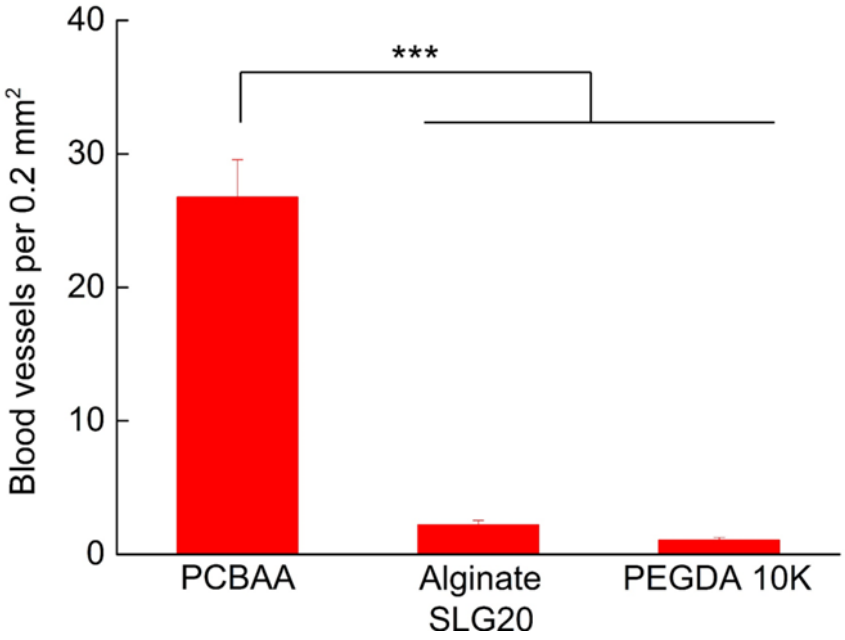

Figure 3-5 Blood vessel density for PCBAA, Alginate SLG20 and PEGDA 10K hydrogel/tissue interface, calculated from FITC-Dextran injection experiment. Data were presented as mean of biological replicates (n=3) ± standard deviation. Statistical analysis: one-way ANOVA with Bonferroni multi-comparison. ***: $p < 0.0001$

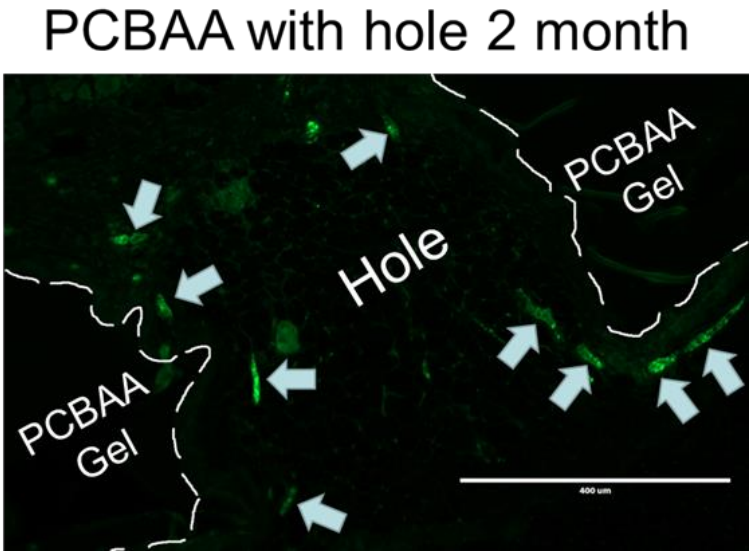

Figure 3-6 Fluorescent image on tissues interfaced with PCBAA hydrogel disk containing a premade hole. The hydrogel disk was implanted for 2 months followed by FITC-Dextran perfusion on blood vessels. Scale bar = 400 µm

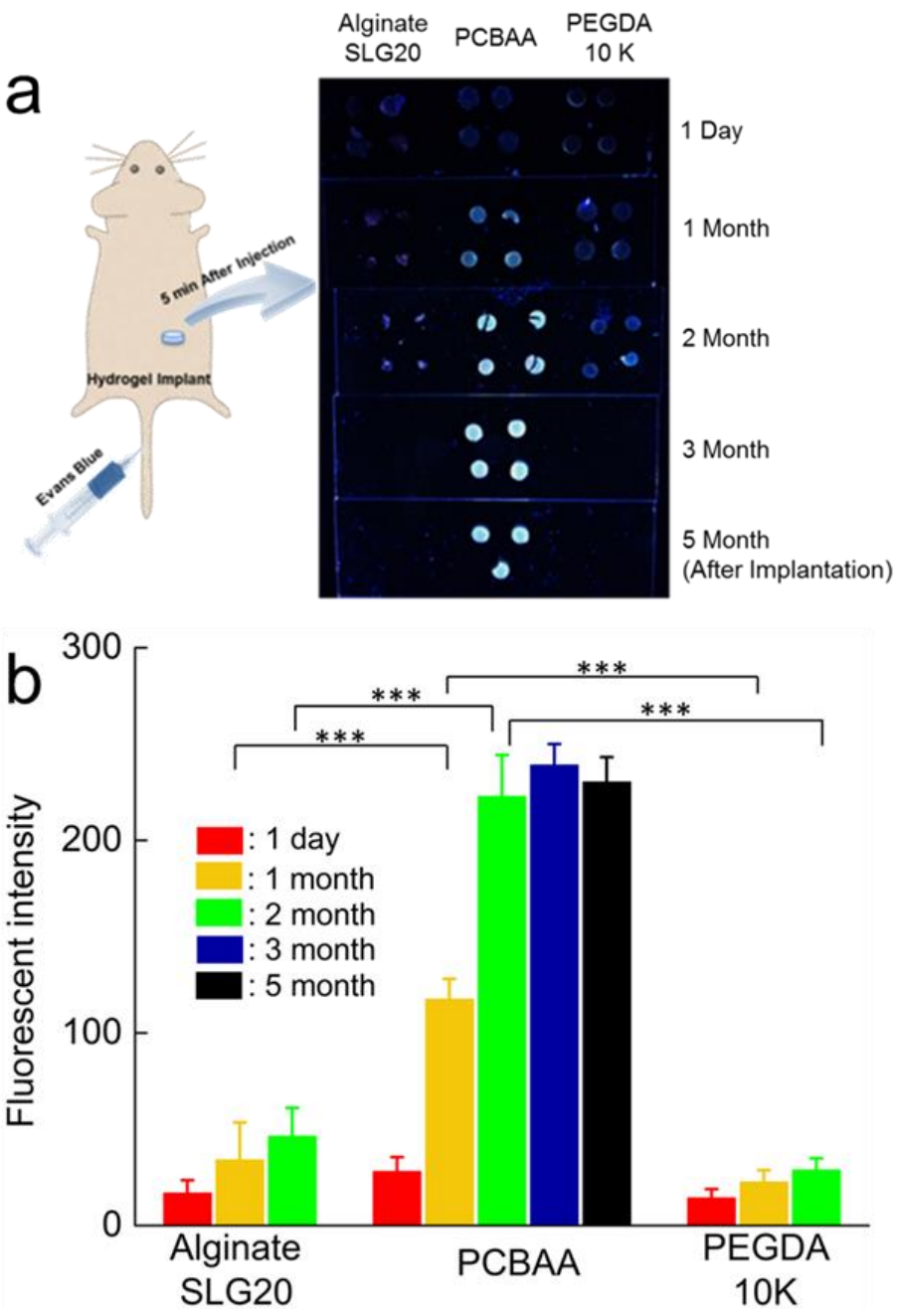

Figure 3-7 (a) dye accumulation of all explanted hydrogel samples (after different time points) under UV lamp after receiving i.v. injection of Evans Blue dye in PBS. (b) Fluorescent intensity quantification from (a). All data are presented as mean of biological replicates ± standard deviation (n=4, (n=3 for PCBAA at 5 months)). Statistical analysis: one-way ANOVA with Bonferroni multi-comparison. ***: $p < 0.0001$.

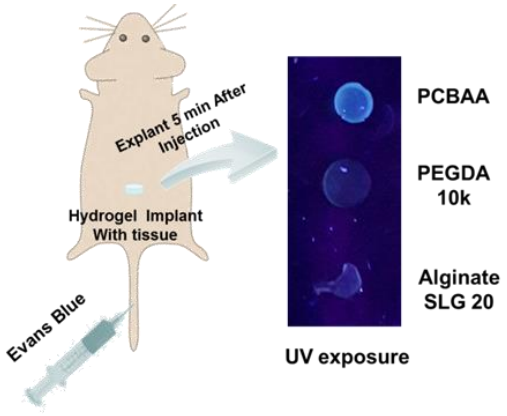

Figure 3-8 Evans Blue dye accumulation on Alginate SLG20, PEGDA 10K and PCBAA hydrogels that have been implanted for 15 days.

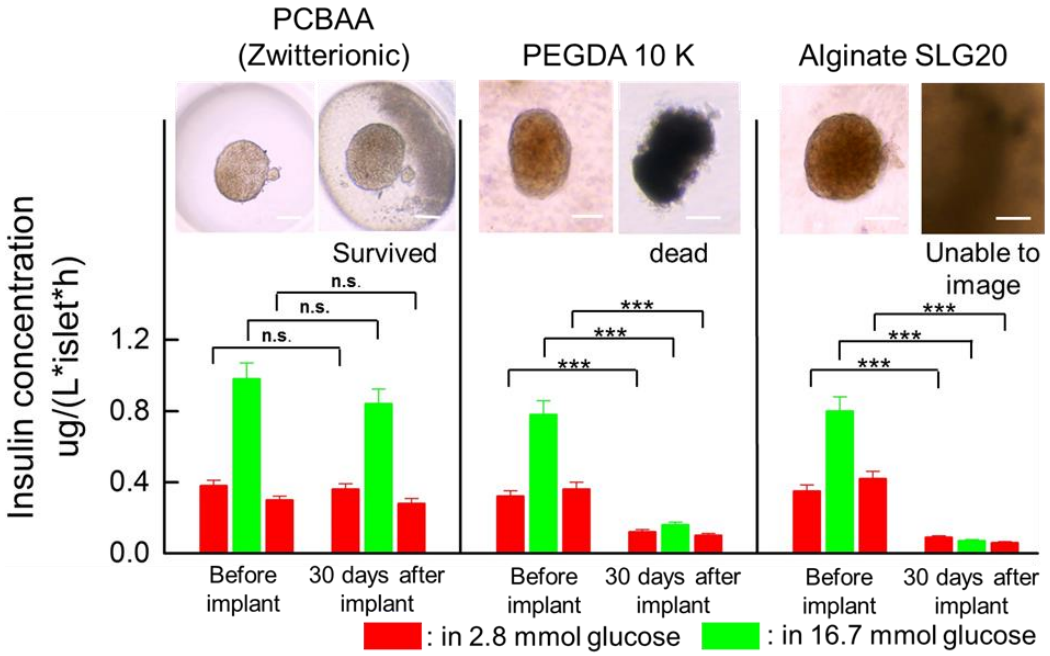

Figure 3-9. The first line exhibited the islets morphology in different materials after 30 days' implantation in normal healthy mice. The second line showed the corresponding glucose response capability of islets in different materials after 30 days' implantation. All data are presented as mean of biological replicates (n=6) ± standard deviation. Statistical analysis: one-way ANOVA with Bonferroni multi-comparison. ***: $p < 0.0001$; n.s.: no significant difference at $p > 0.53$.

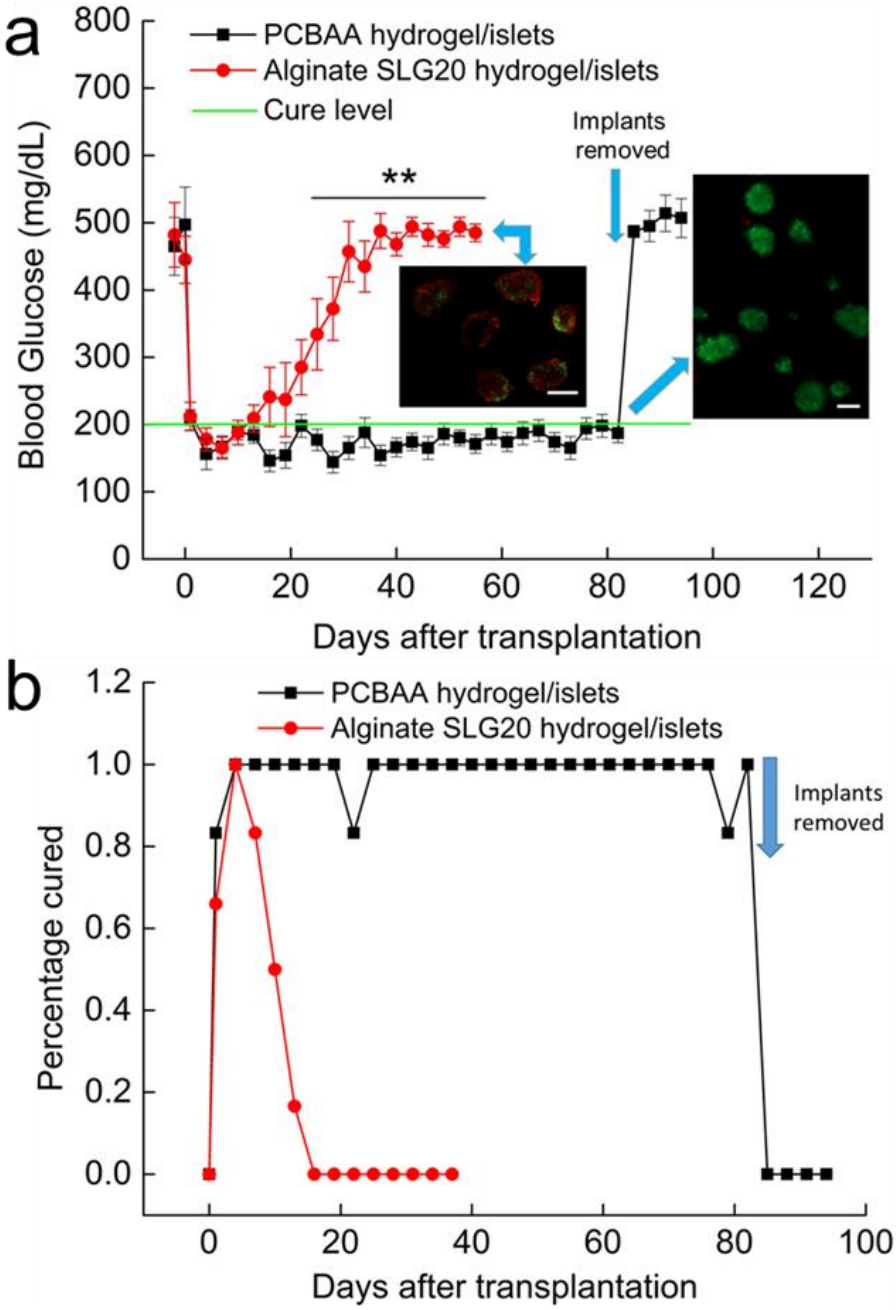

Figure 3-10 (a) Therapeutic curve of PCBAA hydrogel and Alginate SLG20 hydrogel devices with 500 IEq rat islets encapsulated. Live (green) and Dead (red) staining was performed at the end point as indicated. (b) The fraction of cured diabetic mice after being transplanted (non-fasted blood glucose level < 200 mg/dl). All data are presented as mean of animal replicates (n=6) ± standard deviation. Statistical analysis: non-parametric Mann-Whitney test. **: $p < 0.001$.

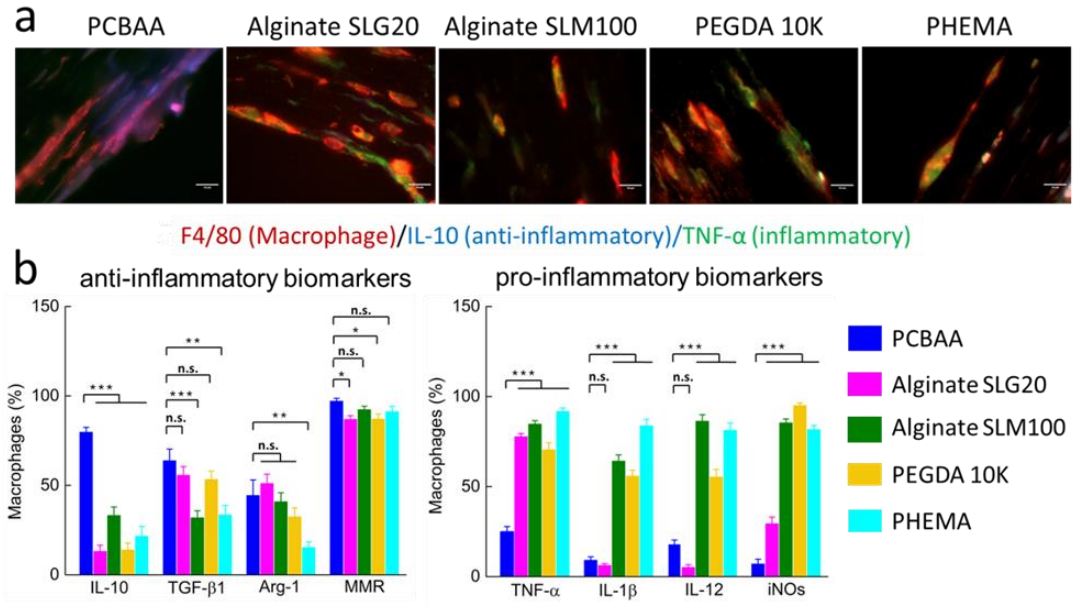

Figure 3-11 (a) Macrophages in the vicinity of different material implants (within ~100 µm from the tissue/hydrogel interface) were analyzed after 1-month implantation. Representative immunofluorescence histological images were obtained through triple staining with the indicated markers. (b) Percentage of macrophages expressing pro-inflammatory (interleukin 10 (IL-10), transforming growth factor beta 1 (TGF-β1), arginase-1 (Arg-1) and macrophage mannose receptor (MMR)) and anti-inflammatory (tumor necrosis factor alpha (TNF- α), interleukin 1 beta (IL-1 β), interleukin 12 (IL-12) and Inducible nitric oxide synthase (iNOs)) biomarkers. All data were showed as mean of biological replicates (n=10) ± SEM. Statistical analysis: one-way ANOVA with Bonferroni multi-comparison. *: $p < 0.01$; **: $p < 0.001$; ***: $p < 0.0001$; n.s.: no significant difference at $P > 0.05$.

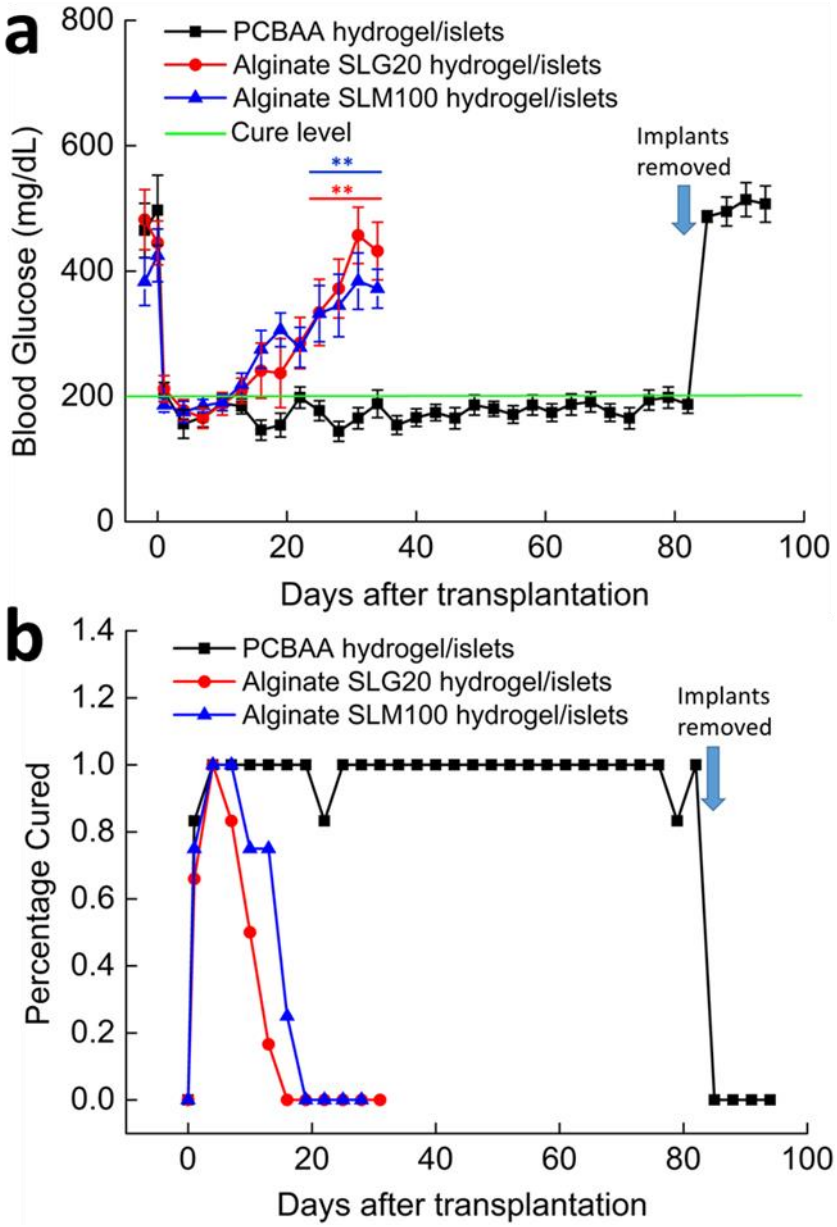

Figure 3-12 (a) Therapeutic curve of PCBAA hydrogel, alginate SLG20 gel and alginate SLM100 gel devices with 500 IEq rat islets encapsulated. (b) The fraction of cured diabetic mice after being transplanted (non-fasted blood glucose level < 200 mg/dl). All data were showed as mean of animal replicates (n=6; for SLM100, n=4) ± standard deviation. Statistical analysis: non-parametric Mann-Whitney test. **: $p < 0.001$.

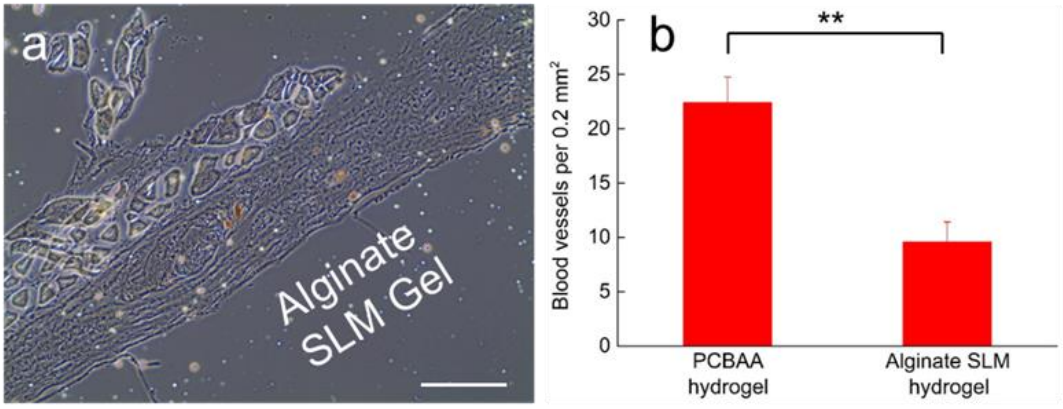

Figure 3-13 (a) Representative image of MECA-32 antibody staining of Alginate SLM100 hydrogel/tissue interface. Scale bar = 50 µm. (b) Calculated blood vessel density of PCBAA hydrogel/tissue interface and alginate SLM hydrogel/tissue interface, based on MECA-32 staining results. Data were showed as mean of biological replicates (n=3) ± standard deviation. Statistical analysis: unpaired, two-tailed t-test. **: $p < 0.001$

CHAPTER 4. A MACRO-CROSSLINKER FOR DURABLE ANTI-FOULING COATING

4.1 Introduction

Zwitterionic polymer coatings were effective to solve Biofouling problem that causes implantable device failure and unwanted microorganism attachment. However, zwitterionic polymer coating is usually fragile with only short-term function since these super-hydrophilic polymers tends to dissolve in water. In this chapter, we described and synthesized a novel zwitterionic macro-crosslinker to overcome the vulnerability of zwitterionic coating. The macro-crosslinker coating was highly crosslinked over the whole surface with much greater thickness than common polymer brush coating and stayed in presence on polyurethane (PU) surface to maintain function even after long term treatment in flowing phosphate buffered saline (PBS). The macro-crosslinker coating enabled the application of zwitterionic polymer in durable anti-biofouling coating for long term function.

For many applications involving surface exposure to biomolecule and microorganism, biofouling is a serious problem that causes implantable device failure[157-158] and unwanted microorganism attachment[159-160]. Recently, surface modification with non-fouling polymer has been utilized to overcome the biofouling problem[161-162]. Encouraging results had been obtained in various applications on different traditional substrates such as anti-thrombosis polyurethane catheters and coatings on metal ship hull to resist marine fouling[163] by using non-fouling zwitterionic polymers. Zwitterionic polymer coatings are super-hydrophilic and attract a dense layer of water molecule to resist non-specific protein binding and

bacteria adhesion[164]. Many methods have been involved in fabricating zwitterionic coatings[165]. Nevertheless, the resulting zwitterionic polymer coatings are typically unstable with only short-term function, regardless of how they are immobilized on the surface[166]. Unlike hydrophobic polymer coatings, super-hydrophilic polymer coatings drastically tend to dissolve into water environment. This leads to gradual exposure of the coated surface over time[167], and hinders the use of zwitterionic coating in applications that require long term durability[46]. Despite significant efforts in this field[168], it remains a challenge to fabricate durable non-fouling coating using super-hydrophilic zwitterionic polymers.

In this work, we synthesized zwitterionic macro-crosslinker to overcome the vulnerability and challenge in developing durable anti-fouling coatings. Double bonds were introduced to high molecular weight (Mw) zwitterionic polymer backbone, which was then crosslinked on polyurethane substrate by graft-from method. Different from single polymer chain which was easily torn away from the surface, the macro-crosslinker coating was highly crosslinked over the whole surface with significantly increased thickness and remained on polyurethane (PU) surface to sustain non-fouling function even after long term shearing in flowing phosphate buffered saline (PBS). Synthesis of the zwitterionic macro-crosslinker was verified by Nuclear Magnetic Resonance (NMR) and coating thickness was characterized by surface ellipsometry and scanning electron microscope (SEM) visualization. Contact angle, protein absorption and bacteria adhesion were utilized to examine the function of the coating after different durability challenges. Results indicated the

macro-crosslinker coating was much more durable than common brush polymer coating and conventional small molecule crosslinking strategy, indicating its potential for durable (or long-term) anti-fouling applications.

4.2 Materials and methods

4.2.1 Materials

2-Aminoethyl methacrylate hydro-chloride (NH_2-MA monomer, 90%), Tert-Butyl bromoacetate (98%), 2-(Dimethylamino) ethyl mathacrylate (DMA 98%), N,N-Methylenebis(acrylamide) (MBAA, 99%), Anhydrous DMF, Anhydrous Acetone (99.99%) and Anhydrous methanol were purchased from Sigma-Aldrich, St. Louis, MO. Triethylamine (TEA, 99%), trifluoroacetic acid (TFA, 99.9%) and Ethyl Ether anhydrous (99.9%) were obtained from Fisher Chemical. Co. Deuterium Oxide (D_2O 99.9%) and Dimethyl sulfoxide-D6 (D-DMSO, 99.9%) were obtained from Cambridge Isotope Laboratories, Inc. USA.

4.2.2 Synthesis of PCBMA-tBu monomer

The synthesis procedure was as reported previously[4]. Briefly 5 g 2-Dimethylamino-ethyl methacrylate and 8.68 g tert-butyl bromoacetate were reacted in 20 ml acetonitrile for 24 h at 50 ^oC under N2 protection. Upon addition of 250 ml ethyl ether to the reaction mixture, the white crystals were isolated and dried. The resulting CBMA-tBu monomers were immediately stored in a desiccator at -20 ^oC (yield 96%)

4.2.3 Synthesis of PCBMA macro-crosslinker

The polymerization solvent was prepared by dissolving 5 mg

2-Hydroxy-4-(2-hydroxyethoxy)-2-methylpropiophenone (photo-initiator, I-2959) in anhydrous DMF. The CBMA-tBu ester monomer was first copolymerized with 2-Aminoethyl methacrylate hydro-chloride (NH_2MA monomer) at different molar ratio (10:1, 30:1 and 50:1) in the polymerization solvent (35% by weight) under UV for 10 min and the resulting polymer A was precipitated in anhydrous acetone. Unreacted monomer was washed away by re-dissolving the product in DMF and precipitated in acetone for additional two times (polymer yield: 56%). The purified copolymer A was then reacted with acryloyl chloride (3 times of the amount of NH_2 function group) in presence of triethylamine in anhydrous DMF (10% by weight) for 5 h at room temperature followed by precipitation in anhydrous ethyl ether and vacuum dry (polymer B, yield: 87%). Lastly, copolymer B was stirred in trifluoroacetic acid (20% by weight) to remove tBul ester protection and neutralized using triethylamine (TEA) to pH=7 in anhydrous methanol on ice bath. The obtained zwitterionic macro-crosslinker C was precipitated in ethyl ether and dried in vacuum (macro-crosslinker C yield: 91%; overall yield: 44%).

4.2.4 Characterization

The molecular weight of the macro-crosslinker and surface initiated polymer (obtained by ultrasonic treatment after coating) were determined by gel permeation chromatography (GPC) on a Waters Alliance 2695 Separations Module equipped with a Waters Ultrahydrogel Linear column and a Waters 2414 reflex detector. The mobile phase was PBS buffer solution at a flow rate of 0.7 ml/min at 35 ^{o}C. Poly(ethylene oxide) from Polymer Laboratories were used as standards. The synthesized products

were examine using a Varian Mercury-400 MHz NMR. In Figure 2 of the main text, the product A and B were dissolved in D-DMSO and product C was dissolved in D_2O. The coating thickness was characterized by surface ellisometry and averaged from three measurements at different surface site (α-SETM, J.A. Woollam Co., Inc.).

4.2.5 Protein absorption

To measure the fibrinogen (Fg, Sigma-Aldrich) adsorption on PCBMA macrocrosslinker coating, coated surface (either by PCBMA brush or PCBMA macrocrosslinker) and bare PU surface were incubated with 1mg/ml Fg in a well plate for 10 minutes at room temperature, followed by 5 washes with PBS buffer. Samples were then incubated with 1 mg/ml bovine serum albumin solution for 10 minutes at room temperature with 5 times wash again with PBS buffer. The tested surface were then removed from the fifth PBS wash and transferred to new wells. They were next incubated with a 1:200-dilution of horseradish peroxidase (HRP)-conjugated anti-fibrinogen in PBS for 10 minutes, followed by another 5 washes with the same buffer. After the fifth wash, the tested surfaces were transfer to new wells and SIGMAFAST OPD was added to each well at 30-second intervals. The surfaces were incubated in the OPD solution for 30 minutes away from light. The supernatant was removed from each test well, transferred to a cuvette, and its absorbance at 490 nm was measured. All samples were measured in triplicate.

4.2.6 Bacteria adhesion and SEM image

After bacteria adhesion on PU, the surface will be immersed in the fix solution of 2.5% gluaraldehyde, 2% paraformaldehyde in 0.1 M sodium phosphate buffer. The

surface was then dehydrate in a gradient ethanol series and dried in vacuum. Before imaging, the surface sample was coated with nano-gold using a SEEVac Conductive IV sputter coater. The bacteria were imaged using a JSM - 6510LV SEM at 5 um magnification and bacteria adhesion density was calculated by counting the bacteria number per 900 um^2.

4.3 Results and discussions

The synthesis of zwitterionic macro-crosslinker, based on polycarboxy betaine methacrylate (PCBMA), involves 3 steps of reaction and each step was monitored by ^{1}H-NMR **(Figure 4-1)**. The CBMA-tBul ester monomer was first copolymerized with 2-aminoethyl methacrylate hydro-chloride (NH_2MA monomer) at different molar ratio (m:n=10:1, 30:1 and 50:1) in anhydrous dimethylformamide (DMF) using random free radical polymerization and the resulting polymer A was precipitated in anhydrous acetone. Unreacted monomer was washed away by re-dissolving the product in DMF and precipitated in acetone for additional two times. NMR spectrum for polymer A showed no peak between 5-6 ppm, indicating the complete removal of both unreacted CBMA-tBu and NH_2MA monomers. An emerging peak (b at 7 ppm) implied successful incorporation of NH_2MA unit into the PCBMA-tBu ester polymer backbone. The purified copolymer A was then reacted with acryloyl chloride in presence of triethylamine in anhydrous DMF followed by precipitation in anhydrous ethyl ether and vacuum dry. The obtained copolymer B had its NMR peak b completely replaced by peak c (5-6 ppm, for acryloyl chloride) with an undetectable peak d (7.9 ppm for -NH-); this indicated that the NH_2 function groups from NH_2MA

were completely reacted with acryloyl chloride. Lastly, copolymer B was treated by trifluoroacetic acid (TFA) to remove tBu ester protection and neutralized using triethylamine (TEA) to pH=7 in anhydrous methanol on ice bath. The obtained zwitterionic macro-crosslinker C was precipitated in ethyl ether and dried in vacuum (overall yield: 44%). Complete removal of tBu ester groups was confirmed by the disappearance of peak a (1.2 ppm) for tBu ester shown in copolymer A and B (spectra for different double bond ratio see **Figure 4-2**). Free radical polymerization was chosen here since there was no any toxic catalyst involving and small molecule could be easily removed, which was crucial for potential *in vivo* application such as coatings for catheters.

The coating on hydrophobic PU substrate was produced by a surface graft-from redox polymerization method which was reported previously[169]. We chose graft-from method because it was able to induce densely distributed polymer chain that was proved to effectively cover the whole surface in various shapes and inner side of tubes[170]. Briefly, our model substrates, PU coupons, were immersed in a 1% solution of tert-butylperoxy 2-ethylhexyl carbonate (TBEC) in isopropyl alcohol (IPA) for 2 hours at room temperature. After a few times of gentle wash with ethanol, the coupons were transferred to a polymerization solution of 10% (weight ratio) PCBMA macro-crosslinker containing 5 mM Fe(II) gluconate at 40°C for 12 h. In our control study, 10% CBMA monomer, or 10% CBMA monomer with commonly used small molecule crosslinker, N,N-Methylenebis(acrylamide) (MBAA), were used in the polymerization solution to produce polymer brush coating or crosslinked coating,

respectively. Unreacted TBEC was removed by repeated gentle rinse with IPA. The coupons with surface coatings were dried in vacuum before test.

The coating thickness was characterized by surface ellipsometry using the bare PU surface as the control **(Figure 4-3)**. Immediate after the coating reaction, the macro-crosslinker coating showed much greater thickness (>300 nm) than the polymer brush coating (11±1.3 nm), and the brush coating with MBAA crosslinker (11.5±1.6 nm) at the same crosslinking density as macro-crosslinker (MBAA/CBMA monomer ratio = double bonds unit/PCBMA unit). Under SEM, the coating for polymer brush and the one crosslinked with MBAA could hardly tell, but the thick coating of macro-crosslinker could be clearly visualized. Gel permeation chromatography (GPC) characterization showed that the macro-crosslinker had an average molecular of 174 KDa, which was much larger than the surface initiated polymer brush (4.5 KDa). There were several reasons explaining the resulting low MW of polymer brush. 1) There was steric hindrance between polymer brush chains preventing the chain from growing larger[171]. 2) Surface redox polymerization was not effective to produce high MW polymer since only monomer near the surface participates the chain growth. 3) The presence of 5 mM Fe(II) gluconate, which was the reducing agent to induce free radical generation on hydrogen peroxide of TBEC, greatly decreased the solubility of zwitterionic monomer (maximum 18% by weight), preventing further increasing the monomer concentration as a way to increase the Mw of resulting polymer. Coating thickness from different methods was further monitored after one week incubation in water. Polymer brush coating lost 80% of its

thickness (from 10±1.2 nm to 2.1±0.2 nm) while macro-crosslinker coating was almost intact (4 % thickness loss).

The durability of the surface coating made through different methods was further examined by measuring water contact angles after different days of incubation in water **(Figure 4-4)**. Without any zwitterionic polymer coating, the bare PU surface was hydrophobic showing a typically water contact angle around 70°. After the coating through all tested methods, the contact angle decreased to around 8°, indicating the efficient introduction of super-hydrophilic zwitterionic polymers onto the PU surface. Nevertheless, as days went by, the contact angles for polymer brush coating and polymer brush coating crosslinked by MBAA gradually increased and reached the original contact angle of 70° (for bare PU) after two weeks. This suggests that coatings were almost completely lost upon two weeks incubation in water. Addition of small molecule crosslinker MBAA to mimic the same theoretical crosslinking density of macro-crosslinker only led to negligible improvement in durability. The contact angle for the macro-crosslinker coating, by contrast, remained unchanged after one week and increased to 19° after two weeks, indicating greater durability of this particular coating.

Zwitterionic material coatings were known for great non-fouling property that resists non-specific protein binding and microorganism attachment, and can be potentially applied on blood-contact biomedical devices, e.g., catheters, to resist thrombosis and ship hulls to resist marine fouling. In these circumstances, coatings would be subject to shear stress in the moving fluid such as blood and sea water; this

required more durable coating technology to maintain long term anti-fouling performance[172]. To test the durable function of the zwitterionic macro-crosslinking coating under shear stress, the coating was exposed to PBS solution under 1500 rpm stirring for one week and taken out for functional test. Human fibrinogen was utilized for protein binding test and results before and after one week of flow condition were compared **(Figure 4-5)**. It was found that all coating methods were able to produce a freshly-made coating that resists fibrinogen binding. However, after one week exposure to flow condition, polymer brush coating and brush coating with MBAA crosslinking lost anti-fouling function with protein binding returning to the level of bare PU surface. The macro-crosslinker coating showed almost the same low level of protein binding before and after the flow treatment, suggesting its superior durability under shear stress condition. We further conducted bacterial attachment assay as additional functional test for the coatings using *E. coli.* as a model bacterium. After flow condition treatment in PBS, the coatings were transferred to high concentration bacteria suspension ($1.12*10^9$ cell/ml) for 0.5 h, followed by repeated washes with sterile PBS, fixation, dehydration and vacuum drying. The bacteria attached on the coating surface were visualized under SEM and their density was calculated **(Figure 4-5)**. Similar results were obtained to the protein adsorption test. After one week flow condition, the macro-crosslinker coating had almost zero bacteria adhesion, but coating of polymer brush and the brush with MBAA crosslinking showed bacterial adhesion as worse as bare PU surface.

So far many coating methods using zwitterionic materials were able to modify

hydrophobic substrate with non-fouling property. However, these coatings were usually vulnerable with only short-term function, since super-hydrophilic polymer chains would be easily washed away by aqueous environment. It is obvious that crosslinking individual polymer brush chains could help stabilize the overall coatings[173]. In a crosslinked surface network, if one polymer chain tended to be torn away from the surface, its neighbouring covalently linked polymers would retain it from dissolving into water environment. Our results showed that different crosslinking strategies had different levels of stabilizing effect on the coatings **(Figure 4-6)**. What we found was small molecule crosslinker MBAA did not improve stability of polymer brush, and the resulting crosslinked coatings was far less durable than macro-crosslinker coatings. This could be potentially explained by 1) low local concentration of MBAA (at the kept CBMA/MBAA ratio) led to relatively inefficient crosslinking and 2) the monomer concentration could not be further increased in presence of Fe(II) gluconate. We did observed that the small crosslinker MBAA strategy was inefficient to further increase the coating thickness (11.5±1.6 nm) compared with macro-crosslinker strategy (>300 nm). A thicker coating has generally shown enhanced durability[174].

In summary, we demonstrated the synthesis of novel zwitterionic macro-crosslinker enabling the formation of durable non-fouling coating on common hydrophobic plastic substrate, PU. Coating formed using the macro-crosslinker exhibited much greater thickness and durability compared to common polymer brush coating and brush coating crosslinked with small molecule crosslinkers. Upon

incubation in water, macro-crosslinker coating was able to sustain hydrophilicity for more than two weeks. Even under shear flow condition, the macro-crosslinker coating was able to retain its non-fouling property to resist protein and bacteria adsorption after one week treatment, while all other methods failed. The durable zwitterionic macro-crosslinker coating can be potentially applied on blood-contact biomedical devices or for marine coating applications.

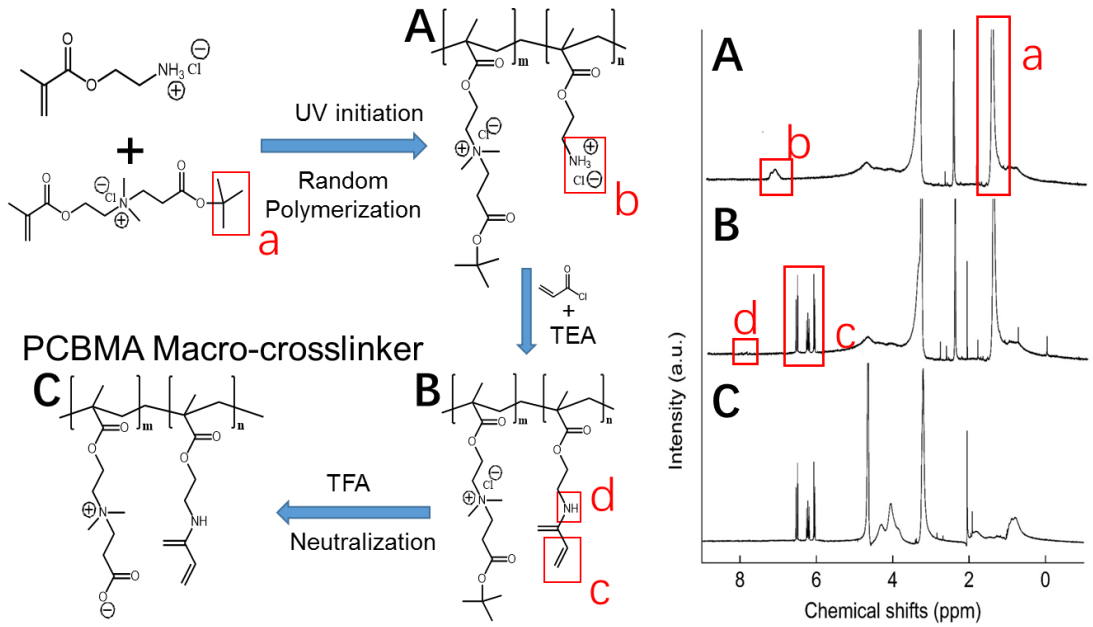

Figure 4-1 Synthetic route and ^{1}H-NMR characterization of the macro-crosslinker

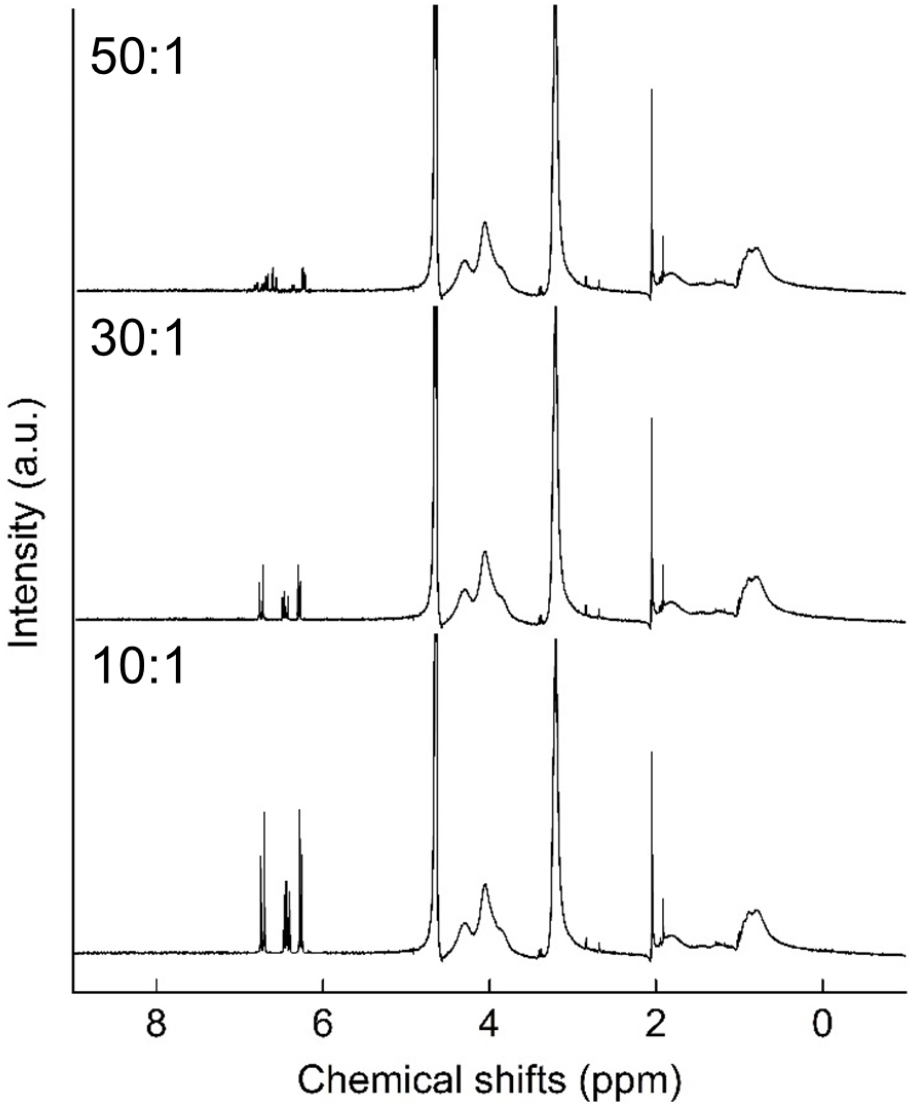

Figure 4-2 ^{1}H-NMR of PCBMA macro-crssolinker with different double bond density (labeled by CBMA/double bond molar ratio).

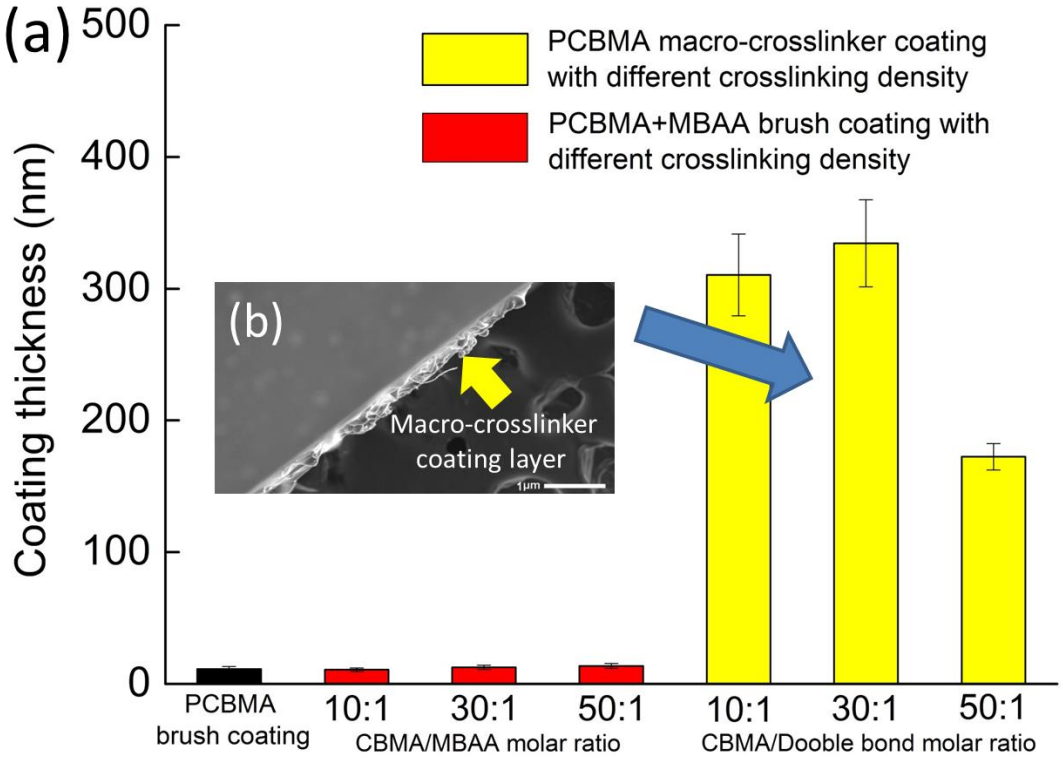

Figure 4-3 (a) Coating thickness of different methods and (b) SEM image of macro-crosslinker coating

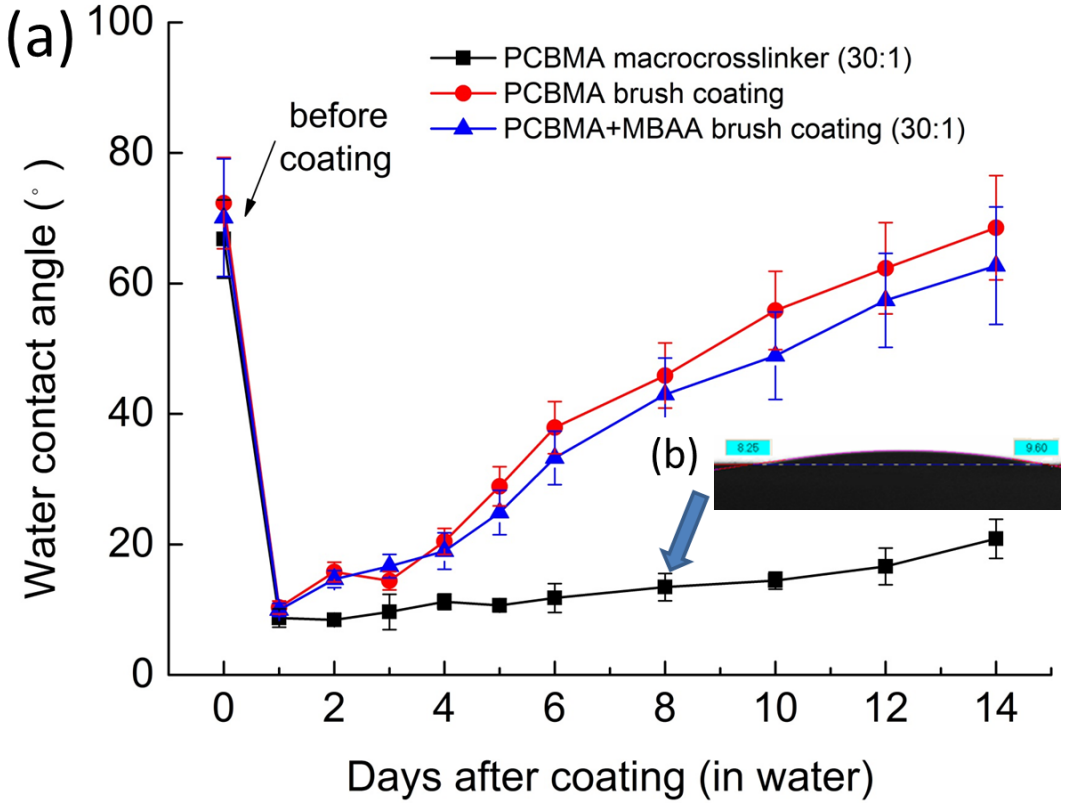

Figure 4-4 (a) Time course contact angles for coating surfaces made from different methods and (b) water drop on macro-crosslinker coating on day 8

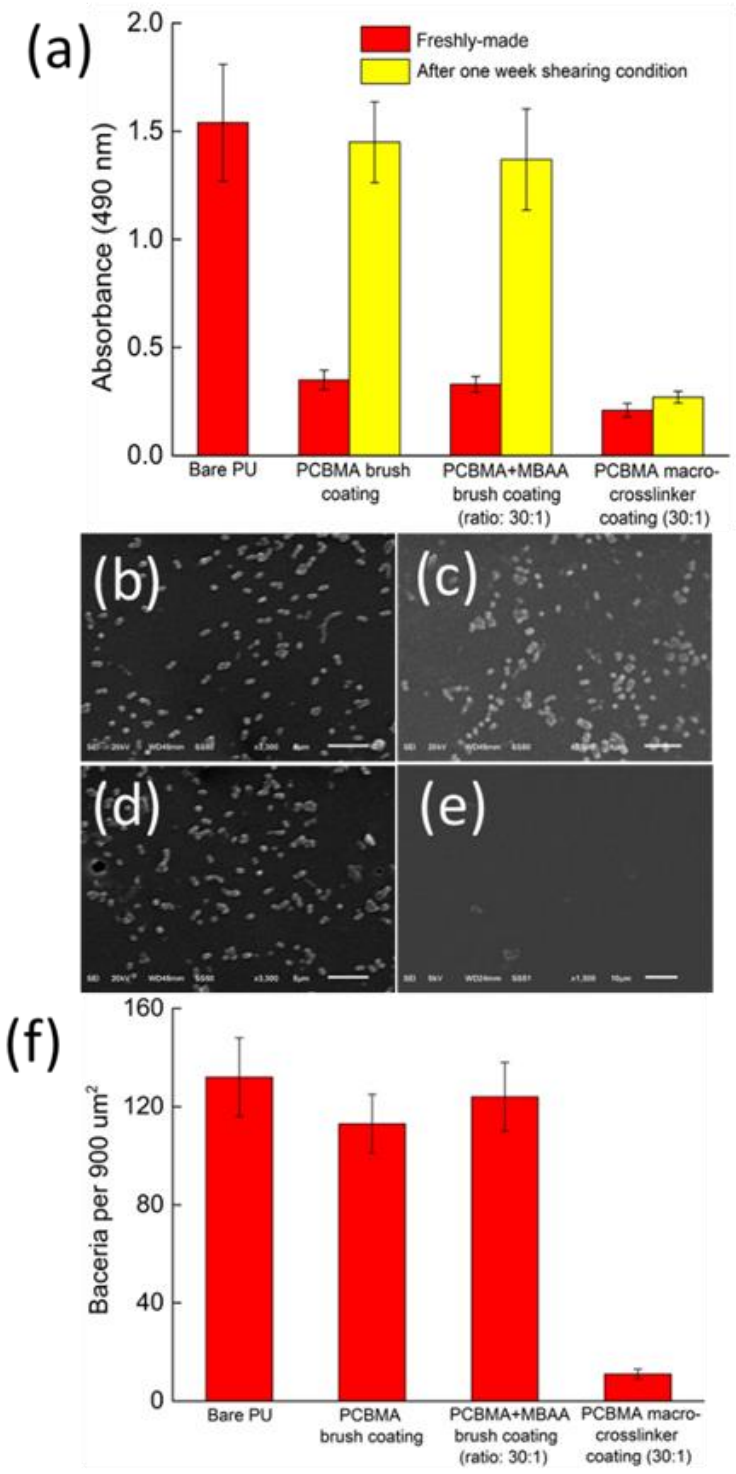

Figure 4-5 (a) Protein binding test on coatings obtained from different methods before and after one week exposure in flowing PBS, and E. coli adhesion test on coatings obtained from (b) bare PU, (c) PCBMA brush coating, (d) PCBMA+MBAA brush coating and (e) PCBMA macro-crosslinker coating with (f) calculated adhesion density

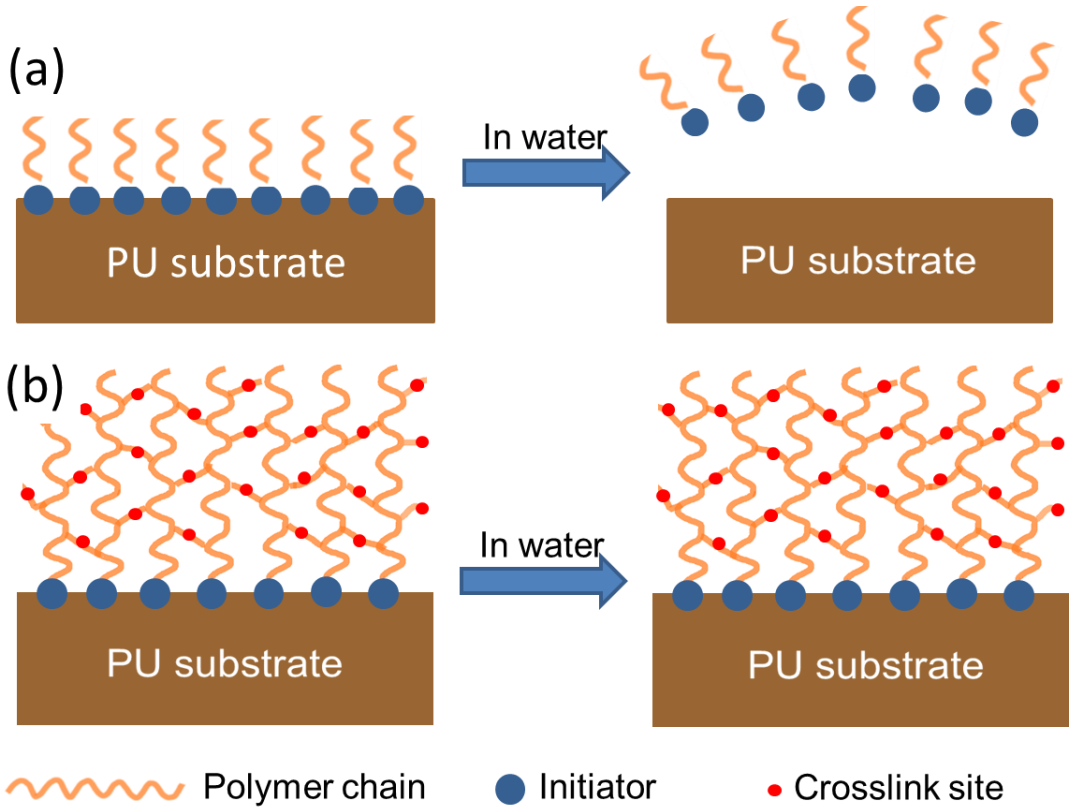

Figure 4-6 Mechanism of (a) fragile brush coating and (b) durable macro-crosslinker coating.

CHAPTER 5. SUPER-DURABLE COATING FABRICATED FROM A DOUBLE-SIDED TAPE WITH LONG TERM "ZERO" BACTERIAL ADHESION

5.1 Introduction

In this Chapter, we will describe a novel durable zwitterionic polymers coating that for the first-time potential addresses the tough biofilm issue. The novel coating can be applied on many common substrates as easy as a double-sided tape. Simply apply superglue on a given surface, apply the coating tape we developed on top, remove the tape liner, and then the coating is obtained. The novel coating shows the toughness and durability that have not yet been achieved by any reported one. Most remarkably, this coating achieved unprecedented capability to resist biofilm. State-of-the-art anti-fouling coatings started to accumulate bacteria after just a few hours of contact and would be covered with dense biofilm usually in less than 7 days. Our coating was able to achieve almost "zero" bacteria adhesion even after one-month continuous contact with high concentration bacteria. Our coating technology is convenient to apply and can promisingly solve the biofilm threat, which deteriorates public health and impedes the function of most biomedical devices.

There is no coating technology currently available that can prevent the notorious biofilm formation issue[175-176], which induces infections[177-179] and impede device function[117, 180]. The state-of-the-art anti-biofilm coatings are complex to fabricate and poor in performance due to instability in working environment[47]. They usually started to accumulate bacteria after immediate contact and would be covered with dense biofilm usually within ~7 days[45-46, 48, 181]. Here, we report the first ever solution

to fully address this tough biofilm issue by developing an easily-applied super-antifouling coating. Our coating was able to achieve almost “zero” bacteria adhesion even after one-month continuous contact with high concentration bacteria.

Our novel Durable and Ultra-Robust Antifouling Zwitterionic (DURA-Z) coating combined the use of a zwitterionic hydrogel tape (a double-sided tape) and commercial superglue, and can be easily fabricated and universally applied on common substrates. Super-hydrophilic zwitterionic polymer materials are known for their superior antifouling properties[182]. But they, like common hydrophilic coatings, drastically tend to dissolve in the aqueous environment resulting in poor coating durability[166, 168]. The vulnerability to mechanical damages further prevents these hydrophilic coatings from being practically applied[183]. Superglue based on ethyl cyanoacrylate is one of the strongest linkages ever known for daily bonding projects, and is known to only glue hydrophobic materials such as metal, plastic or wood. It cannot stably bind to hydrophilic ones, e.g., glass slide which has a water contact angle of ~28°. Against this conventional wisdom, here we were able to immobilize a super-hydrophilic DURA-Z gel network (water contact angle < 2°) with the hydrophobic superglue, through a unique interpenetration mechanism. The obtained DURA-Z coating was super-hydrophilic and retained anti-fouling property after various long-term durability tests in aqueous environments by incubating (90 days), shearing (50 days) and flushing (30 days), as well as mechanical damage tests by knife-scratch and repeated sandpaper abrasion at 570 kPa. The pressure used in our

abrasion test is more than 150 times higher than other similar tests for coating stability[184]. Remarkably, DURA-Z coating was able to achieve almost “zero” bacteria adhesion for at least one month when continuously incubated with highly concentrated bacteria (> 10^9 cells per ml) in culture media at both dynamic and static conditions. This remarkable anti-biofilm performance has rarely been achieved. DURA-Z coating can be easily removed from the substrate and re-applied, which further extends the applicability of this coating strategy.

5.2 Materials and methods

5.2.1 Materials

Polyurethane coupons were purchased from BioSurface Technology. Stainless steel strips were purchased from McMASTER-CARR. All solvents and chemicals were purchased from Sigma-Aldrich and were used as received.

5.2.2 Fabrication of DURA-Z tapes.

DURA-Z tapes were fabricated by in-situ forming of a thin layer of PCBAA hydrogel on commercially available polypropylene liner. Briefly, 5 mg 2-Hydroxy-4’-(2-hydroxyethoxy)-2-methylpropiophenone (I-2959) initiator and 30 mg N,N’-Methylenebis(acrylamide) (MBAA) crosslinker were dissolved in 10 ml DI water. 300 mg CBAA monomer was then dissolved in 300 µl initiator/crosslinker solution to prepare a pre-gel solution, which was transferred to between two polypropylene liners adhered to glass slides separated with a Teflon spacer (1 mm in thickness). UV was applied for a few minutes to crosslink the PCBAA hydrogel. DURA-Z tapes were obtained by removing the hydrogel layer along with the liners

from glass slides.

5.2.3 Fabrication of DURA-Z coating.

The polyurethane (PU), stainless steel, glass and wood substrates were cleaned with alcohol and dried in air (wood and metal were pre-treated by sandpaper to obtain rough surfaces, and glass was pre-coated with a thin layer of EVO-stik glue). Then one drop of cyanoacrylate superglue (ACE Hardware Corp.) was applied onto the dried substrate, followed by pressing the DURA-Z tape (hydrogel layer facing down) onto the superglue for a few seconds. One hour was then allowed to completely solidify the superglue. The liner on top of the hydrogel was removed, and the glued coating was transferred to DI water for equilibrium. 20 mins later, the DURA-Z coating was polished either by a small shovel or tweezer, leaving the surface with a thin layer of coating.

5.2.4 Scanning Electron Microscope (SEM) imaging.

samples were dried in vacuum and then coated with nano-gold using an SEEVac Conductive IV sputter coater before imaged by a JSM - 6510LV SEM. For sectional imaging, all tested coupons (bare PU, superglue coated and DURA-Z coated substrates) were vertically cut into half using a sharp scalpel to expose the cross-section.

5.2.5 Atomic-force Microscopy (AFM) imaging

AFM imaging of the bare PU, superglue coated and DURA-Z coated substrates was conducted on a Dimension 3100 AFM from VEECO. All samples were vacuum dried before imaging. The coating thickness and morphology were measured in the air

through the tapping mode using silicon probes (VEECO) with a nominal frequency of 150 kHz. The AFM images were analyzed using Nanoscope software version 5.12.

5.2.6 Infra-red (IR) characterization

Bare PU, superglue coated and DURA-Z coated substrates were vacuum dried before testing. PCBAA hydrogel was freeze-dried before testing. All samples‘ surfaces were characterized on a NICOLET 6700 IR (Thermo Electron Corporation) equipped with an attenuated total reflectance (ATR) accessory.

5.2.7 Contact angle

The water contact angle on bare PU, superglue coated and DURA-Z coated substrates was conducted using a KSV contact angle instrument equipped with a camera at room temperature and ambient humidity. 2 µl of water was dropped on different surfaces and water contact angle was calculated using by the CAM2008 software.

5.2.8 Durability tests in aqueous environment

PBS shearing was created on a stirring plate by a 5-cm stirring bar at 1500 rpm in a beaker (D = 10 cm). The tested samples were firmly clamped and positioned at the inner wall of the beaker, and subjected to the continuous shear stress of 202 G. Body temperature (37 °C) was controlled by the stirring plate and DI water was added to compensate the evaporation every day to maintain standard PBS concentration. In water flushing test, water was cycled by an electric pump with a flow rate of 42.8 ml/s. Protein adsorption test was conducted on the samples before and after the durability challenge.

5.2.9 Mechanical damage tests

For the knife-scratch test, DURA-Z coating on PU coupon was randomly cut by a sharp scalpel. The abrasion test was conducted on an INSTRON compressor equipped with a precise loading detector. Sandpapers (Gator waterproof sanding 400 grit) were fixed on both sides of the compressor and the pressure was calculated by the loading divided by the area of PU coupon. One cycle of abrasion contains pushing and pulling the coupon for 1-cm displacement back and forth under a given pressure. The samples were subjected to 20 cycles of abrasion. Water wettability and protein adsorption tests were conducted on the samples before and after the mechanical damage challenge.

5.2.10 Protein absorption test (ELISA)

Human fibrinogen (Fg, Sigma-Aldrich) adsorption on a variety of substrates (bare substrates, superglue coated and DURA-Z coated substrates) was measured using ELISA method. All samples were incubated with 1mg/ml Fg for 10 minutes at room temperature, followed by 5 washes with PBS buffer. They were then incubated with 1 mg/ml bovine serum albumin solution for 10 minutes at room temperature with 5 washes again with PBS buffer. The samples were removed from the fifth PBS wash and transferred to new wells. They were next incubated with a 1:200-dilution of horseradish peroxidase (HRP)-conjugated anti-fibrinogen (USBiological, Life Sicences) in PBS for 10 minutes, followed by another 5 washes with PBS buffer. After the fifth wash, the samples were transferred to new wells and SIGMAFAST OPD (Sigma-Aldrich) was added to each well. They were incubated in the OPD solution for

30 minutes in the dark. The supernatant was removed from each test well, transferred to a 96-well plate, and its absorbance at 490 nm was measured using a UV-VIS spectrometer (Thermo Scientific Multiscan Go). All samples were measured in triplicate.

5.2.11 Biofilm resistance of DURA-Z coating.

E. coli bacteria were cultured for 24 h at 37 °C on Luria-Bertani (LB) agar plates. One colony was picked and cultured in 20 mL of LB broth medium overnight at 37 °C on a shaker (Standard Analog Shaker, VWR) at 200 rpm. The resulting culture was used to inoculate a second culture in 50 mL of LB medium until an optical density (OD) of 0.8 at 600 nm was reached. The bacteria were collected by centrifugation at 8,000 x g for 10 min at 4 °C, washed three times with sterile PBS (pH 7.4) and finally suspended in LB broth to get a final concentration of 1.05×10^9 cells per ml (OD = 1.31 at 600 nm) for biofilm formation test. In the dynamic method, PU (stainless steel, wood, and glass) substrates, superglue coated substrates and DURA-Z coated substrates were placed in bacterial culture medium (LB Broth) containing highly concentrated bacteria (1.05×109 cells per ml) at 37 °C for 30 days under continuous shaking (300 rpm). The culture medium was gently refreshed every two days, and the bacterial density within the refreshed medium was kept at 1.05×10^9 cells per ml. In the static method, PU substrates, superglue coated substrates and DURA-Z coated substrates were stationarily placed in bacterial culture medium (LB Broth) containing highly concentrated bacteria (1.05×10^9 cells per ml) at 37 °C for 30 days. Bacteria were allowed to settle on the surface of the substrates through gravity. The culture

medium was gently refreshed day by day, and the bacterial density within the refreshed medium was kept at 1.05×10^9 cells per ml. After long-term incubation, all substrates were rinsed with PBS for 30 mins (samples tested in the static method were also imaged without rinsing). After the challenging periods, the substrates were then immersed in the fix solution of 2.5% glutaraldehyde, 2% paraformaldehyde in 0.1 M sodium phosphate buffer and were then dehydrated in a gradient ethanol series and dried in vacuum before SEM imaging. Adhered bacteria density was counted by averaging 6 randomly selected areas (100 μm^2 each).

5.3 Results and discussion

The formation of DURA-Z coating involves the combined use of a fabricated double-sided DURA-Z tape and superglue obtained from the hardware store. DURA-Z tape was prepared by the in-situ growing of a thin layer of zwitterionic poly-carboxybetaine acrylamide (PCBAA, 3-((3-acrylamidopropyl) -dimethylammonio)-propanoate) hydrogel on a commercial polypropylene (pp) liner **(Figure 5-1(a))**. The fabricated hydrogel tape was mechanically stronger than the pure zwitterionic PCBAA hydrogel and can withstand pulling, bending, wrenching and rolling up **(Figure 5-1(b))**. This ensures ease of storage, transport, and mounting of the DURA-Z tape on substrates to be coated. The fabricated DURA-Z tape can be directly mounted as a coating layer without further treatment.

The DURA-Z coating can be glued on a variety of substrates through a simple procedure **(Figure 5-1(c))**. Briefly, a substrate was firstly cleaned, e.g., the polyurethane (PU) substrate was rinsed with alcohol and dried in air. Then one drop

of cyanoacrylate superglue was applied onto the dried substrate, followed by pressing the DURA-Z tape (hydrogel layer facing down) onto the superglue for a few seconds. One hour was allowed to completely solidify the superglue. The liner on top of the hydrogel was removed, and the glued coating was transferred to DI water for equilibrium. 20 mins later, the DURA-Z coating was polished either by a small shovel or tweezer, leaving the surface with a thin layer of coating.

The resulting DURA-Z coating showed completely different morphology compared to PU substrate or cyanoacrylate superglue surface under Scanning Electron Microscope (SEM, **Figure 5-2(a)**), and Atomic-force Microscope (AFM, **Figure 5-3**). SEM images on coating cross-section provided structural details of a surface hydrogel layer and a hydrogel/glue interpenetrating layer **(Figure 5-2(a))**. The overall thickness of the coating (two layers) was measured to be 324±13 μm. The surface of the DURA-Z coating was characterized by Infrared (IR) spectroscopy and showed almost the same chemical composition as pure zwitterionic PCBAA hydrogel **(Figure 5-2(c))**. This implied the surface of the DURA-Z coating had superior anti-fouling property as good as a zwitterionic hydrogel. Water contact angle **(Figure 5-2(b))** indicated that DURA-Z coating was super-hydrophilic with great wettability (water drop spread out quickly), similar to pure PCBAA hydrogel surface.

Super-hydrophilic polymer coatings were known to be unstable since polymers drastically tended to dissolve in water. Common hydrophilic coatings would fail within a few weeks in an aqueous environment. We incubated the DURA-Z coating in DI water at room temperature for up to three months. The morphology of the

coating was almost unchanged, and anti-fouling property (tested by human fibrinogen binding followed by ELISA quantification of the absorbed protein) was retained at the same level as freshly-made coatings after the long-term incubation **(Figure 5-4(a))**. DURA-Z coating was further examined under various durability tests in the water condition, including (1) exposed to PBS buffer shearing (1500 rpm, 202G) at room temperature for 50 days **(Figure 5-4(b))**, (2) exposed to PBS shearing (1500 rpm, 202G) at body temperature (37 °C) for 30 days **(Figure 5-5(a))**, and (3) subjected to continuous perpendicular water-flush at a flow rate of 42.8 ml/s for 30 days **(Figure 5-5(b))**. These challenging conditions did not change the morphology of the DURA-Z coating, and the antifouling property of the coating was well retained, indicated by the unchanged, significantly lowered human fibrinogen absorption on the coating, compared with uncoated PU **(Figure 5-5(a) and (b))**.

The DURA-Z coating was further subjected to mechanical damage tests. We used a sharp scalpel to randomly scratch the coating **(Figure 5-5(d))**. The coating retained its small water contact angle and great anti-fouling property **(Figure 5-5(d))**. We further examined the coating in an abrasion test, where a PU coupon with both sides coated with DURA-Z was placed between two stationary sandpapers (400 grit) and a pressure of 570 kPa was applied by a compressor **(Figure 5-5(c))**. The coupon was moved back and forth (displacement = 1 cm) for 20 circles and the coating was found to survive this abrasion test with great water wettability, and unchanged great anti-fouling property **(Figure 5-5(c))**. It should be noted that the 570 kPa pressure used in our abrasion test is more than 150 times higher than other similar tests for

coating stability. In our sandpaper abrasion test, a PU coupon without DURA-Z coating applied cannot be moved by manpower under a pressure of 50 kPa. It appears that the slippery surface of DURA-Z coating contributes to its great capability to resist abrasion damage.

Microorganism attachment on surfaces leads to biofilm formation that causes medical device failure, infection and marine fouling related fuel penalty. Hydrophilic polymer coatings, such as zwitterionic polymers, are non-toxic and environmentally friendly and have shown their effectiveness in resisting microorganism adhesion[185-187]. Nevertheless, due to the instability of hydrophilic polymers in an aqueous environment, these coatings were not able to maintain the resistance to microorganism adhesion for a longer period of time. Here we expect the ultra-durable and robust DURA-Z coating can greatly improve long-term microorganism resistance performance. To highlight this property, we utilized *Escherichia coli* (*E. coli*) as a model system to study the coating's resistance to biofilm formation and quantified the bacterial adhesion by SEM. Our initial study has challenged the coating with dynamic bacterial culture condition. DURA-Z coated PU substrate was placed in bacterial culture medium (Luria-Bertani Broth) containing an extremely high number of bacteria (1.05×10^9 cells per ml) at 37 °C for 30 days under continuous shaking (300 rpm). The culture medium was gently refreshed every two days, and the bacterial density within the refreshed medium was kept at 1.05×10^9 cells per ml. After 30 days, bacteria on the substrate surface were fixed, dehydrated, vacuumed and visualized under SEM. Results indicate almost zero adhesion of

bacteria on the zwitterionic DURA-Z coating, while biofilm had developed on the bare PU substrate and the superglue coated surface **(Figure 5-6 (a) and (b))**.

We further challenged the DURA-Z coating with one of the harshest condition, where high-density bacteria (1.05×10^9 cells per ml) were stationarily cultured with the substrate in LB broth at 37 °C, and allowed to settle on the substrate surface through gravity. The culture medium was gently refreshed day by day, and the bacterial density within the refreshed medium was maintained at 1.05×10^9 cells per ml. After 30 days, without any rinsing, only a small amount of bacteria was found to be scattered on DURA-Z coating (no biofilm forming) under SEM **(Figure 5-7)**. With 30 min of rinsing in PBS, these scattered bacteria were easily washed off from the DURA-Z coating **(Figure 5-6(c) and (d))**. By contrast, a biofilm (high-density bacteria adhered) formed on the bare PU substrate and superglue coated substrate, and remained to be firmly attached even after rinsing **(Figure 5-6(c) and (d))**. It should be noted that long-term biofilm resistance was highly desirable to reduce infection and extend medical device lifetime, but remained a challenge in the field[188]. We attribute the observed remarkable long-term biofilm resistance to the combined effect of ultra-low fouling property and ultra-durability of the zwitterionic DURA-Z coating.

The DURA-Z coating can be easily applied to a variety of substrates including stainless steel, wood, and glass **(Fig. 5-8(a))** by combining the use of DURA-Z tape and superglue. It should be noted that the glass substrate was pre-treated with a thin layer of EVO-Stik glue before applying the coating due to the low affinity between cyanoacrylate superglue and glass. DURA-Z coatings obtained on these

substrates were also found to be durable as indicated by unchanged great anti-fouling property even after two months of incubation in water **(Figure 5-9)**. They were also tested for *E. coli* biofilm resistance for 30 days using dynamic bacterial challenge condition. Almost zero bacteria adhesion was achieved on all tested DURA-Z coatings despite different types of substrates were coated **(Figure 5-10)**.

Practically speaking, it is frequently desirable that a coating layer can be fully removed from the substrate, followed by a new coating to be re-applied seamlessly[189]. However, reapplication of coating was hard to realize based on the chemical modification methods[190-192] without significantly damaging the original substrates. Here the DRUA-Z coating binds with the substrate surface through commercial superglues which are dissolvable in organic solvents. Take DURA-Z coated stainless steel for example **(Figure 5-8(b))**, upon 1-hour incubation in acetone, the coating came off spontaneously without any damage to the substrate surface. It is feasible to re-apply a new DURA-Z coating on this same stainless steel substrate, and the new coating resisted protein binding as efficient as when it was first applied **(Figure 5-8(c))**.

The key for the DURA-Z coating to achieve the ultra-durability is because of the use of superglue to strongly bind the super-hydrophilic polymer network (PCBAA hydrogel) and a hydrophobic substrate together. This is against common sense since commercial superglue is known to only bind hydrophobic substrates. Superglues are based on the rapid solidification of hydrophobic cyanoacrylate polymers, which have low affinity with hydrophilic materials such as zwitterionic polymers. In fact, we tried

to glue linear zwitterionic PCBAA polymer powder and highly concentrated PCBAA/water solution on substrates using superglue, but the attached polymers quickly dissolved upon incubation in water and both obtained surfaces showed hydrophobic nature **(Figure 5-11)**. The success of using superglue to strongly bind hydrophilic zwitterionic hydrogel layer (DURA-Z coating) is attributed to the unique inter-penetration structure formed between these two **(Figure 5-2(a) and (d))**. It is expected that during the curing process, liquid cyanoacrylate monomers penetrated into the zwitterionic hydrogel network and were crosslinked. The entanglement between the DURA-Z and superglue networks immobilized the coating on the substrate for as long and strong as the superglue adhesive can last.

For biofilm resistance performance, DURA-Z coating is unprecedented. State-of-the-art anti-fouling coatings started to accumulate bacteria after just a few hours of contact and would be covered with dense biofilm usually within ~7 days. DURA-Z coating was able to achieve almost “zero” bacteria adhesion even after one-month continuous contact with high concentration bacteria. This coating technology is convenient to apply and can promisingly solve the biofilm threat, which deteriorates public health and impedes the function of most biomedical devices.

In summary, we developed an ultra-durable and robust zwitterionic polymer network coating, namely DURA-Z, by combining the use of commercial superglue and the developed DURA-Z tapes. DURA-Z coating showed great stability and durability in a series of long-term challenges in aqueous environments as well as

mechanical damage tests. With superior anti-fouling and durable property, the coating was able to achieve almost zero adhesion of bacteria after one-month continuous co-culture with *E. coli* bacteria at extremely high density. DURA-Z coating is applicable to various common substrates to achieve long term durability and anti-fouling performance, and when needed, it can be easily removed and re-applied. This simple and inexpensive method will find applications as anti-fouling coatings in large, such as anti-biofilm coatings, medical device coatings and marine coatings.

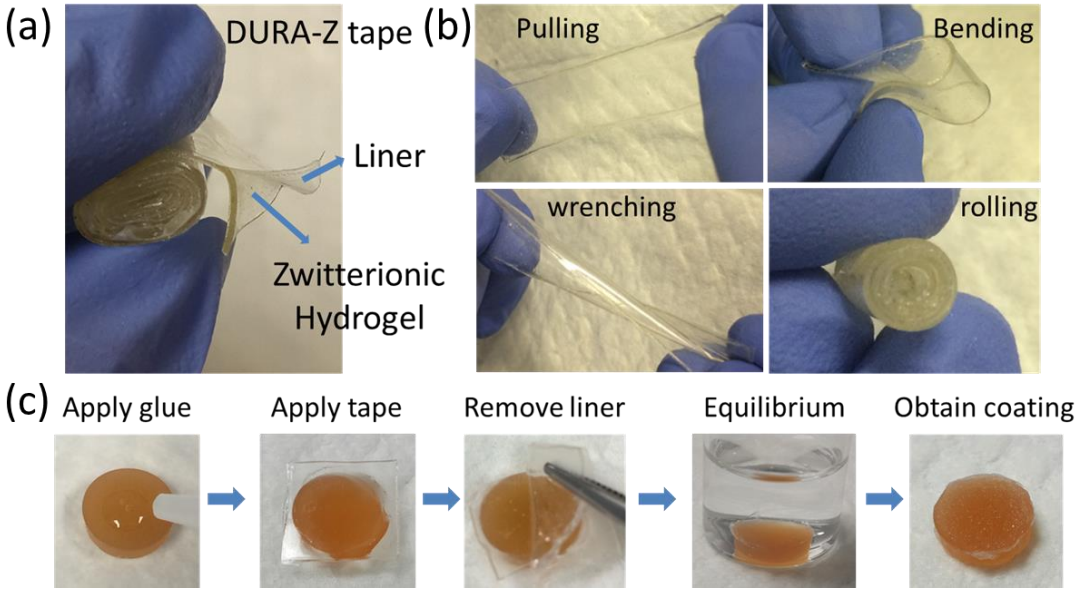

Figure 5-1 (a) structure of DURA-Z tape, (b) DURA-Z tape under pulling, bending wrenching and rolling, and (c) fabrication of DURA-Z coating on PU substrate.

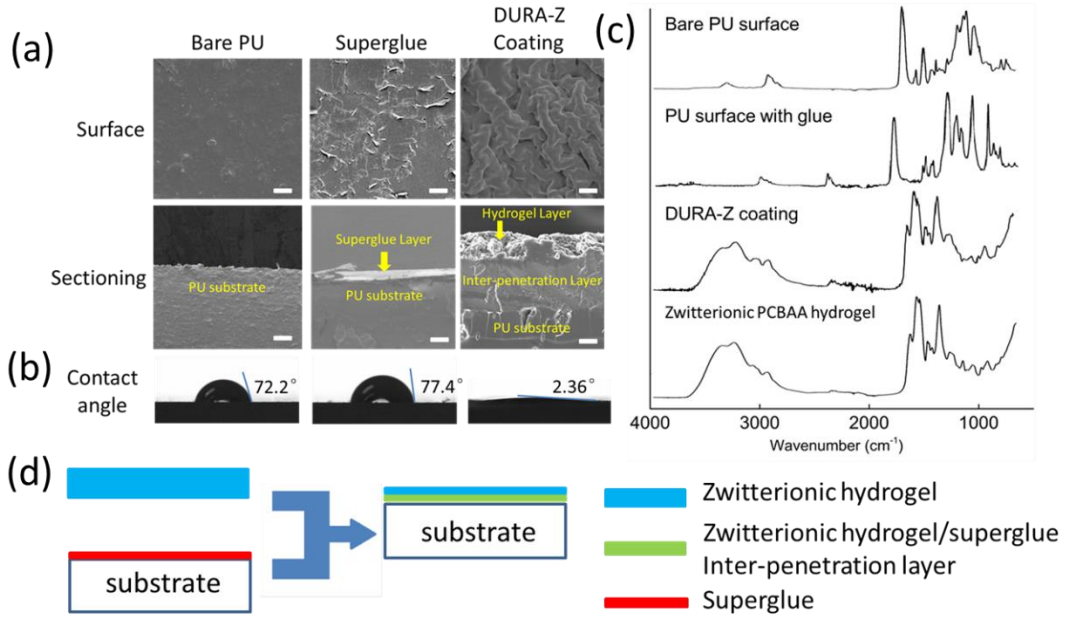

Figure 5-2 (a) SEM imaging on the surface and sectioning of uncoated PU, superglue and DURA-Z coated substrates (scale bar = 100 μm), (b) water contact angles on bare PU, superglue and DURA-Z coated substrates, (c) IR spectra of bare PU surface, superglue coated PU surface, DURA-Z coated surface and zwitterionic PCBAA hydrogel surface, and (d) illustration of the formation of DURA-Z coating.

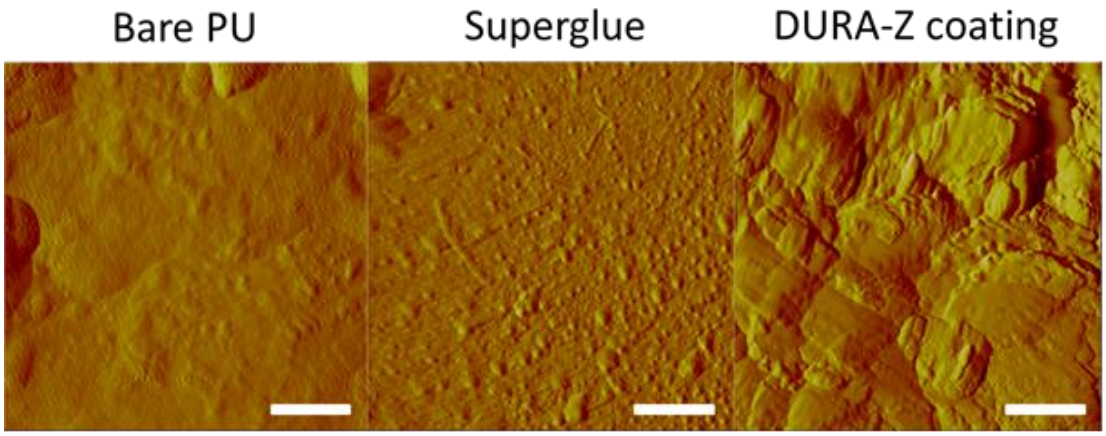

Figure 5-3 AFM images of bare PU substrate, superglue and DURA-Z coated PU substrates. Scale bar = 50 µm.

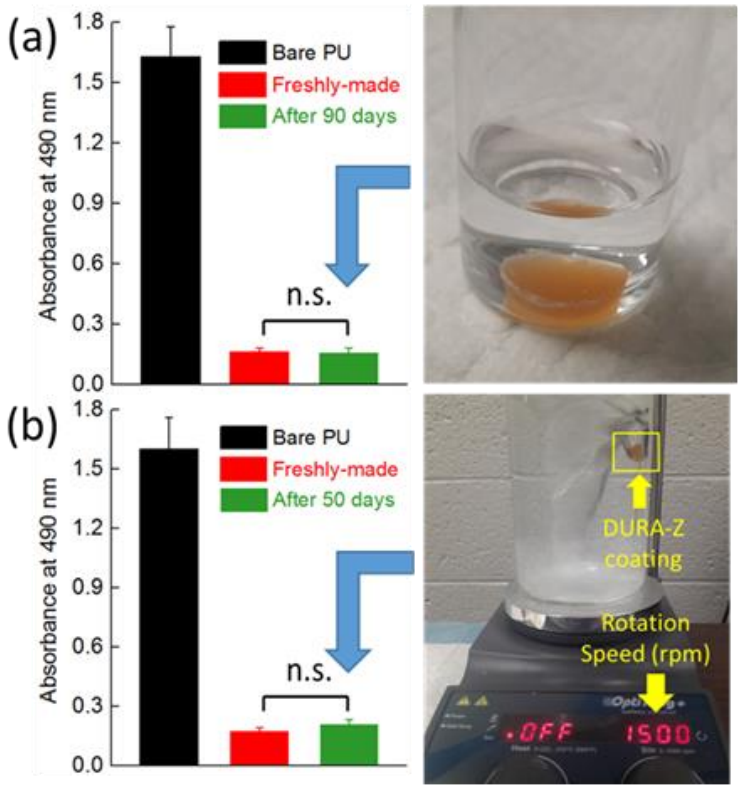

Figure 5-4 Antifouling property of DURA-Z coating after durability tests. (a) 3-month incubation in water and (b) 50 days exposure to PBS shearing at room temperature. Data were showed as mean of replicates (n=3) ± standard deviation. Statistical analysis: unpaired, two-tailed t-test, n.s.: no significant difference at $P > 0.05$, meaning the great anti-fouling property was retained.

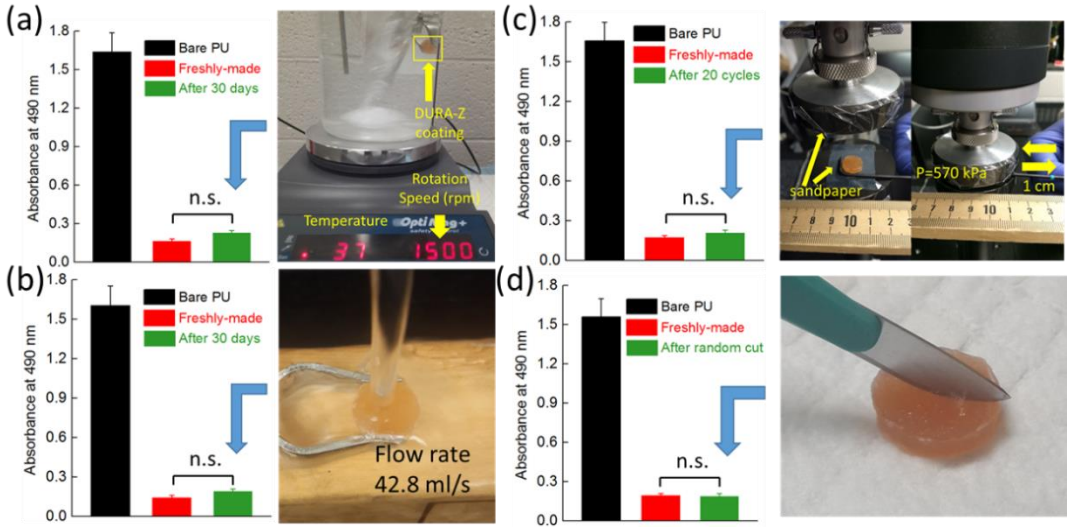

Figure 5-5 Antifouling property of DURA-Z coating after various durability and mechanical damage tests. (a) 30 days exposure to PBS shearing under body temperature, (b) 30 days exposure to perpendicular water flush, (c) 20 cycles of abrasion test under 570 kPa, and (d) random scratch by a scalpel. The antifouling property was evaluated by the resistance of human fibrinogen binding on the surface (absorbed protein) before and after the coating being challenged. All data were showed as mean of replicates (n=3) ± standard deviation. Statistical analysis: unpaired, two-tailed t-test, n.s.: no significant difference at $P > 0.05$, meaning the great anti-fouling property was retained.

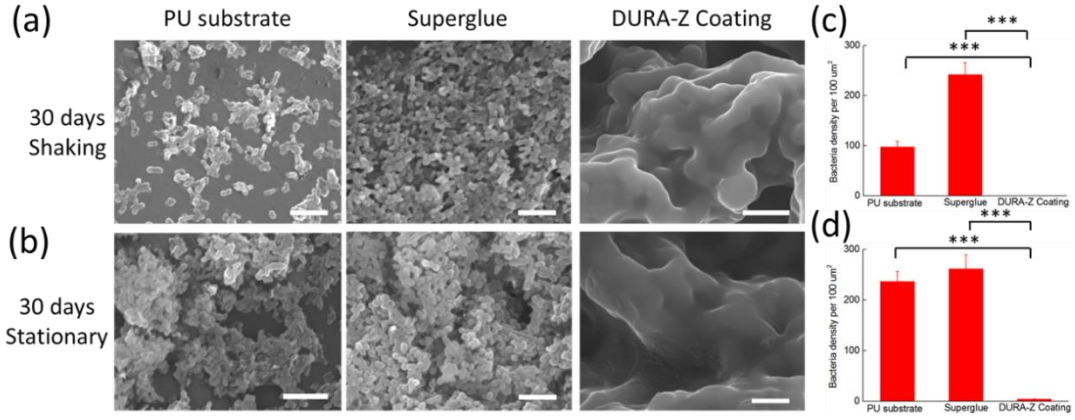

Figure 5-6 representative SEM images of bacteria adhesion on bare PU, superglue and DURA-Z coated PU substrates after 30 days of co-culture with E. coli bacteria at (a) shaking condition and (b) static condition. Attached bacterial density was calculated for (c) shaking condition and (d) static condition. ***: All data are presented as mean of biological replicates (n=6) ± standard deviation. Statistical analysis: one-way ANOVA with Bonferroni multi-comparison. ***: $p < 0.0001$. Scale bar = 5 µm.

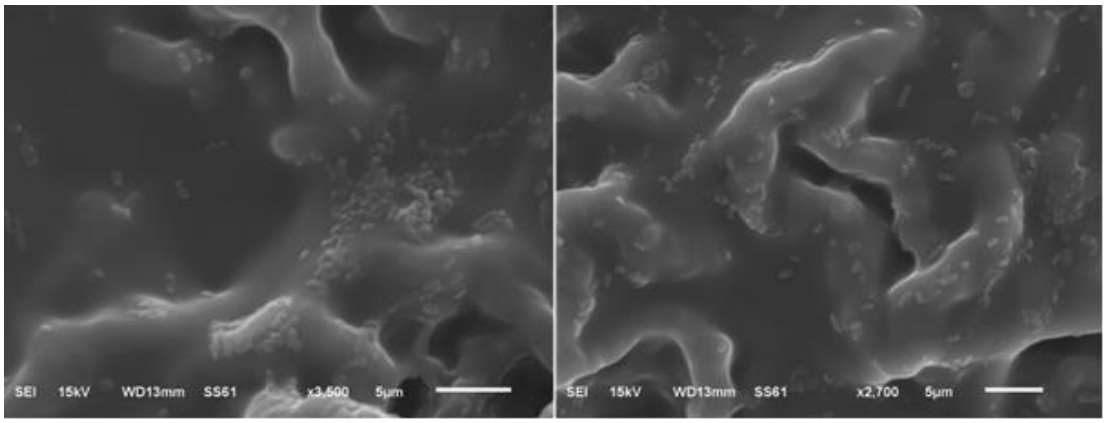

Figure 5-7 representative SEM images showing bacteria adhesion on DURA-Z coating after 30 days of culture with bacteria at static condition without any rinsing. Scale bar = 5 μm.

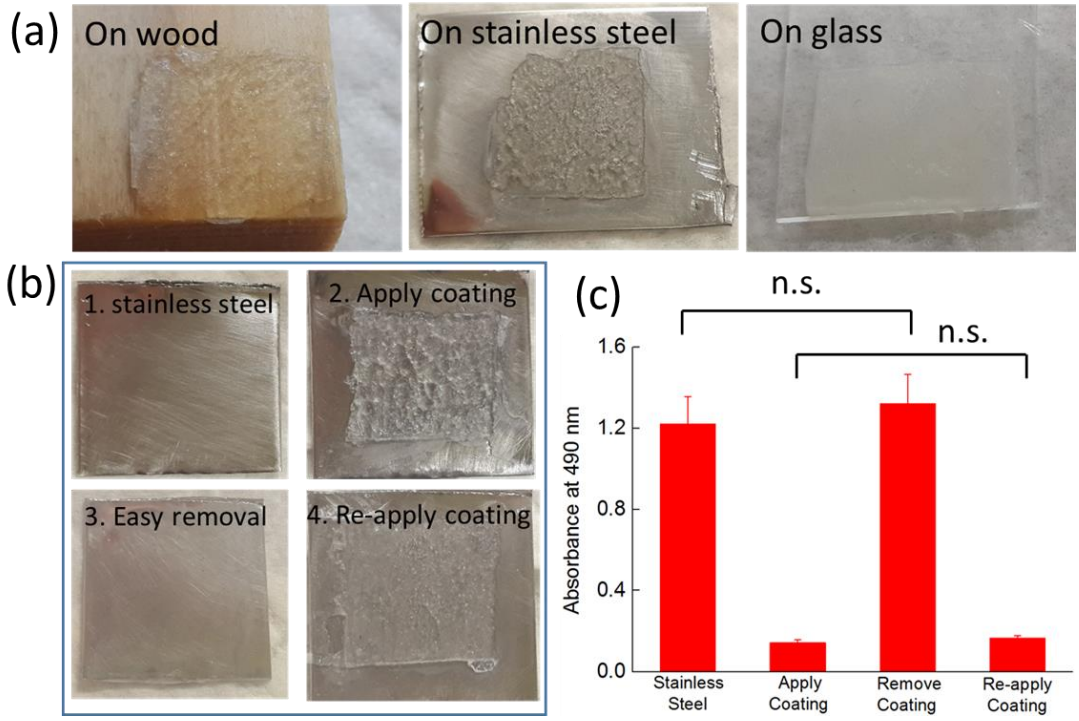

Figure 5-8 (a) DURA-Z coating on wood, stainless steel, and glass substrates. (b) Easy removal and re-application of DURA-Z coating on stainless steel substrate, and (c) corresponding antifouling property. All data were showed as mean of replicates (n=3) ± standard deviation. Statistical analysis: unpaired, two-tailed t-test, n.s.: no significant difference at $P > 0.05$.

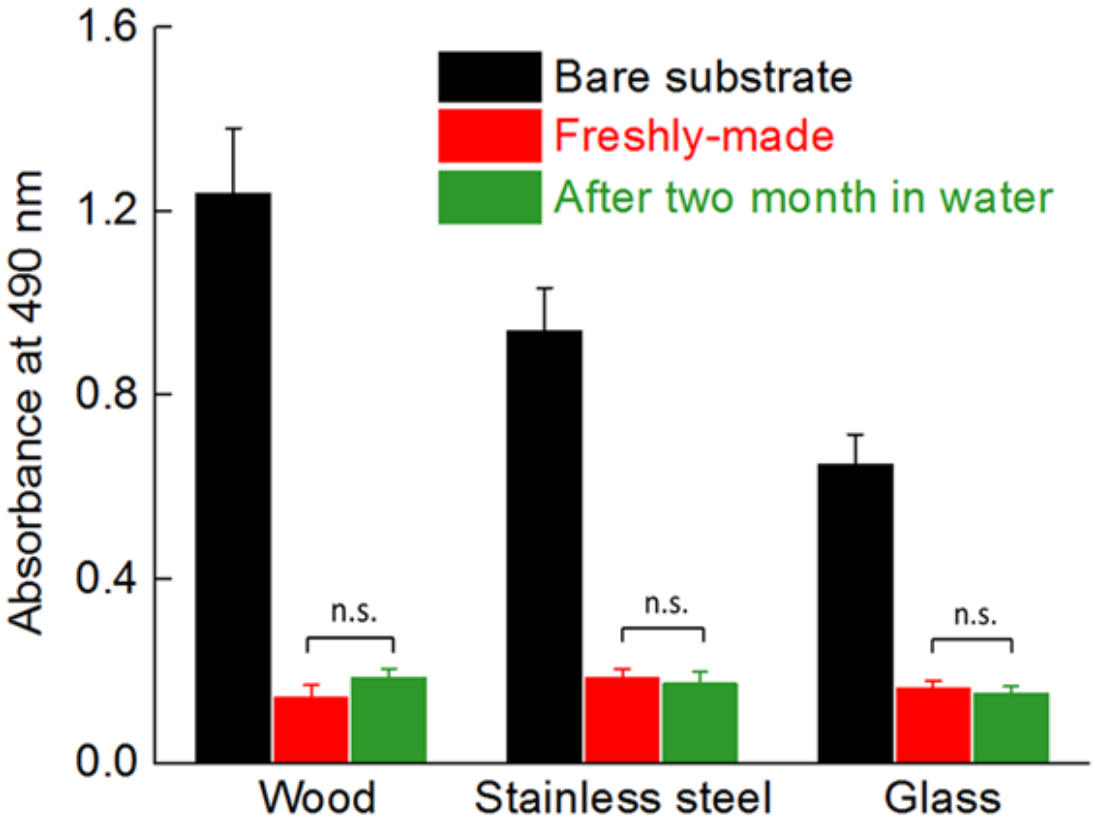

Figure 5-9 Antifouling property of DURA-Z coating on wood, stainless steel and glass substrates after two-month incubation in water. All data were showed as mean of replicates (n=3) ± standard deviation. Statistical analysis: unpaired, two-tailed t-test, n.s.: no significant difference at $P > 0.05$, meaning the great anti-fouling property was retained.

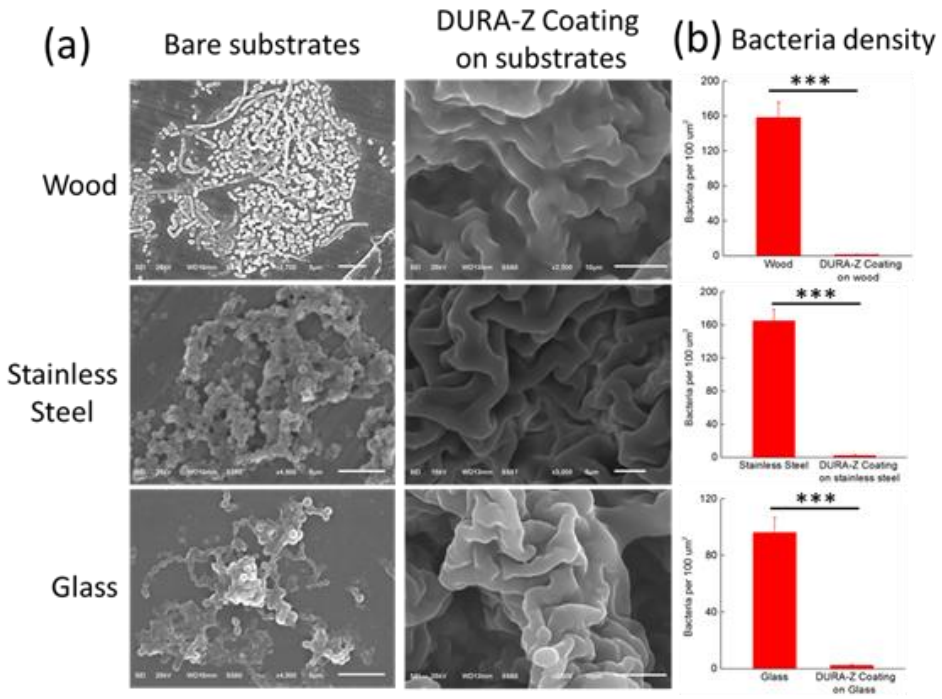

Figure 5-10 (a) representative SEM images of bacteria adhesion on wood, stainless steel, glass and DURA-Z coating on these substrates after 30 days of co-culture with bacteria at shaking condition, and (b) calculated bacterial density on wood, stainless steel, glass and DURA-Z coatings on these substrates. All data are presented as mean of biological replicates (n=6) ± standard deviation. Statistical analysis: unpaired two-tailed t-test, ***: $p < 0.0001$. scale bar = 10 µm.

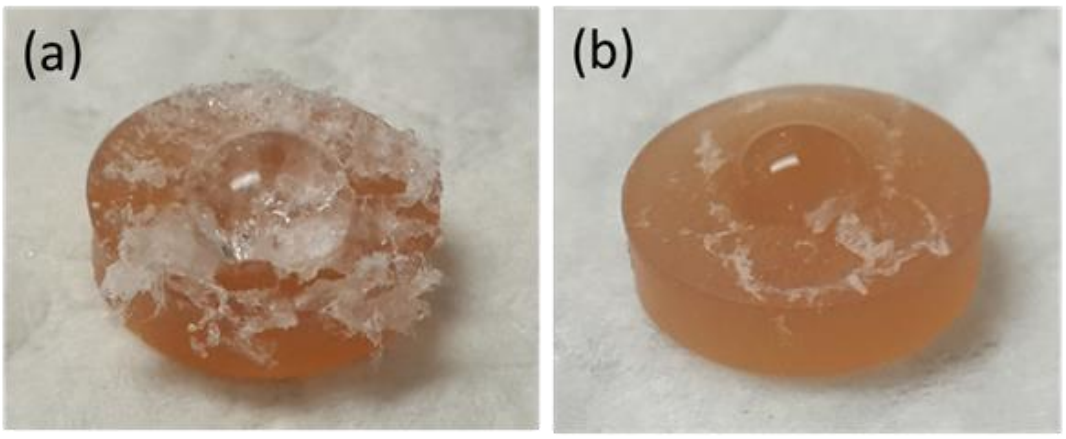

Figure 5-11 (a) PCBAA polymer powder and (b) PCBAA water solution were glued on PU substrates. The coated surface showed hydrophobic nature after incubation in water, as indicated by the non-spread water droplet.

CHAPTER 6. CONCLUSION AND OUTLOOK

The focus of this thesis is to study the potentials of the zwitterionic PCB materials in solving several key challenges in various applications as stabilizing materials for nanoparticles, hydrogels, and surface coatings, respectively. Specifically, this thesis involves the work of a one-step synthesis of zwitterionic polymer modified carbon nanoparticles, pancreatic islets encapsulation by PCB hydrogel materials and subsequent transplantation to achieve long-term diabetic reversal effect, and a durable zwitterionic PCB polymer coating for various substrates to resist long-term biofilm formation. These subjects are introduced separately in the following paragraphs.

The study on the ultra-stable carbon nanoparticles was a novel strategy to fabricate core-shell NPs with superior stability directly and solely from anti-fouling zwitterionic polymers through single step of microwave heating. We found that Only those zwitterionic polymers that are stable through high temperature microwave heating can produce zwitterionic polymer shell-carbon core NPs, which can be further purified through sucrose gradient centrifugation. The resulting nanoparticle showed superior colloid stability in bio-relevant media and even the freeze-drying conditions. We expect this green chemistry in making ultra-stable NPs can inspire future functional NPs to be developed. These ultra-stable florescent carbon nanoparticles will find applications in cell labelling and trackable drug delivery systems.

The project on islet transplantation exhibited the first synthetic polymer material

ever known promoting functional neovascularization as good as natural body system. A zwitterionic carboxy betaine containing hydrogel was found to promote vascularization at the subcutaneous (s.c.) site to the same density level as normal tissue, and to maintain that high-level vasculature for at least 6 months. The newly formed blood vessels were perfused and they approached the implanted zwitterionic gel surface as close as below 20 micrometers away. Consequently, the zwitterionic hydrogel was highly accessible by circulating blood, even after 5 months of implantation. This finding was highlighted by using zwitterionic hydrogel in encapsulating islets for the treatment Type 1 diabetes. The zwitterionic hydrogel based novel system remarkably outperforms the state-of-the-art technology using alginate encapsulating materials at highly challenging s.c. site. We expect, with natural tissue-like blood accessibility, the zwitterionic hydrogel is a promising platform to improve the long-term performance of most current implantable devices to fight against various diseases.

For the study on tough and durable zwitterionic polymer coating to resist micro-organism biofilm, we first developed a novel zwitterionic macro-crosslinker to overcome the vulnerability of zwitterionic coating on common hydrophobic polyrethane substrate. Coating formed using the macro-crosslinker exhibited much greater thickness and durability compared to common polymer brush coating and brush coating crosslinked with small-molecule crosslinkers. Upon incubation in water, macro-crosslinker coating was able to sustain hydrophilicity for more than two weeks. Even under shear flow condition, the macro-crosslinker coating was able to retain its

anti-fouling property to resist protein and bacteria adsorption after one week treatment. The durable zwitterionic macro-crosslinker coating can be potentially applied to resist micro-organism adhesion on blood-contact biomedical devices or for marine coating applications.

For the anti-biofilm purpose, the durability of the macro-crosslinker coating was not enough. We then the developed a DURA-Z coating to further increase the durability and toughness of zwitterionic coating that was able to resist long term biofilm resistance. The DURA-Z coating can be easily and universally applied on common substrates. Against conventional wisdom, commercial superglue only for binding hydrophobic materials was used to strongly immobilize the super-hydrophilic DURA-Z coating through interpenetration. The fabricated DURA-Z coating retained anti-fouling property after 90 days of immersion in water, 50 days of buffer shearing and 30 days of water-flushing, and after repeated knife-scratch and sandpaper abrasion under 570 kPa. The DURA-Z coating achieved a rarely reported long-term biofilm resistance: it remained almost "zero" bacteria adhesion after continuously challenged by more than 10^9 bacterial cells per ml culture medium for 30 days. The DURA-Z coating greatly extended the industrial application of zwitterionic polymer coating by overcoming the durability and toughness challenges, and can be applied in medical devices and marine coating to protect working surfaces from biofilm growth for the long term reliable use.

REFERENCES

1. Lowe, A. B.; McCormick, C. L., *Chem. Rev.* **2002,** *102* (11), 4177-4189.
2. Jiang, S. Y.; Cao, Z. Q., *Adv. Mater.* **2010,** *22* (9), 920-932.
3. Chen, S. F.; Jiang, S. Y., *Adv. Mater.* **2008,** *20* (2), 335-340.
4. Cao, Z. Q.; Yu, Q. M.; Xue, H.; Cheng, G.; Jiang, S. Y., *Angew. Chem. Int. Edit.* **2010,** *49* (22), 3771-3776.
5. Yuan, Y. Y.; Mao, C. Q.; Du, X. J.; Du, J. Z.; Wang, F.; Wang, J., *Adv. Mater.* **2012,** *24* (40), 5476-5480.
6. Zhang, L.; Cao, Z. Q.; Bai, T.; Carr, L.; Ella-Menye, J. R.; Irvin, C.; Ratner, B. D.; Jiang, S. Y., *Nat. Biotechnol.* **2013,** *31* (6), 553-565.
7. Jiang, H.; Wang, X. B.; Li, C. Y.; Li, J. S.; Xu, F. J.; Mao, C.; Yang, W. T.; Shen, J., *Langmuir* **2011,** *27* (18), 11575-11581.
8. Bai, T.; Sun, F.; Zhang, L.; Sinclair, A.; Liu, S. J.; Ella-Menye, J. R.; Zheng, Y.; Jiang, S. Y., *Angew. Chem. Int. Edit.* **2014,** *53* (47), 12729-12734.
9. Klein, J., *Polym. Advan. Technol* **2012,** *23* (4), 729-735.
10. Smith, R. S.; Zhang, Z.; Bouchard, M.; Langer, R.; Loose, C., *Sci. Transl. Med.* **2012,** *4* (153).
11. Zhang, Z.; Finlay, J. A.; Wang, L. F.; Gao, Y.; Callow, J. A.; Callow, M. E.; Jiang, S. Y., *Langmuir* **2009,** *25* (23), 13516-13521.
12. Greim, H.; Ahlers, J.; K.; Bayer, E., *Chemosphere* **1994,** *28* (12), 2203-2236.
13. Chen, S. F.; Liu, L. Y.; Jiang, S. Y., *Langmuir* **2006,** *22* (6), 2418-2421.
14. Ueda, T.; Oshida, H.; Kurita, K.; Ishihara, K.; Nakabayashi, N., *Polym. J.* **1992,** *24*

(11), 1259-1269.

15. Ladenheim, H.; Morawetz, H., *J. Polym. Sci.* **1957,** *26* (113), 251-254.
16. Zhang, Z.; Vaisocherova, H.; Cheng, G.; Yang, W.; Xue, H.; Jiang, S. Y., *Biomacromolecules* **2008,** *9* (10), 2686-2692.
17. Ladd, J.; Zhang, Z.; Chen, S.; Hower, J. C.; Jiang, S., *Biomacromolecules* **2008,** *9* (5), 1357-1361.
18. Ueland, P. M.; Hustad, S., *Clin. Chem. Lab. Med.* **2005,** *43* (10), 1069-1075.
19. Wang, Z.; Ma, G. L.; Zhang, J Chen, S. F., *Langmuir* **2014,** *30* (13), 3764-3774.
20. Zhang, Z.; Chen, S. F.; Jiang, S. Y., *Biomacromolecules* **2006,** *7* (12), 3311-3315.
21. Hadjesfandiari, N.; Yu, K.; Mei, Y.; Kizhakkedathu, J. N., *J. Mater. Chem. B* **2014,** *2* (31), 4968-4978.
22. Cao, Z. Q.; Jiang, S. Y., *Nano Today* **2012,** *7* (5), 404-413.
23. Zhang, L.; Jiang, S. Y., *Acs Nano* **2012,** *6* (8), 6681-6686.
24. Konradi, R.; Acikgoz, C.; Textor, M., *Macromol. Rapid. Comm.* **2012,** *33* (19), 1663-1676.
25. Zhang, Z.; Ratner, B. D.; Jiang, S. Y., *J. Biomat. Sci-Polym. E* **2009,** *20* (13), 1845-1859.
26. Jia, G. W.; Cao, Z. Q.; Xue, H.; Xu, Y. S.; Jiang, S. Y., *Langmuir* **2009,** *25* (5), 3196-3199.
27. Yang, W.; Zhang, L.; Wang, S. L.; White, A. D.; Jiang, S. Y., *Biomaterials* **2009,** *30* (29), 5617-5621.
28. Chen, Y. J.; Xiong, Z. C.; Ye, M. L.; Zou, H. F., *Nanoscale* **2015,** *7* (7), 3100-3108.

29. Wei, W.; Cao, Z. Q., *Sci. China. Technol. Sc.* **2016,** *59* (12), 1968-1970.

30. Weber, L. M.; Cheung, C. Y.; Anseth, K. S., *Cell Transplant.* **2007,** *16* (10), 1049-1057.

31. Weber, L. M.; Lopez, C. G.; Anseth, K. S., *J. Biomed. Mater. Res. A* **2009,** *90a* (3), 720-729.

32. Su, J.; Hu, B. H.; Lowe, W. L.; Kaufman, D. B.; Messersmith, P. B., *Biomaterials* **2010,** *31* (2), 308-314.

33. Davis, N. E.; Beenken-Rothkopf, A. E.; Fontaine, M. J., *Biomaterials* **2012,** *33* (28), 6691-6697.

34. Nguyen, K. T.; West, J. L., *Biomaterials* **2002,** *23* (22), 4307-4314.

35. Weber, L. M.; Anseth, K. S., *Matrix. Biol.* **2008,** *27* (8), 667-673.

36. Christensen, L. H.; Kebuladze, I., *Plast. Reconstr. Surg.* **2003,** *111* (6), 1883-1890.

37. Suzuki, Y.; Nishimura, Y.; Tanihara, Yamawaki, Y.; Kakimaru, Y., *J. Biomed. Mater. Res.* **1998,** *39* (2), 317-322.

38. Li, X. Y.; Chen, H. N.; Epstein, P. N., *J. Biol. Chem.* **2004,** *279* (1), 765-771.

39. Onuki, Y.; Bhardwaj, U.; Papadimitrakopoulos, F.; Burgess, D. J., *J. Diabetes. Sci. Technol.* **2008,** *2* (6), 1003-15.

40. Sakata, S.; Inoue, Y.; Ishihara, K., *Langmuir* **2014,** *30* (10), 2745-2751.

41. Ye, S. H.; Jang, Y. S.; Wagner, W. R., *Langmuir* **2013,** *29* (26), 8320-8327.

42. Lewis, A. L., *Colloid Surface B* **2000,** *18* (3-4), 261-275.

43. Byambaa, B.; Konno, T.; Ishihara, K., *Colloid Surface B* **2012,** *99*, 1-6.

44. Inoue, Y.; Nakanishi, T.; Ishihara, K., *React. Funct. Polym.* **2011,** *71* (3), 350-355.

45. Cheng, G.; Jiang, S. Y., *Biomaterials* **2007,** *28* (29), 4192-4199.

46. Cheng, G.; Li, G. Z.; Xue, H.; Chen, S. F.; Bryers, J. D.; Jiang, S. Y., *Biomaterials* **2009,** *30* (28), 5234-5240.

47. Wang, W.; Lu, Y.; Xie, J. B.; Zhu, H.; Cao, Z. Q., *Chem. Commun.* **2016,** *52* (25), 4671-4674.

48. Zhao, C.; Zheng, J., *Biomacromolecules* **2011,** *12* (11), 4071-4079.

49. Zhang, L.; Gu, F. X.; Chan, J. M.; Wang, A. Z.; Langer, R. S.; Farokhzad, O. C., *Clin Pharmacol. Ther.* **2008,** *83* (5), 761-769.

50. Hotze, E. M.; Phenrat, T.; Lowry, G. V., *J. Environ. Qual.* **2010,** *39* (6), 1909-1924.

51. Kim, T.; Lee, C. H.; Joo, S. W.; Lee, K., *J. Colloid. Interf. Sci.* **2008,** *318* (2), 238-243.

52. Basu, S.; Ghosh, S. K.; Kundu, S.; Panigrahi, S.; Praharaj, S.; Pande, S.; Jana, S.; Pal, T., *J. Colloid. Interf. Sci.* **2007,** *313* (2), 724-734.

53. Yang, W.; Ella-Menye, J. R.; Liu, S. J.; Bai, T.; Wang, D. Q.; Yu, Q. M.; Li, Y. T.; Jiang, S. Y., *Langmuir* **2014,** *30* (9), 2522-2529.

54. Murthy, A. K.; Stover, R. J.; Johnston, K. P., *J. Am. Chem. Soc.* **2013,** *135* (21), 7799-7802.

55. McFarlane, N. L.; Wagner, N. J.; Kaler, E. W.; Lynch, M. L., *Langmuir* **2010,** *26* (17), 13823-13830.

56. Zhang, Y. F.; Yin, Q.; Lu, H.; Xia, H. W.; Lin, Y.; Cheng, J. J., *Acs. Macro. Lett.* **2013,** *2* (9), 809-813.

57. Cheng, J.; Teply, B. A.; Sherifi, I.; Langer, R.; Farokhzad, O. C., *Biomaterials* **2007,** *28* (5), 869-876.

58. Kataoka, K.; Nagasaki, Y., *Adv. Drug. Deliver. Rev.* **2012,** *64*, 37-48.

59. Rosler, A.; Klok, H. A., *Adv. Drug. Deliver. Rev.* **2012,** *64*, 270-279.

60. Wei, H.; Zhuo, R. X., *Prog. Polym. Sci.* **2009,** *34* (9), 893-910.

61. Chang, C.; Zhuo, R. X., *Macromolecules* **2009,** *42* (13), 4838-4844.

62. Pastoriza-Santos, I.; Liz-Marzan, L. M., *Langmuir* **2002,** *18* (7), 2888-2894.

63. Nowinski, A. K.; White, A. D.; Keefe, A. J.; Jiang, S. Y., *Langmuir* **2014,** *30* (7), 1864-1870.

64. Baker, S. N.; Baker, G. A., *Int. Edit.* **2010,** *49* (38), 6726-6744.

65. Wang, W.; Li, Y. M.; Cheng, L.; Cao, Z. Q.; Liu, W. G., *J. Mater. Chem. B* **2014,** *2* (1), 46-48.

66. Liu, C. J.; Zhang, P.; Wang, W.; Liu, W. G., *Biomaterials* **2012,** *33* (13), 3604-3613.

67. Cheng, G.; Mi, L.; Cao, Z. Q.; Xue, H.; Yu, Q. M.; Carr, L.; Jiang, S. Y., *Langmuir* **2010,** *26* (10), 6883-6886.

68. Carion, O.; Mahler, B.; Pons, T.; Dubertret, B., *Nat. Protoc.* **2007,** *2* (10), 2383-2390.

69. Lee, W. F.; Chen, Y. M., *J. Appl. Polym. Sci.* **2003,** *89* (7), 1884-1889.

70. Cao, B.; Li, L. L.; Tang, Q.; Cheng, G., *Biomaterials* **2013,** *34* (31), 7592-7600.

71. Xu, Y.; Takai, M.; Ishihara, K., *Biomacromolecules* **2009,** *10* (2), 267-274.

72. Goto, Y.; Matsuno, R.; Konno, T.; Takai, M.; Ishihara, K., *Biomacromolecules* **2008,** *9* (3), 828-833.

73. Oda, H.; Konno, T.; Ishihara, K., *Biomaterials* **2013,** *34* (24), 5891-5896.

74. Goda, T.; Furukawa, H.; Gong, J. P.; Ishihara, K., *Soft Matter* **2013,** *9* (7),

2166-2171.

75. Zhang, Z.; Chen, S. F.; Chang, Y.; Jiang, S. Y., *J. Phys. Chem. B* **2006,** *110* (22), 10799-10804.

76. Xu, X. Y.; Ray, R.; Gu, Y. L.; Ploehn, H. J.; Gearheart, L.; Raker, K.; Scrivens, W. A., *J. Am. Chem. Soc.* **2004,** *126* (40), 12736-12737.

77. Liu, H. P.; Ye, T.; Mao, C. D., *Angew. Chem. Int. Edit.* **2007,** *46* (34), 6473-6475.

78. Zhai, X. Y.; Liu, W. G., *Chem. Commun.* **2012,** *48* (64), 7955-7957.

79. Ueno, K.; Watanabe, M., *Langmuir* **2008,** *24* (10), 5253-5259.

80. Chan, J. M.; Zhang, L. F.; Yuet, K. P.; Liao, G.; Rhee, J. W.; Langer, R.; Farokhzad, O. C., *Biomaterials* **2009,** *30* (8), 1627-1634.

81. Cao, L.; Wang, X.; Meziani, M. J.; Lu, F. S.; Wang, H. F.; Luo, P. J. G.; Lin, Y.; Harruff, B. A.; Veca, L. M.; Murray, D.; Xie, S. Y.; Sun, Y. P., *J. Am. Chem. Soc.* **2007,** *129* (37), 11318-11332.

82. Wang, W.; Cheng, L.; Liu, W. G., *Sci. China. Chem.* **2014,** *57* (4), 522-539.

83. Li, H. T.; Kang, Z. H.; Liu, Y.; Lee, S. T., *J. Mater. Chem.* **2012,** *22* (46), 24230-24253.

84. Kearney, C. J.; Mooney, D. J., *Nat. Mater.* **2013,** *12* (11), 1004-1017.

85. Hunt, N. C.; Grover, L. M., *Biotechnol. Lett.* **2010,** *32* (6), 733-742.

86. Nichols, S. P.; Schoenfisch, M. H., *Chem. Rev.* **2013,** *113* (4), 2528-2549.

87. Heo, Y. J.; Shibata, H.; Okitsu, T.; Kawanishi, T.; Takeuchi, S., *P. Natl. Acad. Sci. USA* **2011,** *108* (33), 13399-13403.

88. Farra, R.; Sheppard, N. F.; McCabe, L.; Neer, R. M.; Anderson, J. M.; Santini, J. T.;

Cima, M. J.; Langer, R., *Sci. Transl. Med.* **2012,** *4* (122).

89. O'Brien, F. J., *Mater. Today* **2011,** *14* (3), 88-95.
90. Yancopoulos, G. D.; Davis, S.; Gale, N. W.; Rudge, J. S.; Wiegand, S. J.; Holash, J., *Nature* **2000,** *407* (6801), 242-248.
91. Xu, C. Y.; Inai, R.; Kotaki, M.; Ramakrishna, S., *Biomaterials* **2004,** *25* (5), 877-886.
92. Shuaib, A.; Butcher, K.; Mohammad, A. A.; Saqqur, M.; Liebeskind, D. S., *Lancet Neurol.* **2011,** *10* (10), 909-921.
93. Suszynski, T. M.; Avgoustiniatos, E. S.; Papas, K. K., *J. Diabetes Sci. Technol.* **2014,** *8* (3), 575-80.
94. Sekine, H.; Okano, T., *Nat. Commun.* **2013,** *4*, 1399-1407.
95. Takebe, T.; Sekine, K.; Ueno, Y.; Zheng, Y. W.; Koike, N.; Aoyama, S.; Adachi, Y.; Taniguchi, H., *Nature* **2013,** *499* (7459), 481-487.
96. Xue, A. S.; Koshy, J. C.; Brown, R. H.; Hicks, M. J.; Hollier, L. H., Jr., *Craniomaxillofac Trauma. Reconstr.* **2014,** *7* (1), 27-34.
97. Veiseh, O.; Doloff, J. C.; Greiner, D. L.; Langer, R.; Anderson, D. G., *Nat. Mater.* **2015,** *14* (6), 643-651.
98. Brauker, J. H.; Carrbrendel, V. E.; Martinson, L. A.; Crudele, J.; Johnston, W. D.; Johnson, R. C., *J. Biomed. Mater. Res.* **1995,** *29* (12), 1517-1524.
99. Madden, L. R.; Mortisen, D. J.; Murry, C. E.; Ratner, B. D., *P. Natl. Acad. Sci. USA* **2010,** *107* (34), 15211-15216.
100. Khanna, O.; Moya, M. L.; Opara, E. C.; Brey, E. M., *J. Biomed. Mater. Res. A* **2010,**

95a (2), 632-640.

101. Olsson, R.; Maxhuni, A.; Carlsson, P. O., *Transplantation* **2006,** *82* (3), 340-347.
102. Phelps, E. A.; Headen, D. M.; Taylor, W. R.; Thule, P. M.; Garcia, A. J., *Biomaterials* **2013,** *34* (19), 4602-4611.
103. Phelps, E. A.; Taylor, W. R.; Garcia, A. J., *P. Natl. Acad. Sci. USA* **2010,** *107* (8), 3323-3328.
104. Narang, A. S.; Cheng, K.; Henry, J.; Zhang, C. X.; Sabek, O.; Fraga, D.; Kotb, M.; Gaber, A. O.; Mahato, R. I., *Pharm. Res.* **2004,** *21* (1), 15-25.
105. Luo, J. Z. Q.; Luo, L. G., *Bone Marrow Transpl.* **2011,** *46* (8), 1128-1137.
106. Veriter, S.; Dufrane, D., *Cell Transplant.* **2014,** *23* (11), 1349-1364.
107. Grainger, D. W., *Nat. Biotechnol.* **2013,** *31* (6), 507-509.
108. Vaisocherova, H.; Jiang, S. Y., *Anal. Chem.* **2008,** *80* (20), 7894-7901.
109. Lacy, P. E., *Cc/Life Sci.* **1981,** (8), 21-21.
110. Shapiro, A. M. J.; Hao, E.; Rajotte, R. V.; Kneteman, N. M *Cell Transplant.* **1996,** *5* (6), 631-638.
111. Carter, J. D.; Dula, S. B.; Corbin, K. L.; Wu, R. P.; Nunemaker, C. S., *Biol. Proced. Online* **2009,** *11* (1), 3-31.
112. de Haan, B. J.; van Willigen, J. W.; de Haan, A.; de Vos, P., *Pancreas* **2004,** *29* (1), E15-E22.
113. Amoli, M. M.; Moosavizadeh, R.; Larijani, B., *Cytotechnology* **2005,** *48* (1-3), 75-78.
114. Tagler, D.; Makanji, Y.; Shea, L. D., *Biotechnol. Bioeng.* **2014,** *111* (7), 1417-1429.

115. Lee, T. T.; Garcia, A. J., *Nat. Mater.* **2015,** *14* (3), 352-360.

116. Khoo, X.; Grinstaff, M. W., *Mrs Bull.* **2011,** *36* (5), 357-366.

117. Ding, X.; Yang, C.; Yang, Y. Y., *Biomaterials* **2012,** *33* (28), 6593-6603.

118. Scharp, D. W.; Marchetti, P., *Adv. Drug Deliver. Rev.* **2014,** *67-68*.

119. Ma, M. L.; Vegas, A.; Chen, D. L.; Bratlie, K. M.; Dang, T.; York, R. L.; Hollister-Lock, J.; Weir, G. C.; Anderson, D. G., *Adv. Healthc. Mater.* **2013,** *2* (5), 667-672.

120. Dang, T. T.; Gu, Z.; Cheng, H.; Weir, G. C.; Langer, R.; Anderson, D. G., *Biomaterials* **2013,** *34* (23), 5792-5801.

121. Lin, C. C.; Anseth, K. S., *Biomacromolecules* **2009,** *10* (9), 2460-2467.

122. Weber, L. M.; He, J.; Bradley, B.; Haskins, K.; Anseth, K. S., *Acta Biomater.* **2006,** *2* (1), 1-8.

123. Cruise, G. M.; Hegre, O. D.; Scharp, D. S.; Hubbell, J. A., *Biotechnol. Bioeng.* **1998,** *57* (6), 655-665.

124. Cruise, G. M.; Hubbell, J. A., *Cell Transplant.* **1999,** *8* (3), 293-306.

125. Phelps, E. A.; Barker, T. H.; Garcia, A. J., *Adv. Mater.* **2012,** *24* (1), 64-70.

126. Schweicher, J.; Nyitray, C.; Desai, T. A., *Front. Biosci-Landmrk* **2014,** *19*, 49-76.

127. Jain, R. K., *Nat. Med.* **2001,** *7* (9), 987-989.

128. Levy, B. I.; Schiffrin, E. L.; Mourad, J. J.; Agostini, D.; Vicaut, E.; Safar, M. E.; Struijker-Boudier, H. A. J., *Circulation* **2008,** *118* (9), 968-976.

129. Patterson, C. E.; Rhoades, R. A.; Garcia, J. G. N., *J. Appl. Physiol.* **1992,** *72* (3), 865-873.

130. Barkai, U.; Bloch, K.; de Vos, P.; Rotem, A., *Cell Transplant.* **2013,** *22* (8),

1463-1476.

131. Pedraza, E.; Coronel, M. M.; Fraker, C. A.; Ricordi, C.; Stabler, C. L., *P. Natl. Acad. Sci. USA* **2012,** *109* (11), 4245-4250.

132. Steele, J. A. M.; Neufeld, R. J., *Adv. Drug. Deliver. Rev.* **2014,** *67-68*, 74-83.

133. Kerby, A.; Bohman, S.; Westberg, H.; Jones, P.; King, A., *Artif. Organs.* **2012,** *36* (6), 564-570.

134. Vegas, A. J.; Weir, G. C.; Melton, D. A.; Langer, R.; Anderson, D. G., *Nat. Med.* **2016,** *22* (3), 306-311.

135. Jacobs-Tulleneers-Thevissen, D.; Keymeulen, B.; Pipeleers, D.; Consortium, B. C. T., *Diabetologia* **2013,** *56* (7), 1605-1614.

136. Dufrane, D.; Goebbels, R. M.; Gianello, P., *Transplantation* **2010,** *90* (10), 1054-1062.

137. Orlando, G.; Gianello, P.; Salvatori, M.; Stratta, R. J.; Soker, S.; Ricordi, C.; Dominguez-Bendala, J., *Diabetes* **2014,** *63* (5), 1433-1444.

138. Espevik, T.; Otterlei, M.; Skjakbraek, G.; Ryan, L.; Wright, S. D.; Sundan, A., *Eur. J. Immunol.* **1993,** *23* (1), 255-261.

139. Krishnan, R.; Foster, C. E., 3rd; Lakey, J. R., *Rev. Diabet. Stud.* **2014,** *11* (1), 84-101.

140. Anderson, J. M.; Rodriguez, A.; Chang, D. T., *Semin. Immunol.* **2008,** *20* (2), 86-100.

141. Ratner, B. D., *J. Control. Release.* **2002,** *78* (1-3), 211-218.

142. Hetrick, E. M.; Prichard, H. L.; Klitzman, B.; Schoenfisch, M. H., *Biomaterials*

2007, *28* (31), 4571-4580.

143. Kenneth Ward, W., *J. Diabetes Sci. Technol.* **2008,** *2* (5), 768-77.

144. Lee, R. J.; Springer, M. L.; Blanco-Bose, W. E.; Shaw, R.; Ursell, P. C.; Blau, H. M., *Circulation* **2000,** *102* (8), 898-901.

145. Distler, O.; Gay, S., *Circ. Res.* **2004,** *95* (1), 109-16.

146. Lim, F.; Sun, A. M., *Science* **1980,** *210* (4472), 908-910.

147. Calafiore, R.; *Adv. Drug. Deliver. Rev.* **2014,** *67-68*, 84-92.

148. Lanza, R. P.; Hayes, J. L.; Chick, W. L., *Nat. Biotechnol.* **1996,** *14* (9), 1107-1111.

149. Pipeleers, D.; Keymeulen, B., *Trends Endocrin. Met.* **2016,** *27* (5), 247-248.

150. Bratlie, K. M.; York, R. L.; Invernale, M. A.; Langer, R.; Anderson, D. G., *Adv. Healthc. Mater.* **2012,** *1* (3), 267-284.

151. O'Sullivan, E. S.; Vegas, A.; Anderson, D. G.; Weir, G. C., *Endocr. Rev.* **2011,** *32* (6), 827-844.

152. Tuch, B. E.; Keogh, G. W.; Williams, L. J.; Wu, W.; Foster, J. L.; Vaithilingam, V.; Philips, R., *Diabetes Care* **2009,** *32* (10), 1887-1889.

153. Ludwig, B.; Rotem, A.; Bornstein, S. R.; Barkai, U., *P. Natl. Acad. Sci. USA* **2012,** *109* (13), 5022-5027.

154. Colton, C. K., *Adv. Drug. Deliver. Rev.* **2014,** *67-68*, 93-110.

155. Ludwig, B.; Reichel, A.; Gendler, Z.; Rotem, A.; Barkai, U.; Bornstein, S. R., *P. Natl. Acad. Sci. USA* **2013,** *110* (47), 19054-19058.

156. Otterlei, M.; Ostgaard, K.; Skjakbraek, G.; Smidsrod, O.; Soonshiong, P.; Espevik, T., *J. Immunother.* **1991,** *10* (4), 286-291.

157. Ratner, B. D.; Bryant, S. J., *Annu. Rev. Biomed. Eng.* **2004,** *6*, 41-75.

158. Amoako, K. A.; Cook, K. E., *Adv. Mater. Interfaces.* **2016,** *3* (6) 446-448.

159. Callow, J. A.; Callow, M. E., *Nat. Comm.* **2011,** *2 1-6*.

160. Bauer, S.; Arpa-Sancet, M. P.; Finlay, J. A.; Callow, M. E.; Callow, J. A.; Rosenhahn, A., *Langmuir* **2013,** *29* (12), 4039-4047.

161. Hu, Y. C.; Ye, X. S., *Acta Biomater.* **2015,** *13*, 142-149.

162. Kyomoto, M.; Ishihara, K., *Acta Biomater.* **2015,** *24*, 24-34.

163. Banerjee, I.; Pangule, R. C.; Kane, R. S., *Adv. Mater.* **2011,** *23* (6), 690-718.

164. Fukazawa, K.; Ishihara, K., *Acs. Appl. Mater. Inter.* **2013,** *5* (15), 6832-6836.

165. Blanco, C. D.; Navarro, A.; Mendoza, E.; Tzanov, T., *Acs. Appl. Mater. Inter.* **2014,** *6* (14), 11385-11393.

166. Yang, R.; Gleason, K. K., *Langmuir* **2012,** *28* (33), 12266-12274.

167. Gao, G. Z.; Kizhakkedathu, J. N., *Biomaterials* **2011,** *32* (16), 3899-3909.

168. Wang, G. Z.; Yuan, Z. F.; Chen, S. F., *Acs Appl. Mater. Inter.* **2015,** *7* (31), 16938-16945.

169. Zhang, L.; Yang, H. C.; Liu, H.; Ni, Q. T.; Gong, F. H., *Polym. Eng. Sci.* **2015,** *55* (4), 889-895.

170. Yang, Y.; Yan, X. H.; Cui, Y.; He, Q.; Li, D. X.; Wang, A. H.; Fei, J. B.; Li, J. B., *J. Mater. Chem.* **2008,** *18* (47), 5731-5737.

171. Zhang, P.; Henthorn, D. B., *Aiche J.* **2010,** *56* (6), 1610-1615.

172. Chlupac, J.; Bacakova, L., *Physiol. Res.* **2014,** *63* (2), 167-177.

173. Wei, Q.; Becherer, T.; Noeske, P. L.; Grunwald, I.; Haag, R., *Adv. Mater.* **2014,** *26*

(17), 2688-93, 2615.

174. Lin, P.; Ding, L.; Lin, C. W.; Gu, F., *Langmuir* **2014,** *30* (22), 6497-507.

175. Swartjes, J. J. T. M.; Krom, B. P.; Busscher, H. J.; van der Mei, H. C., *Adv. Funct. Mater.* **2013,** *23* (22), 2843-2849.

176. Lu, Y.; Yue, Z. G.; Wang, W.; Cao, Z. Q., *Front. Chem. Sci. Eng.* **2015,** *9* (3), 324-335.

177. Tamboto, H.; Vickery, K.; Deva, A. K., *Reconstr. Surg.* **2010,** *126* (3), 835-842.

178. Francolini, I.; Donelli, G., *Fems. Immunol. Med. Mic.* **2010,** *59* (3), 227-238.

179. Williams, D. L.; Sinclair, K. D.; Jeyapalina, S.; Bloebaum, R. D., *J. Biomed. Mater. Res. B* **2013,** *101b* (6), 1078-1089.

180. Zhao, L. Z.; Wang, H. R.; Huo, K. F.; Cui, L. Y.; Zhang, W. R.; Ni, H. W.; Zhang, Y. M.; Wu, Z. F.; Chu, P. K., *Biomaterials* **2011,** *32* (24), 5706-5716.

181. Buskens, P.; Wouters, M.; Rentrop, C.; Vroon, Z., *J. Coat. Technol. Res.* **2013,** *10* (1), 29-36.

182. Carr, L. R.; Xue, H.; Jiang, S. Y., *Biomaterials* **2011,** *32* (4), 961-968.

183. Holmes, P. F.; Norde, W., *J. Biomed. Mater. Res. A* **2009,** *91a* (3), 824-833.

184. Lu, Y.; Parkin, I. P., *Science* **2015,** *347* (6226), 1132-1135.

185. Mahmud, G.; Huda, S.; Yang, W.; Kandere-Grzybowska, K.; Pilans, D.; Jiang, S. Y.; Grzybowski, B. A., *Langmuir* **2011,** *27* (17), 10800-10804.

186. Cheng, G.; Xue, H.; Li, G. Z.; Jiang, S. Y., *Langmuir* **2010,** *26* (13), 10425-10428.

187. Fernandez, I. C. S.; Busscher, H. J., *Biomaterials* **2007,** *28* (28), 4105-4112.

188. Costerton, J. W.; Stewart, P. S.; Greenberg, E. P., *Science* **1999,** *284* (5418),

1318-1322.

189. Owen, S. J.; Volmer, D. A., *Rapid Commun. Mass. Sp.* **2003,** *17* (21), 2439-2449.

190. Yang, W. J.; Kang, E. T.; Teo, S. L. M.; Rittschof, D., *Prog. Polym. Sci.* **2014,** *39* (5), 1017-1042.

191. Goda, T.; Konno, T.; Takai, M.; Moro, T.; Ishihara, K., *Biomaterials* **2006,** *27* (30), 5151-5160.

192. Ganewatta, M. S.; Decho, A. W.; Tang, C. B., *Biomacromolecules* **2015,** *16* (10), 3336-3344.

ABSTRACT

ZWITTERIONIC POLYMER MATERIALS FOR NANOPARTICLE STABILIZATION, CELL ENCAPSULATION AND ANTI-FOULING COATING

by

WEI WANG

August 2017

Advisor: Dr. Zhiqiang Cao

Major: Materials Science and Engineering

Degree: Doctor of Philosophy

Based on the superior anti-fouling property, the zwitterionic materials had great potential in applications such as medical implants, medical device coating, and marine coating industry. This dissertation will focus on the applications of zwitterionic materials in stabilizing carbon nanoparticles, as implantable devices and durable coating on medical devices for long-term anti-microbial purposes. Chapter 2 of the thesis will discuss a simple method to synthesis carbon nanoparticles stabilized by zwitterionic polymers. Chapter 3 of the thesis reports the use of zwitterionic hydrogel to encapsulate islet of Langerhans to treat Type 1 diabetes. In Chapter 4 and 5, several methods were developed to improve the stability and durability of zwitterionic anti-fouling coating. The improved coatings were able to address the notorious biofilm issue on medical devices by resisting the bacteria adhesion for a long term in highly concentrated bacteria culture media. These works greatly extend the applicability of zwitterionic materials for long-term anti-fouling purposes.

AUTOBIOGRAPHICAL STATEMENT

Education

B.Engn. in Polymer Materials & Engineering, Tianjin University – 2013

Ph.D. in Materials and Engineering, Wayne State University – 2017

Publications

1. **Wei Wang**, Jianhai Yang, Ershuai Zhang, Yang Lu and Zhiqiang Cao*, Carnitine Derived Zwitterionic Betaine Materials, **submitted**
2. **Wei Wang**, Hui Zhu, Zhigang Wang, Zhanguo Yue, Yang Lu and Zhiqiang Cao* Zwitterionic hydrogel implant promotes functional blood vessel growth as good as natural body system, **Nature Biomedical Engineering, in revision**
3. **Wei Wang,** Yang Lu, Hui Zhu and Zhiqiang Cao*, Super-durable coating fabricated from a double-sided tape with long term "zero" bacterial adhesion, **Advanced Materials, in revision**
4. J.B. Xie, Y. Lu, **W. Wang,** H. Zhu, Z.G. Wang and Z.Q. Cao*, Simple Protein Modification Using Zwitterionic Polymer to Mitigate the bioactivity Loss of Conjugated Insulin, **Advanced Healthcare Materials**, (2017).
5. **Wang W** and Cao Z Q. Opinion on the recent development of environmentally friendly marine anti-fouling coating, **Science China Technological Sciences**, 2016, 59(12): 1968-1970.
6. **Wang W,** Lu Y, Xie J, et al. A zwitterionic macro-crosslinker for durable non-fouling coatings, **Chemical Communications**, 2016, 52(25): 4671-4674.
7. **W. Wang,** J. Amin, Z.Q. Cao*, Advances in Smart Hydrogels for Biosensing Applications, in Gels Handbook: Fundamentals, Properties and Applications, U. Demirci and A. Khademhosseini, Editors. 2016, **World Scientific Publishing Company**. 3, 189 (2016)
8. Lu Y, Yue Z, **Wang W,** et al. Strategies on designing multifunctional surfaces to prevent biofilm formation, **Frontiers of Chemical Science and Engineering,** 2015, 9(3): 324-335.
9. **Wang W,** Lu Y, Yue Z, et al. Ultrastable core–shell structured nanoparticles directly made from zwitterionic polymers, **Chemical Communications**, 2014, 50(95): 15030-15033.
10. **Wang W,** Li Y, Cheng L, et al. Water-soluble and phosphorus-containing carbon dots with strong green fluorescence for cell labeling, **Journal of Materials Chemistry B,** 2014, 2(1): 46-48.